LUND UNIVERSITY

Improvements to air mass calculations for ground-based infrared measurements

Meier, Arndt; Goldman, A; Manning, PS; Stephen, TM; Rinsland, CP; Jones, NB; Wood, SW

Published in:
Journal of Quantitative Spectroscopy & Radiative Transfer

DOI:
10.1016/S0022-4073(02)00018-3

2004

Link to publication

Citation for published version (APA):
Meier, A., Goldman, A., Manning, PS., Stephen, TM., Rinsland, CP., Jones, NB., & Wood, SW. (2004). Improvements to air mass calculations for ground-based infrared measurements. *Journal of Quantitative Spectroscopy & Radiative Transfer*, *83*(1), 109-113. https://doi.org/10.1016/S0022-4073(02)00018-3

Total number of authors:
7

General rights
Unless other specific re-use rights are stated the following general rights apply:
Copyright and moral rights for the publications made accessible in the public portal are retained by the authors and/or other copyright owners and it is a condition of accessing publications that users recognise and abide by the legal requirements associated with these rights.
• Users may download and print one copy of any publication from the public portal for the purpose of private study or research.
• You may not further distribute the material or use it for any profit-making activity or commercial gain
• You may freely distribute the URL identifying the publication in the public portal

Read more about Creative commons licenses: https://creativecommons.org/licenses/

Take down policy
If you believe that this document breaches copyright please contact us providing details, and we will remove access to the work immediately and investigate your claim.

LUND UNIVERSITY

PO Box 117
221 00 Lund
+46 46-222 00 00

Download date: 12. Jul. 2024

PERGAMON

Journal of Quantitative Spectroscopy & Radiative Transfer 83 (2004) 109–113

Journal of Quantitative Spectroscopy & Radiative Transfer

www.elsevier.com/locate/jqsrt

Note

Improvements to air mass calculations for ground-based infrared measurements

Arndt Meier[a,*], Aaron Goldman[b], Paul S. Manning[b], Thomas M. Stephen[b], Curtis P. Rinsland[c], Nicholas B. Jones[d], Stephen W. Wood[d]

[a] *Department of Chemistry, University of Wollongong, NSW 2522, Australia*
[b] *Department of Physics, University of Denver, Denver, CO 80208, USA*
[c] *NASA Langley Research Center, Mail Stop 401A, Hampton, VA 23681-2199, USA*
[d] *NIWA (National Institute of Water and Atmospheric Research Ltd.), Lauder, Private Bag 50061, Omakau, Central Otago, New Zealand*

Received 22 October 2001; received in revised form 8 January 2002; accepted 29 January 2002

Abstract

High-resolution ground-based infrared solar spectra are routinely recorded at the Network for the Detection of Stratospheric Change (NDSC) stations. These data sets play a key role in providing a long-term record of atmospheric composition and their links to climate change. The analysis of observed infrared spectra involves comparison to a computer-modeled atmosphere where knowledge of the air mass distribution is an essential component. This note summarises improvements made to an existing and widely used computer code (FSCATM) to perform refractive ray-tracing and calculation of the air mass distribution. Changes were made towards higher vertical resolution in the troposphere and increased numerical precision. The revised FSCATM improves the analysis of infrared spectra mostly through the more accurate representation of the temperature profile. Air mass differences with respect to earlier versions are documented and are typically $<0.7\%$, exceptions being extreme cases of inversion layers. The current version provides ray tracing and air mass calculations for any terrestrial observation site. The output files are reported in a format compatible with the SFIT and SFIT2 retrieval algorithms, which are widely used for NDSC infrared atmospheric studies. The improved computer code, documentation, reference profiles, and test cases are available electronically.
Published by Elsevier Ltd.

1. Introduction

The Air Mass Computer Program for Atmospheric Transmittance/Radiance Calculation FSCATM [1] has been widely used for over a decade with a variety of atmospheric radiative transfer applications. Ray tracing and optical paths integrals based on this program have been applied extensively

* Corresponding author. Tel.: +61-2-9310-1800; fax: +61-2-9699-8615.
E-mail address: a.meier@apollolifesciences.com (A. Meier).

0022-4073/04/$ - see front matter Published by Elsevier Ltd.
PII: S0022-4073(02)00018-3

by the LOWTRAN codes [2]. Several improvements, including better accuracy with more effective use of the atmospheric layers and preserving the hydrostatic equation, were developed for the widely used Line-by-Line program known as LBLRTM and its FASTCODE predecessors [3]. In another widely used Line-by-Line code, known as GENLN2 [4] independent calculations are applied for this purpose, which are based on an algorithm similar to that of FSCATM [1], and allow to obtain high-accuracy optical paths for the atmospheric trace gases.

The ray-tracing program FSCATM has been implemented in the SFIT (e.g. [5,6]) and in the SFIT2 retrieval programs [7–10] to determine the slanted optical path of sunlight as seen from the ground. These particular implementations of FSCATM have a set of SFIT-specific auxiliary programs and are referred to as SFIT-FSCATM. These programs are widely used by the atmospheric infrared remote sensing community, in particular within the NDSC [11,12].

SFIT retrieves total column amounts of atmospheric trace gases from ground-based solar infrared spectra based on the observed absorption features, the observation geometry, and the model atmosphere provided by SFIT-FSCATM. The latter consists of total air masses, pressures, temperatures, and volume mixing ratios (VMRs) for infrared active species in vertically-stratified layers. This revision of FSCATM also improves the quality of satellite validation and long-term monitoring programs. The full report on which this Note is based is available from *J. Quant. Spectrosc. Radiat. Transfer* as an electronic supplement [13].

2. Changes to FSCATM

The new version of FSCATM is backward compatible and incorporates the minimal number of changes in the source code. All SFIT-FSCATM releases prior to version 2.01 (July 1999), had a number of limitations which can lead to errors when the user atmosphere is defined with vertical resolutions better than 2 km. The main limitations arise from the internal layering scheme of FSCATM which is used for needed interpolations. Consequently, the total number of internal model layers has been increased, the numerical precision has been improved, the maximum number of output layers has been raised, the number of standard molecules has been increased from 57 to 63, and the fundamental constants used were updated to be in agreement with the latest CODATA recommendations [14]. The new molecules added include some important replacement CFCs which are increasing rapidly in abundance.

SFIT uses its own auxiliary programs to have FSCATM perform the necessary ray tracing. Thus, some changes were required in these programs to comply with the new FSCATM. Besides changes in data formats the default boundary layer selections have been made self-consistent, the iterative run for the determination of the apparent from the astronomical zenith angle has been automated and can be achieved following either an internal or external iteration procedure, the number of pre-stored observation sites was tripled (Table 1), the set of default a priori VMR profiles was updated, the user interface has been improved, and a new ab initio calculation of the atmospheric bending has been implemented resulting in an accuracy of better than 0.0012° for solar zenith angles of up to 85° for any terrestrial site. The improvements made to the iterative determination of the atmospheric bending result in faster convergence. The user is given the option to define his own output altitude scheme and to provide his own set of VMR profiles to suit a particular retrieval code or site-specific atmospheric conditions. In the case of profile retrieval codes such as SFIT2 the use of an output

Table 1
List of observation sites supported by SFIT-FSCATM, most of which have NDSC status

Site	Latitude	Longitude	Altitude (m)
Eureka, Canada	80.05°N	86.42°W	610
Ny-Ålesund, Spitsbergen	78.92°N	11.94°E	20
Kiruna, Sweden	67.84°N	20.41°E	419
Poker Flat RR, Alaska	65.119°N	147.433°W	505
Harestua, Norway	60.217°N	10.753°E	596
Bremen, Germany	53.107°N	8.854°E	27
NPL Teddington, UK	51.424°N	0.343°W	30
Zugspitze, German Alps	47.422°N	10.987°E	2964
Jungfraujoch, Swiss Alps	46.549°N	7.986°E	3580
Moshiri, Japan	44.367°N	142.267°E	280
Rikubetsu, Japan	43.457°N	143.766°E	370
Mt Bancroft, CA	37.584°N	118.235°W	3801
Denver, CO	36.673°N	104.963°W	1643
Billings, Oklahoma	36.605°N	97.485°W	317
Tsukuba, Japan	36.048°N	140.116°E	31
Table Mountain, CA	34.382°N	117.677°W	2258
JPL Pasadena, CA	34.200°N	118.172°W	350
Kitt Peak, AZ	31.90°N	111.60°W	2090
Teneriffe, Canarian Islands	28.294°N	16.490°W	2367
Mauna Loa, Hawaii	19.539°N	155.578°W	3398
Wollongong, Australia	34.45°S	150.88°E	30
Lauder, New Zealand	45.045°S	169.684°E	370
Arrival Heights, Antarctica	77.83°S	166.67°E	200
South Pole, Antarctica	89.83°S		2850
User specified at run time	any	any	0–4000

altitude scheme of constant stepsize throughout the lower atmosphere is found to reduce unwanted profile oscillations.

3. Impacts of the revision of FSCATM

Two case studies have been carried out for two locations each in order to evaluate the impacts of the changes made. The first part of this study revealed that differences in air mass, pressure, and temperature are small in the troposphere ($<0.42\%$) except for inversion layers. FSCATM data products for altitudes above 12 km altitude agreed within the numerical precision.

The second part of the study investigated the impacts of the changes in SFIT-FSCATM on the total column amounts (TCAs) retrieved from ground-based solar FTIR spectra recorded in Kiruna, Sweden, under a wide range of meteorological conditions. The spectra were analysed using SFIT 1.09*e* [5,6]. The TCAs were retrieved from 125 different absorption lines located in more than 100 atmospheric micro-windows.

The detailed studies [13] reveal that in the absence of an inversion layer the effects of the changes in SFIT-FSCATM on the TCAs retrieved with SFIT 1.09*e* are $<0.7\%$ for any species except water vapor (2.5%) and $<0.2\%$ for any stratospheric species. Compared to other uncertainties in the retrieval of TCAs, which typically add to several percent, a re-processing of spectra previously analysed with SFIT-FSCATM 1995 is not necessary. However, the differences become significant for all tropospheric species if a strong inversion layer is present. This does not affect molecules with a mostly stratospheric distribution. An exception is $ClONO_2$ where a change in TCAs of several percent is seen, which is caused by strong interference from an overlapping temperature-sensitive CO_2 line [13].

The temperature sensitivity of a transition depends on its lower state energy E'' and the partition function [15]. The full report [13] discusses the differences in retrieved TCAs as a function of the lower state energies involved and the magnitude of the temperature misrepresentation, which in our case is also a function of altitude and of the distribution of the molecule over altitude [13]. A systematic error in the retrieved TCAs of $0.2\%\,K^{-1}$ in temperature misrepresentation and per $100\,cm^{-1}$ above $300\,cm^{-1}$ in the transition's lower state energy E'' can be estimated for a molecule entirely contained in the altitude range where the temperature error occurs. It is noted that, this relation applies to ground-based FTIR observations irrespective of the source of a temperature misrepresentation.

It is noted that, while it is common practice to select lines with minimal temperature sensitivity, transitions with high-temperature sensitivity were also included in the studies for demonstrating the behaviour of unavoidable interference lines.

4. Conclusions

The limited vertical resolution in the troposphere implemented in the 1995 version of SFIT-FSCATM can result in misrepresentations in pressure, temperature and air mass. The changes made to SFIT-FSCATM substantially improve the representation of the tropospheric part of the model atmosphere, which is particularly significant if inversion layers are encountered. The differences between the current version 2.03 (Oct 2001) and versions before 1999 are small if the temperature and VMR profiles provided are fairly smooth. High-altitude sites are generally less affected than low-altitude observation sites.

Consistent with the conclusion that temperature errors are the main cause of problems with using the previous SFIT-FSCATM version is the fact that differences in the TCAs retrieved show a clear correlation with the lower state energies of the corresponding absorption lines [13].

In addition, the number of molecules has been expanded to include replacement-CFCs, which are expected to reach detection limits in the near future. The corresponding default VMRs have been updated according to recent measurements.

Acknowledgements

Research at the University of Denver was supported in part by NSF and in part by NASA. Acknowledgement is made to the National Center for Atmospheric Research, which is supported

by the National Science Foundation, for computer time used in this research. We wish to thank the Australian Research Council and the New Zealand Foundation for Research, Science, and Technology for funding; the Upper Atmosphere Research Program for funding NASA Langley; our colleagues at the Swedish Institute of Space Physics and their collaboration partners for their support in recording the solar spectra, the Atmospheric Watch Section of the Australian Bureau of Meteorology and the Swedish Space Corporation at Esrange for use of their PTU sonde data, and all our colleagues from the infrared working group of the NDSC for their encouraging support.

References

[1] Gallery WO, Kneizys FX, Clough SA. Air mass computer program for atmospheric transmittance/radiance calculation: FSCATM. Environmental research paper ERP-828/AFGL-TR-83-0065, Air Force Geophysical Laboratory, Hanscom AFB, MA, 1983.

[2] Kneizys FX, Shettle EP, Abreu LW, Chetwynd JH, Anderson GP, Gallery WO, Selby JEA, Clough SA. Users guide to LOWTRAN7, AFGL-TR-88-0177. Hanscom AFB, MA, Air Force Geophysical Laboratory AFGL(OPI): 1988.

[3] Clough SA, Iacono MJ. Line-by-line calculations of atmospheric fluxes and cooling rates 2: application to carbon dioxide, ozone, methane, nitrous oxide, and the halocarbons J Geophys Res 1995;100:16 519–35.

[4] Edwards DP. GENLN2 a general line-by-line atmospheric transmittance and radiance model. NCAR technical note, NCAR/TN-367+STR, Boulder, CO, 1992.

[5] Rinsland CP, Levine JS, Zander R, Goldman A, Sze ND, Ko MKW, Johnson DW. Infrared measurements of HF and HCl total column abundances above Kitt Peak, 1977–1990: seasonal cycles, long-term increases, and comparisons with model calculations J Geophys Res (D: Atmosph) 1991;96:15 523–40.

[6] Rinsland CP, Smith MAH, Rinsland PL, Goldman A, Brault JW, Stokes GM. Ground-based infrared spectroscopic measurements of atmospheric hydrogen cyanide. J Geophys Res (D: Atmosph) 1982;87:11 119–25.

[7] Rinsland CP, Goldman A, Connor BJ, Stephen TM, Jones NB, Wood SW, Murcray FJ, David SJ, Blatherwick RD, Zander R, Mahieu E, Demoulin P. Correlation relationships of stratospheric molecular constituents from high spectral resolution, ground-based infrared solar absorption spectra. J Geophys Res (D: Atmosph) 2000;105:14 637–52.

[8] Rinsland CP, Jones NB, Connor BJ, Logan JA, Pougatchev NS, Goldman A, Murcray FJ, Stephen TM, Pine AS, Zander R, Mahieu E, Demoulin P. Northern and southern hemisphere ground-based infrared spectroscopic measurements of tropospheric carbon monoxide and ethane. J Geophys Res (D: Atmosph) 1998;103:28 197–217.

[9] Connor BJ, Jones NB, Wood SW, Keys JG, Rinsland CP, Murcray FJ. Retrieval of HCl and HNO_3 profiles from ground-based FTIR data using SFIT2. In: Bojkov RD, Visconti G, editors. Proceedings of the XVIII Quadr Ozone Symposium. L'Aquila, Italy, Parco Scientifico e Technologico d'Abruzzio, 1998. p. 485–88.

[10] Pougatchev NS, Connor BJ, Rinsland CP. Infrared measurements of the ozone vertical distribution above Kitt Peak. J Geophys Res (D: Atmosph) 1995;100:16689–97.

[11] Kurylo MJ. Network for the detection of stratospheric change. Proc Soc Photo Opt Instrum Eng 1991;1491: 169–74; see also http://www.ndsc.ws/.

[12] Kurylo MJ, Zander R. The NDSC—its status after 10 years of operation. Proceedings of the XIX Quad. Ozone Symposium. Sapporo, Japan, Hokkaido University, 2000. p. 167–8.

[13] Meier A, Goldman A, Manning PS, Stephen TM, Rinsland CP, Jones NB, Wood SW. Improvements to air mass calculations for ground-based infrared measurements—full report. Unpublished Research Report, 2001; http://www.uow.edu.au/science/research/acrg/staff/fscatmf.pdf.

[14] Mohr PJ, Taylor BN. CODATA recommended values of the fundamental physical constants: 1998. Rev Mod Phys 2000;72:351–495; also available online from NIST: http://physics.nist.gov/cuu/Constants/index.html.

[15] Penner SS. Quantitative molecular spectroscopy and gas emissivities. Reading, MA: Addison-Wesley, 1959. LCCC 59–7546.

Electronic Supplement*

Improvements to Air Mass Calculations for Ground-Based Infrared Measurements

Arndt Meier**†, Aaron Goldman‡, Paul S. Manning‡, Thomas M. Stephen‡,
Curtis P. Rinsland§ Nicholas B. Jones¶, and Stephen W. Wood¶

†University of Wollongong, Dept. of Chemistry, NSW 2522, Australia, fax 61-2-42214287, email arndt@uow.edu.au ‡University of Denver, Dept. of Physics, Denver CO 80208, USA §NASA Langley Research Center, Mail Stop 401A, Hampton VA 23681-2199, USA ¶NIWA (National Institute of Water and Atmospheric Research Ltd.), Lauder, Private Bag 50061, Omakau, Central Otago, New Zealand

Abstract – High-resolution ground-based infrared solar spectra are routinely recorded at the Network for the Detection of Stratospheric Change (NDSC) stations. These data sets play a key role in providing a long-term record of atmospheric composition and their links to climate change. The analysis of observed infrared spectra involves comparison to a computer-modeled atmosphere where knowledge of the air mass distribution is an essential component. This note summarises improvements made to an existing and widely used computer code (FSCATM) to perform refractive ray-tracing and calculation of the air mass distribution. Changes were made towards higher vertical resolution in the troposphere and increased numerical precision. The revised FSCATM improves the analysis of infrared spectra mostly through the more accurate representation of the temperature profile. Air mass differences with respect to earlier versions are documented and are typically less than 0.7 %, exceptions being extreme cases of inversion layers. The current version provides ray tracing and air mass calculations for any terrestrial observation site. The output files are reported in a format compatible with the SFIT and SFIT2 retrieval algorithms, which are widely used for NDSC infrared atmospheric studies. The improved computer code, documentation, reference profiles, and test cases are available electronically.

1 Introduction

The Air Mass Computer Program for Atmospheric Transmittance/Radiance Calculation FSCATM [1] has been widely used for over a decade with a variety of atmospheric radiative transfer applications. Raytracing and optical paths integrals based on this program have been applied extensively by the LOWTRAN codes [2]. Several improvements, including better accuracy with more effective use of the atmospheric layers and preserving the hydrostatic equation, were developed for the widely used Line-by-Line program known as LBLRTM and its FASTCODE predecessors [3]. In another widely used Line–by–Line code, known as GENLN2 [4] independent

*The major findings of this manuscript are published as a Note in the Journal of Quantitative Spectroscopy and Radiative Transfer, 2002.

**To whom all correspondence should be addressed

calculations are applied for this purpose, which are based on an algorithm similar to that of FSCATM [1], and allow to obtain high accuracy optical paths for the atmospheric trace gases.

The ray-tracing program FSCATM has been implemented in the SFIT (e.g. [5, 45, 6]) and in the SFIT2 retrieval programs [7, 8, 9, 10] to determine the slanted optical path of sunlight as seen from the ground. These particular implementations of FSCATM have a set of SFIT–specific auxiliary programs and are referred to as SFIT–FSCATM. These programs are widely used by the atmospheric infrared remote sensing community, in particular within the NDSC [11, 12]. This revision of FSCATM improves the quality of satellite validation and long–term monitoring programs.

FSCATM performs a ray-tracing calculation to determine the air mass distribution along the optical path and creates a model atmosphere according to user–specified parameters. This model atmosphere consists of total air masses, pressures, temperatures, and volume mixing ratios (VMRs) for infrared active species in vertically–stratified layers. SFIT infers total column amounts (TCAs) of atmospheric trace gases from ground–based solar infrared spectra based on the observed absorption features, the observation geometry and the model atmosphere provided by SFIT–FSCATM. It is noted that a brief summary of this report is published as a Note in the *Journal of Quantitative Spectroscopy and Radiative Transfer* [13].

Prior to SFIT 1.09, a 36 layer input model atmosphere was commonly used with SFIT–FSCATM (*refmod92, tape9*), which was handled correctly by FSCATM. With the need for better tropospheric resolution, the number of layers provided to FSCATM was increased from 36 to 41 and became the standard for the SFIT 1.09 distribution through its *refmod95* file. Unfortunately it was overlooked that the finer 1 *km* spaced tropospheric resolution of the *refmod95* volume mixing ratio and pressure temperature profiles handed to FSCATM were not matched by the same vertical resolution within FSCATM. At that time, FSCATM used a fixed 47–layer, internal model with 2 *km* spacing in the troposphere and lower stratosphere. Under certain conditions (see below) the pressures, temperatures and VMRs provided at the additional altitudes were ignored by FSCATM.

SFIT–FSCATM requires two input files. The first, called *Tape7*, is a control file specifying the geometry of the observation, the altitude layering scheme for the output and other required parameters such as the number of trace gases in the input atmosphere. The second input file, called *Tape9*, defines the model atmosphere that is used as input to FSCATM, specifying pressure, temperature and volume mixing ratios (VMRs) for all molecules at a self–consistent set of altitudes. The current distribution of SFIT 1.09e defaults to 41 layers for tape9 and 29 layers for the output of FSCATM, but allows the use of up to 205 input layers and 74 output layers.

In the files distributed[2] with SFIT 1.09e, the program *traceinp* is provided to create the *Tape7* input file from user input and pre–stored or user–specified site and layering information. The program *buildex* is provided to create the *Tape9* input file by combining a file with just the VMR information (known as the *refmod* file) with a file containing pressure and temparature at the same heights where the VMRs are specified[3]. A third program, *fastcon2*, calculates the pressure weighted air masses and reformats the FSCATM output into the three files that are required by SFIT containing air mass factors (*fasmas*), VMR profiles (*fasmix*) and pressure–temperature profiles (*faspt*). A batch or script file is provided to run these programs in the correct sequence[4]. Although the programs *traceinp*, *buildex* and *fastcon2* can be used to prepare

[2]Please note that the executable distributed earlier with SFIT was named *fastcod* rather then *fscatm*.

[3]Please note that this height scheme must start at 0 *km* altitude regardless of the observer's altitude.

[4]The order in which *buildex* and *traceinp* are executed has been reversed. Note also that in the case of SFIT-FSCATM the FSCATM output files *Tape6f* and *Tape8f* are renamed by the raytrace batch to *fastcod.bf* and *Tape7*, respectively. This *Tape7* file is different from the one mentioned earlier.

FSCATM input and reformat FSCATM output, their use is not mandatory. Denver University's *Zephyr2*, for instance, is eaqually suitable and the test cases we compared against *Zephyr2* are consistent with all results presented here. The SFIT suite of programs does however serve as an example of how to carry out these operations.

It is important to note that there are three seperate altitude layering schemes in use. The first is the one used for the input atmosphere supplied to FSCATM in *Tape9*. The second one is stored in binary format inside the executable program and remains normally hidden from the user and which we refer to as the internal layering scheme of FSCATM. And the third one is the requested output layering scheme for SFIT as specified in the initial *Tape7*.

2 Limitations of the old SFIT–FSCATM (1995)

All SFIT–FSCATM releases prior to the parameterized version, v2.01 (July 1999), have a number of limitations which can lead to errors when the user atmosphere is defined with vertical resolutions better than 2 km, as is the case with the 41 layer input data typical in using SFIT 1.09 or SFIT2. The main limitations arise from the internal layering scheme of FSCATM which is used for needed interpolations. It consisted of 47 fixed levels and was constructed using 2 km steps from sea level up to 16 km, 1 km steps from 16 to 30 km, 2 km steps from 30 to 50 km, 5 km steps from 50 to 110 km and two final levels at 120 and 130 km.

If the user provides data at exactly each boundary layer of the internal scheme; i.e. at 0, 2, 4, .. km, FSCATM uses this data and skips the interpolation subroutine which is called only if for any internal boundary layer no exact match is found. Thus, user data provided at 0, 1, 3, 5, .. km only would also lead to reasonable profiles with the old FSCATM 1995 version, because the interpolation routine would be called. However, in the practical case of a user provided input atmosphere defined at the altitudes of 0, 1, 2, 3, 4, 5,..15,16,18, 20,.., 100 km information is found both at each internal boundary layer and at in–between altitudes. Since FSCATM 1995 finds matching pressure, temperature, and VMR data at each of its internal boundary layers 0, 2, 4, 6, 8, 10, 12, 14, and 16 km the interpolation routine is not executed and data provided by the user at the additional altitudes of 1, 3, 5, 7, 9, 11, 13 and 15 km are not considered. Consequently, the physical data provided by the user at odd values of altitudes below 16 km had no effect on the calculations.

3 Changes in FSCATM resulting in Versions 2.01 (June 1999), 2.02 (Aug 2000) and 2.03 (Oct 2001)

It was decided that the new version of FSCATM should be backward compatible and incorporate the minimal number of changes in the source-code. Consequently, a set of additional model layers was added to cover the needs of most applications. The most significant changes implemented since Version 2.01 are:

1) The total number of internal model layers was increased from 47 to 58. The new boundary layers are located at 0, 0.5, 1, 1.5, 2, 2.5, 3, 4, 5, 6, 7, 8, 9, 10, 11, 12, 13, 14, 15 and 16 km altitude, while above they are as in earlier versions of FSCATM. (in the latest version the number was increased to 209, see below.)

2) The number of model layers, internal and external, as well as the number of molecules, are no longer defined in multiple locations throughout the source code. These are now specified once with a FORTRAN PARAMETER statement, hence also the name Parameterized

Air Mass Computer Program for Atmospheric Transmittance/Radiance Calculation (parameterised FSCATM).

3) The maximum number of output layers has been increased to 74.

4) The number of standard molecules has been increased from 57 to 63. The six new molecules added are 58 = OClO, 59 = F134A, 60 = C_3H_8, 61 = F142B, 62 = CFC113, and 63 = F141B. The molecular weights assigned to these molecules are 67.46, 83.033, 44.097, 100.46, 187.359, and 116.95 u, respectively.

5) The molecular weight of H_2S has been corrected from 0.00 to 34.0 u

6) The error handling has been improved. Error messages now include filenames, show the name of the calling routine and give specific hints towards the possible causes.

Changes applied to version 2.02 since the release of version 2.01 include:

7) The accuracy in the final output has been increased. All 4 reported digits are exact, while previously the 4^{th} digit was subject to significant numerical round-off errors. (Technically the intermediate results of the optical path length, the total number of air molecules and the number of each of the individual molecules are stored with 6 rather than 4 significant digits for each layer (*Fastcod1c* output in file *Tape7*)).

8) The fundamental constants used were updated and are now in agreement with the latest CODATA recommendations [14]. However, all values affected changed by substantially less than 0.1 %.

Changes applied to version 2.03 since the release of version 2.02 include:

9) The total number of internal model layers was increased to 209 implementing 0.2km steps from 0 to 30km altitude, 0.5km steps from 30 to 40km, 1.0km steps from 40 to 60km, 2.0km steps from 60 to 80km, 5.0km steps from 80 to 130km, and a final boundary at 99999.0km as in previous versions. The user may provide input data at up to 205 altitudes.

4 Improvements in the SFIT auxiliary programs

This section describes the changes made to the auxiliary programs *buildex, traceinp* and *fastcon2*, which are specific to SFIT applications. *Traceinp* now allows for the optional reading of a user defined external boundary layer definition file. This new feature overrides the built-in defaults at runtime, if desired. This allowed us to reorganise the default boundary layer scheme in a self-consistent manner, while giving the user means to continue to use the old boundary layer scheme (if different) and to meet the emerging needs of profiling tools (see below).

The auxiliary programs now support user-provided REFMOD and matching pressure–temperature files with any number of boundary layers between 30 and 205 (previously fixed to 41 layers). An additional auxiliary program, *refmap*, is provided that allows to map an existing set of *REFMOD* and corresponding pressure–temperature file onto any new boundary layer scheme. It performs a logarithmic interpolation on pressures and VMRs and a linear interpolation on temperature values.[5]

This revision of the programs associated with FSCATM incorporates three more features to improve the program's consistency and computing speed. Altitudes in *Tape9* are now written with 1 meter resolution (previously $1000m$) - this required no changes in FSCATM. The boundary layer selections within *traceinp* have been made self-consistent (see section 4.1) and an

[5]Intended use is for the 'master set' of VMR profiles only. The pressure-temperature profile is expected to be replaced by high-resolution PTU sonde data – otherwise there is little advantage in using a high-resolution input scheme.

improved algorithm was implemented into *traceinp* to determine the first guess for the observed zenith angle (see section 4.2). The latter requires that *buildex* is executed before *traceinp*; i.e. their order is reversed as compared to the 1995 edition. *Traceinp* reads the output from *buildex* to calculate the air number density at the observation altitude and it counts the number of molecules stored in *Tape9*, which allows the use of a flexible number of molecules at runtime.

4.1 Changes in the Layering Schemes

The old default selection of boundary layers in the 29-layers output model atmosphere is given below. (ordered by observation altitude for convenience):

```
0.020,1,2,3,4,5,6,7,8,9,10,   12,   14,   16,18,20,..,100/ NyAlesund
0.370,1,2,3,4,5,6,7,8,9,10,   12,   14,   16,18,20,..,100/ Lauder
0.600,  2,  4,  6,7,8,9,10,11,12,13,14,15,16,18,20,..,100/ Eureka
1.620,      4,5,6,7,8,9,10,11,12,13,14,15,16,18,20,..,100/ Denver
2.090,      4,5,6,7,8,9,10,11,12,13,14,15,16,18,20,..,100/ KittPeak
2.800,      4,5,6,7,8,9,10,11,12,13,14,15,16,18,20,..,100/ SouthPole
3.459,      4,5,6,7,8,9,10,11,12,13,14,15,16,18,20,..,100/ MaunaLoa
3.580,      4,5,6,7,8,9,10,11,12,13,14,15,16,18,20,..,100/ ISSJ
```

And for any unknown site with an observation altitude below or above 1.0 km:

```
0.xxx,  2,  4,  6,7,8,9,10,11,12,13,14,15,16,18,20,..,100/ 'Unknown'
1.xxx,    3,  5,6,7,8,9,10,11,12,13,14,15,16,18,20,..,100/ 'Unknown'
```

This layering scheme could result in different output layering schemes for a single site. For example, selecting Lauder via option '9' rather than option '3' in panel 1 of *traceinp* resulted in different output layering schemes, which caused some confusion in the past.

The new version of *traceinp* resolves this layering problem by using the following default boundary layer schemes:

Observation sites located at altitudes below 0.65 km (e.g. Eureka):

```
0.610,1,2,3,4,5,6,7,8,9,10,   12,   14,   16,18,20,..,100/ Eureka
```

Observation sites located at altitudes between 0.65 km and 1.5 km (e.g. 1.2 km):

```
1.200,  2,3,4,5,6,7,8,9,10,11,12,   14,   16,18,20,..,100/ Unknown
```

Observation sites located at altitudes between 1.5 km and 2.5 km (e.g. Denver):

```
1.620,    3,4,5,6,7,8,9,10,11,12,13,14,   16,18,20,..,100/ Denver
```

Observation sites located at altitudes between 2.5 km and 4.0 km (e.g. Mauna Loa):

```
3.398,      4,5,6,7,8,9,10,11,12,13,14,15,16,18,20,..,100/ MaunaLoa
```

The resulting changes primarily affect Kitt Peak, Denver, and Eureka and all low altitude sites that were not known to the previous release of *traceinp*; i.e. sites that calculated their model atmosphere via 'option 9'. Generally, this scheme gives all unknown stations the most reasonable and consistent profile structure. Please note that the observation altitude for South Pole and Mauna Loa have been corrected. For a complete list of all locations inherently supported and the elevations assigned to them, see Appendix A.1.

Note that the default output layering schemes for the prestored sites in *traceinp* have been chosen as being optimum for use with SFIT1, which is coded to use a 29 layer atmosphere. If using FSCATM with other programs the choice of output layering scheme may be restricted in a different way and the best choice may be different from the default *traceinp* schemes. For example, a VMR profile retrieval algorithm such as SFIT2, in which the VMR in each layer of the retrieved gas or gases can be allowed to vary independently. This means the choice of layering scheme can influence the quality and stability of the retrievals considerably (see section 5.3). Therefore, the user is now given the means to override the default layering schemes if needed.

4.2 The bending functions

At this point we have to destinguish carefully between the **astronomical** solar zenith angle (SZA) and the **apparent** or observed SZA. Calculation of the true optical path requires knowledge of the atmospheric refraction with the latter depending on pressure, temperature and the SZA. If the apparent SZA and hence the refraction is already known, SFIT–FSCATM can perform all its calculations straightforward in one go. If only the astronomical SZA is known, an iteration procedure is required, until a traced ray that uses the actual pressures and temperatures is consistent with the astronomical zenith angle. There are two ways to obtain the correct atmospheric bending for astronomical angles with FSCATM (and others that are not).

If the variable IASTRO (last integer on line 4 of initial *Tape7*) is set to '1', this will cause FSCATM to interpret the SZA as an astronomical one and FSCATM runs an internal iteration. Disadvantages of this otherwise correct operation mode were an instability in previous versions of FSCATM if the SZA should become zero (now fixed). Traditionally, both *traceinp* and the *zephyr2* shell use a different approach: They estimate their own apparent angle, hand this first guess to FSCATM and flag it correctly as an apparent SZA (IASTRO=0). These programs then compare the desired astronomical SZA with the one found in the output of FSCATM and adjust their first guess after each iteration until the desired astronomical SZA agrees within a user-specified accuracy. Only the latest revision level of *traceinp* (v1.13) supports both approaches with the former resulting in some advantages in performance. Please note that the variable IASTRO must at all times be consistent with the type of SZA you are using and that in case of astronomical SZAs either an internal iterative run or multiple external runs with active adaptive

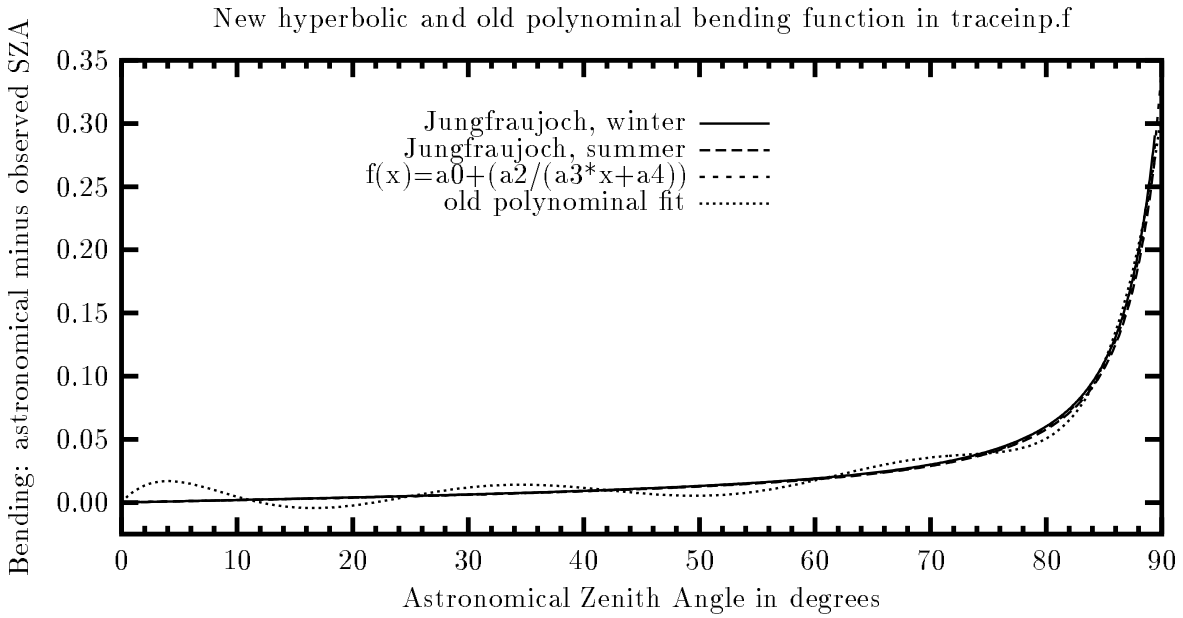

Fig. 1: The refractive bending retrieved iteratively with SFIT–FSCATM is compared against its first estimates as obtained with the old polynominal fit and with the new hyperbolic functions f(x). Even without the small correction term of equation (2), the new functions fit already so well that they can only be distinguished in the residual plot shown in the next figure. The example shown here is for the observation site at the Jungfraujoch, Swiss Alps (46.5°N, 8.0°E, elev. 3580 m).

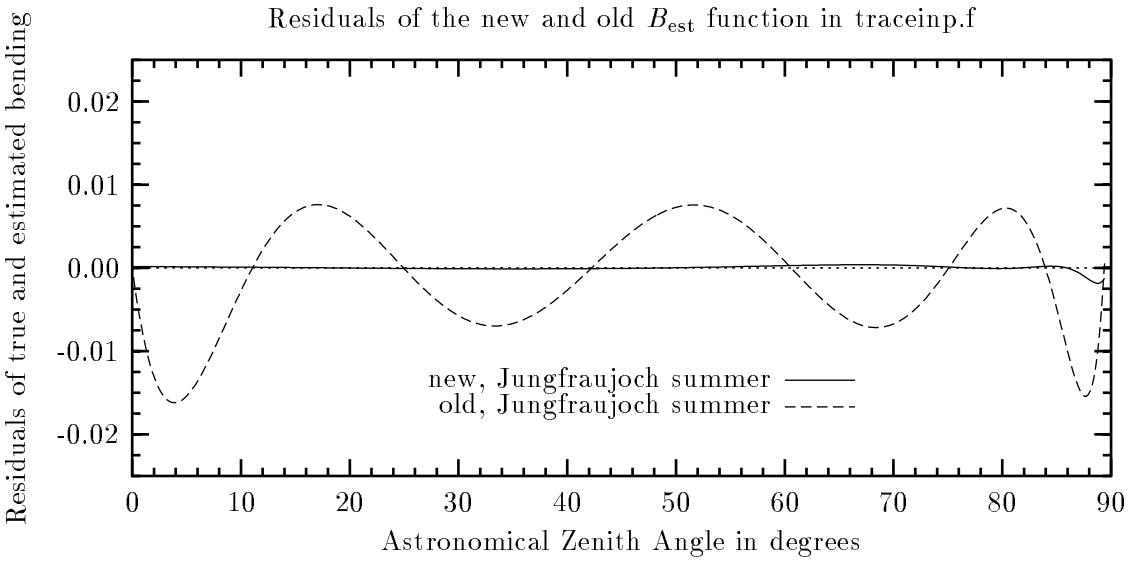

Fig. 2: This figure shows the differences between the curves of the previous figure (initial guess minus final bending vs. astronomical SZA). The estimates obtained with the new functions are much closer to the true bending and result in a faster convergence.

adjustments are mandatory.

In the revision process of SFIT–FSCATM, The function $B_{\rm est}$ in *traceinp* has been improved. This function provides the initial **B**est **est**imate ($B_{\rm est}$) for the refractive bending; i.e. the difference between the astronomical and the apparent or observed zenith angle (Figures 1 and 2). The old first guess was derived from a polynomial fit to a limited number of calculations involving a subset of NDSC sites and did not consider seasonal variability. It was decided to replace the old algorithm with functions that more closely approximate the zenith angle dependencies. These functions are hyperbolic functions of the form a/(b+c*SZA). This results in fewer iterations of SFIT–FSCATM to achieve the same accuracy in the air mass factors for any given astronomical angle. However, a minimum of two runs is always required to calculate any differences in the first place before a decision can be made whether they fullfill the convergence criterium. In most cases 3 to 4 iteration steps will only be required at high to very high zenith angles. As in the previous versions of *traceinp.exe* the convergence criterium monitors the remaining error in the bending, which is to become smaller than 0.0005 before convergence is indicated.

The best estimate for the observed zenith angle $B_{\rm est}$ is the astronomical zenith angle x (in degrees) minus the result of $B_{\rm est}$, which is the estimated bending due to the atmosphere, (the contribution from the correction term 'corr' is small, but improves the quality at very high SZAs significantly):

$$B_{\rm est}(x) = a0 + a1 \cdot x + \frac{a2}{a3 \cdot x + a4} + corr \qquad (1)$$

$$corr = b0 \cdot \left(b1 + e^{b2 \cdot (90 - x)}\right) \cdot cos^2\left(\frac{b3 \cdot x}{\sqrt{b4 - x}}\right)$$

Extensive calculations of observed versus astronomical zenith angles were performed with SFIT–FSCATM v2.02 for different seasons at all 24 observation sites supported resulting in over 30000 geometries considered. The $B_{\rm est}$ functions were then fitted to the resulting data for each

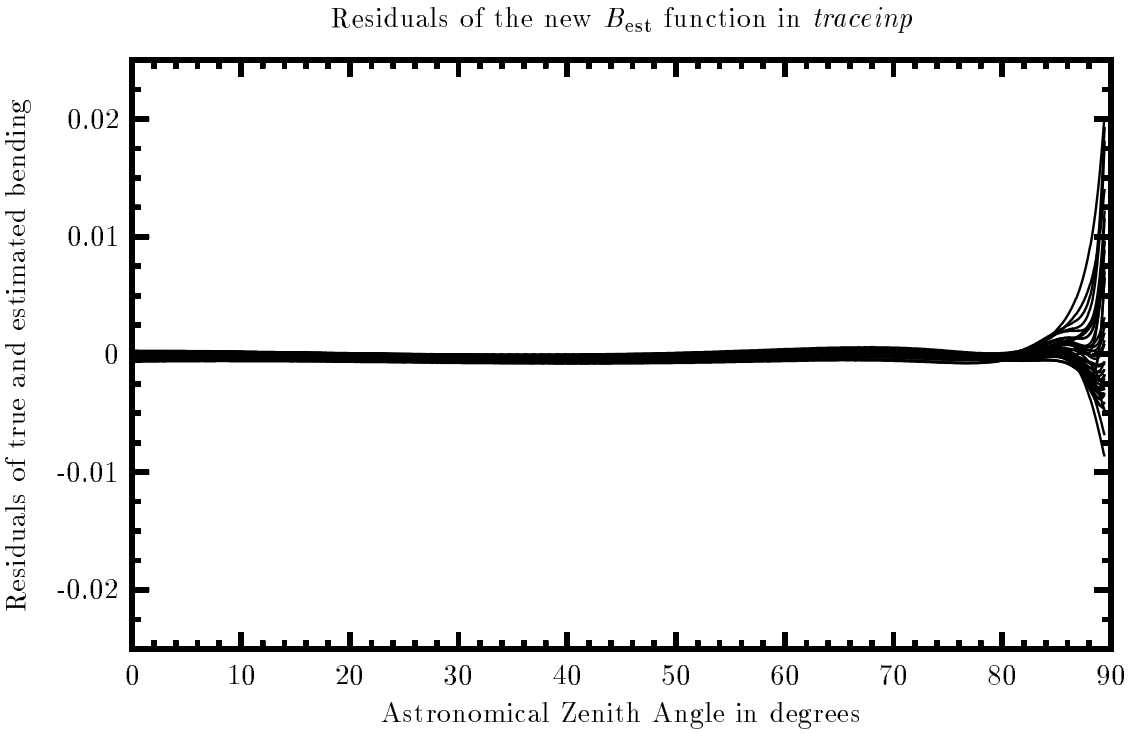

Fig. 3: This figure illustrates the differences between the true atmospheric bending and the estimates calculated from equation (2) with the coefficients from Table 1 for all 24 sites supported. The agreement for the 30768 geometries considered is close to the numerical precision for zenith angles smaller than 85°.

site and season individually. Plotting the resulting coefficients versus the density of air at the observation altitude revealed that all $B_{\rm est}$ functions could be unified into one function depending on astronomical zenith angle and local air density only. Note that $B_{\rm est}$ is not dependent on local pressure or site altitude, but rather on the ratio of local pressure and temperature. The universal coefficients for equation (2) are listed in Table 1. A comparison of the estimated bending to

Table 1: Universial coefficients for calculating atmospheric bending as a function of local air density. The coefficients for equation (1) can be calculated from the air density ϱ (in kg/m^3) at the observer's altitude by the following expressions:

ϱ = pressure/(ambient temperature $\cdot 287\ J \cdot K^{-1} \cdot kg^{-1}$)
a0= 0.06665911$\cdot\varrho^2$ - 0.15464624$\cdot\varrho$ + 0.05387
a1= -6.6704522e-05$\cdot\varrho^2$ + 0.000206288$\cdot\varrho$ - 6.92471e-05
a2= -3.74457759$\cdot\varrho$ + 1.44391
a3= 1.27177688$\cdot\varrho$ + 0.39079
a4= -119.86857346$\cdot\varrho$ -36.70420
b0= 0.36460440$\cdot\varrho^3$ - 1.10194538$\cdot\varrho^2$ + 1.14673294$\cdot\varrho$ - 0.33905
b1= -0.74633976$\cdot\varrho^2$ + 1.44222720$\cdot\varrho$ - 0.42230
b2= -0.07664094 $\cdot\varrho$ - 0.15417
b3= 0.4213820$\cdot\varrho$ + 3.61834
b4= -12.99361791$\cdot\varrho^2$+ 26.21537753$\cdot\varrho$ + 82.07139

the final observation angle is illustrated in Figure 3 for all 30768 geometries. They span SZAa from 0^o to 89.5^o, air densities from 0.81 to 1.38 kg/m^3, site elevations from 20 to 3801 m, and locations between 19.5^o and 89.8^o latitude and conditions from inside and outside the polar vortices. In all calculations the gas constant R is assumed to be 287 J/Kkg. With the given coefficients the approximation in equation (2) may be assumed to be accurate to within 0.0012^o for SZAs up to 85^o, except under exceptional meteorological conditions.

As an example B_{est} is evaluated for the US-Standard atmosphere 1976 at sea level. With pressure 1013.25 hPa, temperature 288.15 K, and gas constant R=287 J/Kkg a local air density of ϱ of 1.2252257 kg/m^3 is obtained. With the coefficients from Table 1 this yields the following best estimate for the atmospheric bending under the specific meteorological conditions chosen:

$$B_{\text{est}} = -0.035544 + 0.0000834 \cdot x + \frac{-3.144043}{1.949007 \cdot x - 183.570255} \qquad (2)$$
$$+0.082351 \cdot \left(0.224366 + e^{-0.248073 \cdot (90-x)}\right) \cdot cos^2\left(\frac{4.134628 \cdot x}{\sqrt{94.685415 - x}}\right)$$

4.3 Summary of changes to *traceinp*, *buildex* and *fastcon2*

1) *Traceinp*, *buildex* and *fastcon2* can now handle up to 70 molecules, while maintaining downward compatibility. At run-time, *Refmod9x*-type input files with up to 70 molecules may be used.

2) The **default** SFIT–FSCATM input and output model atmospheres remain unchanged in their data formats of 41 (*tape9*) and 29 layers (*tape7*), respectively.

3) However, the user may provide input data at up to 205 user-defined altitudes. He or she may also override the default output altitude scheme by passing a boundary layer definition file to *traceinp.exe*. An example is provided in the file '*mysite.bnd*'.

4) True rounding of angles has been incorporated into *fastcon2*. In previous versions, .0001 was added to the angle's value and then the angle was truncated to 2 decimals. Now .005 is added before truncating it.

5) *Buildex* writes the user supplied VMRs (*tape9*) with 4 instead of 3 significant digits and thereby matches the precision used in the output files of FSCATM. Temperatures and pressures are written with 6 and 5 significant digits, respectively, and altitudes with a precision of 1 meter. This change is particularly significant for altitudes, which had been written with only one significant digit previously (1 km resolution). *Buildex* is downward compatible and can read user supplied VMRs in either 3 or 4 digit precision (e.g. *refmod95* and *refmod99* files).

6) *Traceinp* and *buildex* exchange information through the use of message files. These message files allow fully automated batch processing, including the iterative case of astronomical zenith angles. In the latter case *traceinp* actively checks for convergence and creates the file *converge.msg* when the convergence criterion is fulfilled. Alternatively the user may select to have the astronomical SZA case handled by FSCATMs internal iteration procedure.

7) Sixteen new sites have been added to *traceinp*, resulting in a total of 25 pre-stored sites[6]. The new sites are Arrival Heights, Harestua, Kiruna, Table Mountain, Wollongong, Zugspitze (added in July 1999), Moshiri, Rikubetsu, and Tsukuba (added in May

[6]including the '*Unknown site*' which allows the user to create data for any site not defined in the program.

2000), and Billings, Bremen, JPL Pasadena, Mt Bancroft, NPL Teddington, Poker Flat, and Teneriffe (added in June 2000). A complete list of all sites and their locations are given in Appendix A.1, page 37.

8) The *refmod* file was updated, adding some important replacement CFCs, replacing some VMR profiles with newer measurements and scaling all *a–priori* profiles to typical atmospheric loads for 1999. Details are provided in Appendix 3.

9) If a temporary output file already exists, it is overwritten without warning. This caused previous batch jobs to stop with an error.

10) Improved error logging provides the user with more specific information.

11) Comment lines in *refmod95*-type files may now be 80 characters long (previously 72).

12) The observation altitude of the South Pole station was corrected from 2800 m to 2850 m in revision 2.01 and Mauna Loa from 3459 to 3398 m in revision level 2.02.

13) Apart from the aformentioned significant elevation corrections, a number of minor corrections have been applied to observation latitudes, longitudes, and elevations and the polar and equatorial earth radii have been updated in release level 2.02 (for details see Appendix A.1, page 37). Differences resulting from these minor corrections are less than 0.1 % for any number found in the output files of *traceinp* as compared to version 2.01 used in the case studies (section 5).

14) The fundamental constants used were updated and are now in agreement with the latest CODATA recommendations [14].

5 Resulting differences in the output of SFIT–FSCATM and their impacts

As mentioned earlier, FSCATM is used not only with SFIT 1.09 but also with SFIT2 [7, 8, 9, 10] and in other spectroscopic retrieval and radiative transfer models. The changes made to FSCATM itself and the impacts discussed in section 6.1 thus apply to all applications of FSCATM, while the second and third part (sections 5.2 and 5.3) are specific to SFIT applications.

5.1 Part 1: Differences in the output of FSCATM

Two case studies with solar zenith angles of 60^o and 80^o have been carried out for two locations each in order to evaluate the impact of the changes made. This first study investigates the differences in the immediate output of the FSCATM versions 2.01 and 2.02 as compared to the 1995 version. The latest changes of increasing the number of internal model layers from 59 to 209 is discussed seperately at the end of this section.

The first observation site chosen was the Mauna Loa Observatory (19.54^{o}N, 155.58^{o}W, 3459 m amsl). The high elevation of the site and the absence of strong inversion layers make it a location for which the changes in SFIT–FSCATM are expected to have the least effect. Comparisons were made for an apparent solar zenith angle (SZA) of 60^o and an astronomical SZA of 80^o (iterative run), both using the US-Std atmosphere 1976. The tests were accomplished using the new *refmod99* file to provide the a priori VMR profiles and with the refraction calculation performed at 1000 cm^{-1}.

Please note that for this case study we used the old observation altitude of the Mauna Loa observatory throughout (3.46 km). The more accurate recently determined observation altitude is 3398 m. This increases the thickness of the first output layer from 540 to 588 m resulting in

a 10 % increase in the air mass factors and in the number of molecules for that output layer. SFIT–FSCATM *v2.02* as available to end users uses 3398 m for Mauna Loa.

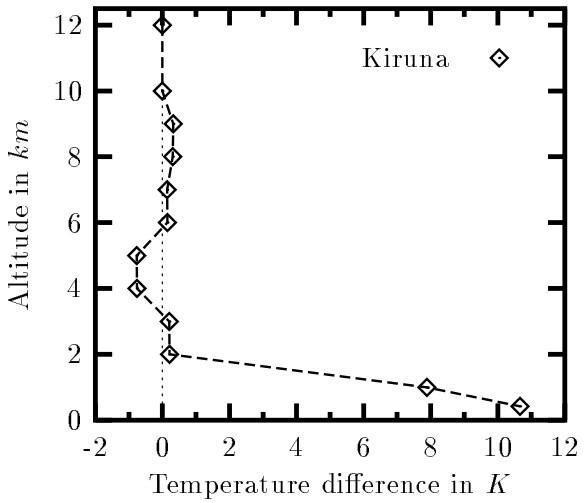

Fig. 4: This figure illustrates the temperature differences between the output of SFIT–FSCATM v2.0x and of the older SFIT–FSCATM release from 1995 as listed in Table 2 for the NDSC site at Kiruna. (There are no differences in the Mauna Loa case.)

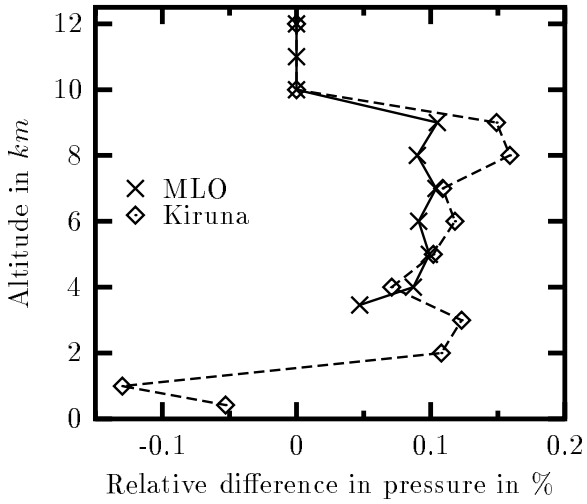

Fig. 5: This figure illustrates the pressure differences between the output of SFIT-FSCATM v2.0x and of the older SFIT–FSCATM release from 1995 as listed in Table 3 for the NDSC sites at Kiruna and at Mauna Loa. Observation altitudes are 419 and 3459 m, respectively.

Kiruna (67.84°, 20.41°E, 419 m amsl) is a low altitude site often subject to strong inversion layers and for this reason was chosen as the second test site. Potential vorticity maps from the ECMWF (European Center for Medium Range Weather Forecast) combined with data from a local PTU sonde (970217.zpt, Figure 8, page 18) indicated that Kiruna was located both inside the polar vortex and under a strong tropospheric inversion layer for the observation day we selected. Comparisons were made for the same SZAs as in the Mauna Loa case, but a customised set of VMR profiles corrected for subsidence was used. The old and new versions of *traceinp* default to different boundary layer schemes for the Kiruna site. In order to obtain a comparison at common boundary layers in the output files, we modified the old version of *traceinp* to default to the new altitude scheme. However, these differences are found of no concern to the following discussion.

A comparison of the results of the old SFIT–FSCATM (1995) distribution to the results from SFIT-FSCATM v2.01 and v2.02 is made for temperature (Table 2 and Figure 4), pressure (Table 3 and Figure 5), and air mass distributions (Table 5 and Figure 6). Temperature differences are listed in Kelvin. All other differences are listed in percent relative to the output from SFIT–FSCATM 1995.

Differences in the calculated air mass distribution factors for the individual output layers are presented in Table 4 and Figure 6. This data shows the differences for the air mass factors for both the slant paths, as well as for the vertical paths. Differences in the total number of molecules are listed in Table 5. In the case of Mauna Loa with the perfectly smooth temperature profile of the US Standard Atmosphere 1976, virtually no differences are observed between the

Table 2: This table compares the temperature profiles in the output of SFIT–FSCATM. The temperature profiles obtained with either of the new FSCATM versions (2.01 or 2.02) are identical and are compared against the ones created with the older SFIT–FSCATM release from 1995 for the NDSC sites Mauna Loa and Kiruna. There are no differences above $12km$ altitude between any of the FSCATM versions.

Mauna Loa US-Std.atmosphere,1976				Kiruna PTU sonde, inversion layer			
Altit. z [km]	Fscatm 1995 T [K]	Fscatm 2.0x T [K]	diff[K]	Altit. z[km]	Fscatm 1995 T [K]	Fscatm 2.0x T [K]	diff[K]
14.00	216.65	216.65	0.00	12.00	208.62	208.62	0.00
13.00	216.65	216.65	0.00	10.00	207.37	207.37	0.00
12.00	216.65	216.65	0.00	9.00	209.76	210.08	0.32
11.00	218.34	218.34	0.00	8.00	218.11	218.42	0.31
10.00	221.64	221.64	0.00	7.00	225.60	225.74	0.14
9.00	226.54	226.54	0.00	6.00	232.23	232.38	0.15
8.00	233.02	233.02	0.00	5.00	238.51	237.74	-0.77
7.00	239.50	239.51	+0.01	4.00	244.43	243.67	-0.76
6.00	245.99	245.99	0.00	3.00	251.46	251.66	0.20
5.00	252.48	252.48	0.00	2.00	259.61	259.82	0.21
4.00	258.97	258.97	0.00	1.00	257.18	265.07	7.89
3.46	263.93	263.93	0.00	.42	247.51	258.17	10.66

Table 3: This table compares the pressure profiles in the output of SFIT–FSCATM v2.02 against the profiles created with the older SFIT–FSCATM release from 1995 for the NDSC sites Mauna Loa and Kiruna. There are no differences above 12 km altitude between any of the SFIT–FSCATM versions.

Mauna Loa, US-Std.atmosphere,1976				Kiruna, PTU sonde 970217			
Altit. z[km]	Fscatm1995 p [hPa]	Fscatmv2.0x p [hPa]	rel. diff[%]	Altit. z [km]	Fscatm1995 p [hPa]	Fscatmv2.0x p[hPa]	rel. diff[%]
14.00	1.314E+02	1.314E+02	0.00	12.00	1.521E+02	1.521E+02	0.00
13.00	1.537E+02	1.537E+02	0.00	10.00	2.118E+02	2.118E+02	0.00
12.00	1.799E+02	1.799E+02	0.00	9.00	2.678E+02	2.682E+02	0.15
11.00	2.103E+02	2.103E+02	0.00	8.00	3.141E+02	3.146E+02	0.16
10.00	2.458E+02	2.458E+02	0.00	7.00	3.665E+02	3.669E+02	0.11
9.00	2.861E+02	2.864E+02	0.10	6.00	4.254E+02	4.259E+02	0.12
8.00	3.318E+02	3.321E+02	0.09	5.00	4.920E+02	4.925E+02	0.10
7.00	3.833E+02	3.837E+02	0.10	4.00	5.671E+02	5.675E+02	0.07
6.00	4.411E+02	4.415E+02	0.09	3.00	6.506E+02	6.514E+02	0.12
5.00	5.057E+02	5.062E+02	0.10	2.00	7.437E+02	7.445E+02	0.11
4.00	5.779E+02	5.784E+02	0.09	1.00	8.490E+02	8.479E+02	-0.13
3.46	6.385E+02	6.388E+02	0.05	.42	9.390E+02	9.385E+02	-0.05

Table 4: This table compares the air mass factors in the *fasmas* output files of SFIT–FSCATM v2.01 and SFIT–FSCATM v2.02 against the ones obtained with SFIT–FSCATM 1995 for the NDSC sites Mauna Loa and Kiruna for zenith geometry, for an apparent solar zenith angle (SZA) of 60^o, and for an astronomical SZA of 80^o each. Differences are within 0.2 %.

Mauna Loa, US-Std.atmosphere,1976					Kiruna, PTU sonde 970217, inversion layer				
Altit.	Fsc1995	Fsc2.01	Fscatm2.02		Altit.	Fsc1995	Fsc2.01	Fscatm2.02	
$[km]$	$[hPa \cdot m]$	$[hPa \cdot m]$	$[hPa \cdot m]$	Δ [%]	$[km]$	$[hPa \cdot m]$	$[hPa \cdot m]$	$[hPa \cdot m]$	Δ [%]
SZA	0^o	0^o	0^o		SZA	0^o	0^o	0^o	
14.00	129.4	129.4	129.4	0.000	12.00	297.5	297.5	297.5	0.000
13.00	151.4	151.4	151.4	0.000	10.00	413.8	413.8	413.9	0.024
12.00	177.1	177.1	177.1	0.000	9.00	263.8	264.3	264.2	0.152
11.00	207.1	207.1	207.1	0.000	8.00	309.6	310.0	309.9	0.097
10.00	242.1	242.1	242.1	0.000	7.00	361.1	361.3	361.4	0.083
9.00	281.8	282.1	282.1	0.106	6.00	419.2	419.4	419.6	0.095
8.00	326.9	327.3	327.2	0.092	5.00	484.8	485.1	485.2	0.083
7.00	377.8	378.1	378.0	0.053	4.00	558.7	559.3	559.2	0.089
6.00	434.6	434.9	435.0	0.092	3.00	641.2	642.1	642.0	0.125
5.00	498.4	498.7	498.8	0.080	2.00	733.1	733.7	733.7	0.082
4.00	569.4	570.1	570.0	0.105	1.00	835.9	835.5	835.6	-0.036
3.46	340.7	340.8	340.8	0.029	.42	537.8	537.4	537.5	-0.056
SZA	60^o	60^o	60^o		SZA	60^o	60^o	60^o	
14.00	257.6	257.6	257.6	0.000	12.00	592.0	592.0	591.9	-0.017
13.00	301.6	301.6	301.5	-0.033	10.00	824.3	824.3	824.2	-0.012
12.00	353.0	353.0	352.9	-0.028	9.00	525.8	526.6	526.6	0.152
11.00	412.8	412.8	412.9	0.024	8.00	616.8	618.0	617.8	0.162
10.00	482.8	482.8	482.7	-0.021	7.00	720.0	720.8	720.9	0.125
9.00	562.3	562.9	562.8	0.089	6.00	836.1	837.3	837.2	0.132
8.00	652.3	652.9	653.1	0.123	5.00	967.6	968.3	968.5	0.093
7.00	754.0	754.6	754.8	0.106	4.00	1116.0	1117.0	1117.0	0.090
6.00	868.2	868.9	868.9	0.081	3.00	1281.0	1282.0	1282.0	0.078
5.00	996.0	996.7	996.8	0.080	2.00	1465.0	1466.0	1466.0	0.068
4.00	1138.0	1139.0	1140.0	0.176	1.00	1671.0	1671.0	1671.0	0.000
3.46	681.3	681.3	681.4	0.015	.42	1076.0	1074.0	1075.0	-0.093
SZA	80^o	80^o	80^o		SZA	80^o	80^o	80^o	
14.00	706.2	706.2	706.2	-0.014	12.00	1612.0	1612.0	1612.0	0.000
13.00	829.6	829.6	829.6	0.012	10.00	2262.0	2262.0	2262.0	0.000
12.00	975.1	975.1	975.1	-0.010	9.00	1450.0	1453.0	1453.0	0.207
11.00	1145.0	1145.0	1145.0	0.000	8.00	1708.0	1711.0	1711.0	0.176
10.00	1344.0	1344.0	1344.0	0.000	7.00	2002.0	2004.0	2004.0	0.100
9.00	1571.0	1573.0	1573.0	0.127	6.00	2333.0	2336.0	2336.0	0.129
8.00	1831.0	1832.0	1832.0	0.109	5.00	2710.0	2713.0	2713.0	0.111
7.00	2124.0	2126.0	2126.0	0.094	4.00	3137.0	3139.0	3139.0	0.064
6.00	2455.0	2458.0	2458.0	0.122	3.00	3614.0	3620.0	3619.0	0.138
5.00	2828.0	2830.0	2830.0	0.071	2.00	4148.0	4155.0	4154.0	0.145
4.00	3246.0	3248.0	3248.0	0.062	1.00	4751.0	4752.0	4750.0	-0.021
3.46	1948.0	1949.0	1949.0	0.051	.42	3065.0	3064.0	3064.0	-0.033

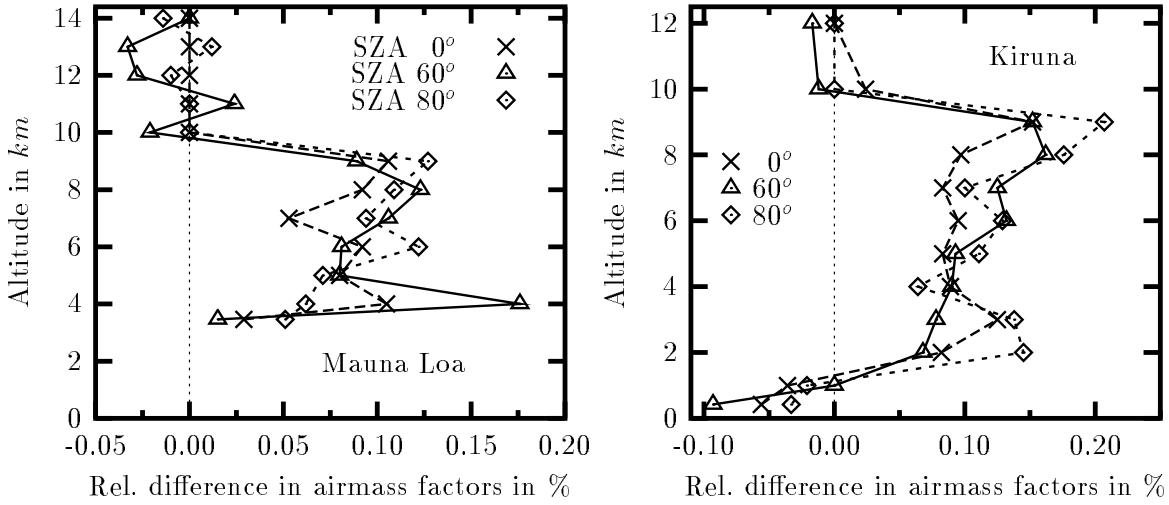

Fig. 6: The **left panel** shows the relative differences in the pressure weighted air masses for zenith angles of 60^o and 80^o (Table 4a). "SZA 0" indicates the air masses for zenith path required to calculate the vertical columns from the slanted columns and are identical for either zenith angle of 60^o and 80^o. The changes in the air masses calculated with SFIT–FSCATM v2.02 are shown relative to the output of the older SFIT–FSCATM release from 1995 for the NDSC site at Mauna Loa. **Right panel:** Same quantities but for the NDSC site at Kiruna. At either site there are no significant differences above 14 km altitude.

new and old SFIT–FSCATM versions in terms of temperature and all other paramters show only very small differences close to the numerical precision.

However, if temperature values at 1, 3, 5, 7, 9 and 11 km altitude differ significantly from the assumed smooth profile based on the temperatures at altitudes 0, 2, 4, 6, 8, 10, and 12 km, as is the case in the Kiruna example, the problems in the 1995 version of SFIT–FSCATM are revealed. Temperature misrepresentations exceeding 10 Kelvin are observed in the inversion layer. It is noted that the improvements to the internal layering scheme of SFIT–FSCATM v2.0x allow the detail in the input profiles to be carried through correctly in the calculation (compare Figures 8 and 9).

There were no differences between the air masses calculated with SFIT–FSCATM versions v2.01 and 1995 for altitudes above 12 km for either site in agreement with our understanding that there was no conflict between the input and the internal layering scheme above this height, in either the old or new calculations. However, the latest SFIT–FSCATM version shows differences of up to ± 2 in the last of its 4 significant digits throughout all altitudes, which is the result of reduced round–off errors as described in section 4.

On the whole, differences exceeding 0.5 % are only seen in the Kiruna case and are restricted to altitudes below 4 km and occur only in temperature and in the total number of molecules.

When the results described above and in the following section 5.2 were presented at the Infrared Working Group Meeting of the NDSC in Bordeaux in Sep 2001, the FTIR community expressed interest in the effects the changes may have on VMR profile retrieval, not just TCAs, and what influence the choice of altitude scheme may have. Moreover, discussion at the NDSC 2001 Symposium with one of the original authors of FSCATM (S.A. Clough) revealed shortcomings in the design of our version of FSCATM that may lead to small errors due to non-thermal equilibrium effects and achromatic behaviour that ideally would require individual

Table 5: *The total number of molecules per output layer are compared for zenith geometry. The data is taken from the same fasmas files as discussed in Table 4a (bottom section of the file "Scancode 999"). Differences are presented as SFIT–FSCATM v2.0x relative to SFIT–FSCATM 1995. There are no differences between the outputs of versions 2.01 and 2.02.*

Mauna Loa, US-Std.atmosphere,1976				Kiruna, PTU sonde 970217, inversion layer			
Altit.	Fscatm1995	Fscatm2.0x		Altit.	Fscatm1995	Fscatm2.0x	
[km]	[molec.]	[molec.]	Δ [%]	[km]	[molec.]	[molec.]	Δ [%]
14.00	.4384E+24	.4384E+24	0.000	12.00	.1047E+25	.1047E+25	0.000
13.00	.5129E+24	.5129E+24	0.000	10.00	.1465E+25	.1465E+25	0.000
12.00	.6002E+24	.6002E+24	0.000	9.00	.9233E+24	.9234E+24	0.011
11.00	.6964E+24	.6964E+24	0.000	8.00	.1042E+25	.1042E+25	0.000
10.00	.8018E+24	.8018E+24	0.000	7.00	.1175E+25	.1175E+25	0.000
9.00	.9133E+24	.9142E+24	0.099	6.00	.1325E+25	.1325E+25	0.000
8.00	.1030E+25	.1031E+25	0.097	5.00	.1492E+25	.1498E+25	0.402
7.00	.1158E+25	.1159E+25	0.086	4.00	.1678E+25	.1685E+25	0.417
6.00	.1297E+25	.1298E+25	0.077	3.00	.1872E+25	.1873E+25	0.053
5.00	.1449E+25	.1450E+25	0.069	2.00	.2073E+25	.2073E+25	0.000
4.00	.1614E+25	.1616E+25	0.124	1.00	.2386E+25	.2314E+25	-3.018
3.46	.9476E+24	.9480E+24	0.042	.42	.1595E+25	.1528E+25	-4.201

air mass files for each molecule. Individual air mass files for each molecule would require a fundamental redesign of the code and would make housekeeping much more complicated. However, the improvement achievable is indeed very small and it was concluded that simply using a small enough altitude stepsize (200m) would reduce any interpolation errors to within the numerical precision, hence avoiding the need for a fundamental redesign.

A conservatively small stepsize to minimise all interpolation errors to within the numerical precision envisaged (4 significant digits) was implemented in FSCATM Version 2.03 by raising the nuber of internal layers from 59 to 209, as described in the previous section. Again we chose real–world data, this time from the Wollongong site, located 30 m above sea level on the Australian Pacific coast (34.46°S, 150.88°E). The study of this data is further deepened in section 5.3 where the effects on the retrieval of VMR profiles are studied. At the Wollongong site inversion layers are normally absent and local PTU sondes are available daily from the Sydney Kingsford–Smith airport.

The observation day chosen is the 9^{th} Oct, 1999. The local PTU sonde reached a ceiling altitude of 29km and data was spline fitted into NCEP observations above 29km to provide pressure and temperature profiles to FSCATM. The PTU sonde temperature profile is shown in Figure 7a.

With this input data we created 4 sets of model atmospheres for later use in the analysis of solar FTIR spectra with SFIT2 (section 5.3). Set-1, referred to as 41/59/S, provides data to FSCATM at the 41 default altitudes, it uses FSCATM Version 2.02 with 59 internal layers, and selects the Standard altitude scheme for the 29 output layers. Set-2, referred to as 41/209/S, uses FSCATM Version 2.03 with its 209 internal layers and all other selections identical to Set-1. Set-3, referred to as 205/209/S, provides data to FSCATM V2.03 at 205 altitudes matching the internal grid up to 100km. Set-4, referred to as 205/209/E, is identical to Set-3 except that the output altitude scheme uses an Equidistant stepsize of 1.5km from ground to 33km altitude (and larger steps above).

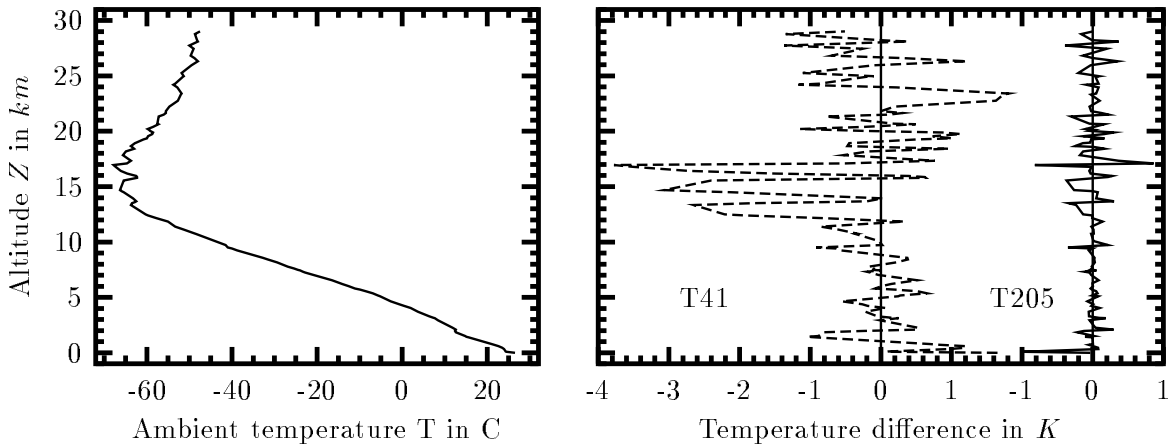

Fig. 7: This figure shows the temperature profile from the Sydney PTU sonde *99100915.syd* (left panel). Interpolation errors are introduced if simple routines are used to map the sonde data onto the 41 standard altitudes (T41) normally handed to FSCATM. These errors are reduced significantly if the data is sampled at a much higher frequency (T205) as has become possible with the latest version of FSCATM (right panel).

The differences caused by pushing the number of internal layers from 59 to 209 alone has only a very marginal effect on the output. Comparing the output from Set-1 and Set-2 shows agreement of better than 0.01% for all air masses and pressures below 50km and better than 0.1% above 50km. Temperatures agree within 0.01K below 60km.

However, interpolation errors, in particular in the temperature profile, are significantly reduced if the PTU sonde is sampled with much higher resolution (Set-3). The interpolation errors in the input temperatures introduced by the simple PTU sonde data conversion program used (*ptwconv* from [[15]]) are illustrated in Figure 7b. These errors are the responsibility of the user, not the FSCATM code, and are expected to be smaller if only smoothed pT profiles (e.g. NCEP data) or more sophisticated PTU-sonde conversion programs are employed, which smooth or integrate the sounding data. Hence, from a practical point of view, the higher number of internal model layers in FSCATM offer an advantage where high resolution input data is available – by shifting the problem of proper integration of geophysical parameters from the user to FSCATM.

However, the VMR profiles indicate that there might be more merit in the four times higher number of internal model layers. The VMR profile of nitrogen handed to FSCATM is assumed constant at a concentration of 78.1%. Hence, we expect the output VMR profile to be the same. This is true to the last digit if 209 model layers are used, but deviations of up to 1.04% are seen if FSCATM V2.02 with only 59 layers is used. The price in CPU time for running the 209 layer version is small and and more than outweighted by the higher precision achieved in the VMRs.

5.2 Part 2: Effects on the total column amounts retrieved with SFIT 1.09e

This case study was not prepared with the latest version of SFIT–FSCATM, but with the version 2.01 as of 20 July, 1999. However, as discussed in sections 4 and 5.1, the differences between these two versions are so marginal that they do not result in any significant differences in any of the results presented here.

This second case study investigates the impacts of the changes in SFIT–FSCATM on the TCAs retrieved with SFIT 1.09e from spectra recorded at Kiruna. The two observation days were selected because of the near perfect observing conditions. The first day chosen exhibits no inversion layer, while the second day exhibits a very strong inversion layer. These case studies show that in the absence of an inversion layer, the TCAs retrieved change by less than 0.2 % for any stratospheric species and less than 0.7 % for most tropospheric species. The only exception is water vapour with a change of 2.5 %. The diffeences are even smaller if some of the more temperature sensitive lines are avoided (see below). In the case of an inversion layer the effects are much stronger, resulting in changes in the retrieved TCAs as high as 20 % for ammonia and up to 35 % for the extreme case of a water vapour line with a very high lower state energy. The unmodified results of SFIT–FSCATM 1995 and of SFIT–FSCATM v2.01 were used in these calculations, i.e. the boundary layer schemes are different for the SFIT–FSCATM 1995 run as compared to the SFIT–FSCATM 2.01 run as described in the section on layering schemes (section 4.3). However, this minor difference is found to be of little concern to the subsequent comparison as has been shown in retrieval and algorithm intercomparisons of the NDSC (e.g. [16]).

A total of 125 different absorption lines are included in this study. The selection of these absorption lines is based on [17]. A detailed illustration of all interfering species for each absorption line studied is found in that reference work. The spectroscopic database used is HITRAN96 [18] with CFC–12 and HCFC–22 added from [19], which are based on the cross-sections by P. Varanasi [20, 21, 22]. The analysis script follows a strict order starting with absorption lines completely free of significant interferences from other lines. The *a priori* VMR profiles are rescaled after every microwindow to represent the best known TCAs. By the time microwindows with significant interferences from other lines are encountered in the script and where seperation may become difficult, most interfering molecules can be held constant, because the *a prioris* are already known to represent reasonable amounts.

The first observation day chosen was the 24^{th} June, 1998 (980624). This was a clear, 'warm' summer day with basically no diurnal changes (polar day). 34 solar spectra split over 6 optical filter regions covering the 650 to 4300 cm^{-1} spectral region were recorded with solar zenith angles ranging from 44.47^{o} to 58.36^{o}. In these spectra a total of 773 microwindows were analysed with SFIT 1.09e twice: once running SFIT with the output from the old SFIT–FSCATM 1995 for all microwindows and a second time using the output from SFIT–FSCATM v2.02 under otherwise identical conditions (including identical input files for the two versions of SFIT-FSCATM). The TCAs retrieved from both SFIT runs were then compared. Any subjectivity in the analysis was removed by using the same fully automated SFIT-Tools V2.13u script for both analyses [15].

The exercise was repeated for spectra recorded on the 17^{th} February, 1997 (970217), comprising a total of 781 microwindows. This day has one of the most extreme inversion layers that occurred on an otherwise perfect observation day. The temperature step from ground to 1000 m altitude was roughly 25 K. All solar zenith angles of the 36 spectra recorded on this Arctic late winter day are very large (all $>79.9^{o}$) though almost constant throughout the day.

Figure 8 illustrates the temperature profiles for the two observation days as recorded by a local PTU sonde. Figures 9a and 8b present the output temperature profiles of SFIT–FSCATM 1995 as compared to SFIT–FSCATM v2.01 for days 980624 and 970217, respectively. Significant differences are seen on both days but are more pronounced in the presence of an inversion layer.

Figure 10 shows the relative differences in the total air mass factors as a function of the astronomical zenith angle for the two observation days (which also illustrates the distribution of zenith angles encountered). The total air mass factor here is the one listed in the FSCATM output file *Tape6f (=fastcod.bf)*. It is defined as the air mass relative to a vertical path from ground to space and is the same one displayed by *traceinp* after convergence is achieved in an

iterative run. As can be seen readily from the plot, there are no differences in the air mass factors on day 980624 when air mass factors between 1.4 and 1.9 occurred, while on day 970217 differences of up to 0.5 % are observed with air mass factors ranging from 5.4 to 19.3. In either case these differences are insufficient to explain the differences in the TCAs discussed below.

Figures 11 and 12 present the effects of using the different SFIT–FSCATM versions with SFIT 1.09e in the retrieval of daily mean TCAs for days 980624 and 970217, respectively. For each spectrum and each absorption line studied the following differences (D_i) in TCAs were calculated individually for each fit:

$$D_i = \frac{\mathrm{TCA}[fscatm\_v2.01] - \mathrm{TCA}[fscatm1995]}{TCA[fscatm1995]} \cdot 100 \qquad (3)$$

The mean D over these differences D_i was calculated a) for each absorption line (Table 6a) and b) for each trace gas (Figures 11 and 12 for observation days 980624 and 970217, respectively). The latter case thus represents the mean over typically several absorption lines commonly used. Figures 11 to 13 are a graphical interpretation of the numbers listed in Table 6b. The actual TCAs from which the differences discussed here were calculated are found in Tables A.2.1 and A.2.2 of Appendix A.2 together with a number of additional parameters. For each of these mean values 'D' the corresponding 1-σ uncertainty was calculated and a t–test was performed to decide which of the observed changes are significant within our uncertainties. If for a given absorption line the mean difference over N spectra is D, with the individual differences

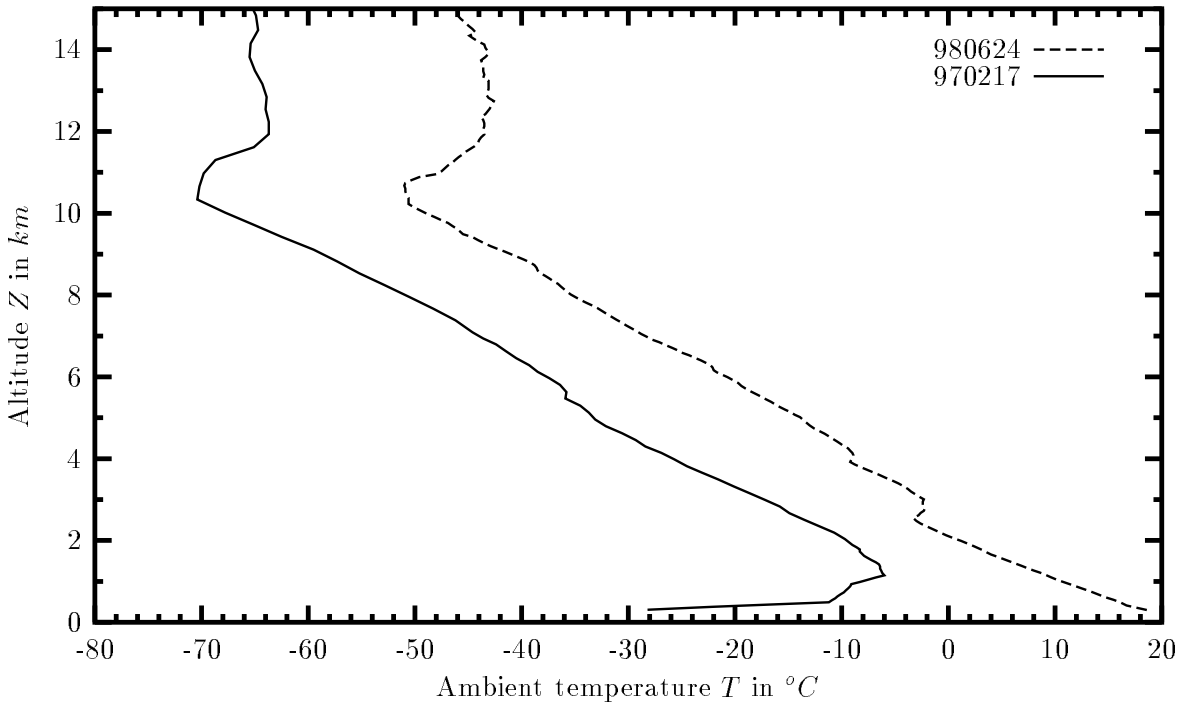

Fig. 8: This figure shows the temperature profile from ground to 15 km altitude as recorded by a local PTU sonde for the observation days selected for case study 2. The temperature profile on day 970217 (solid line) shows a strong inversion layer with a step of 25 K near ground.

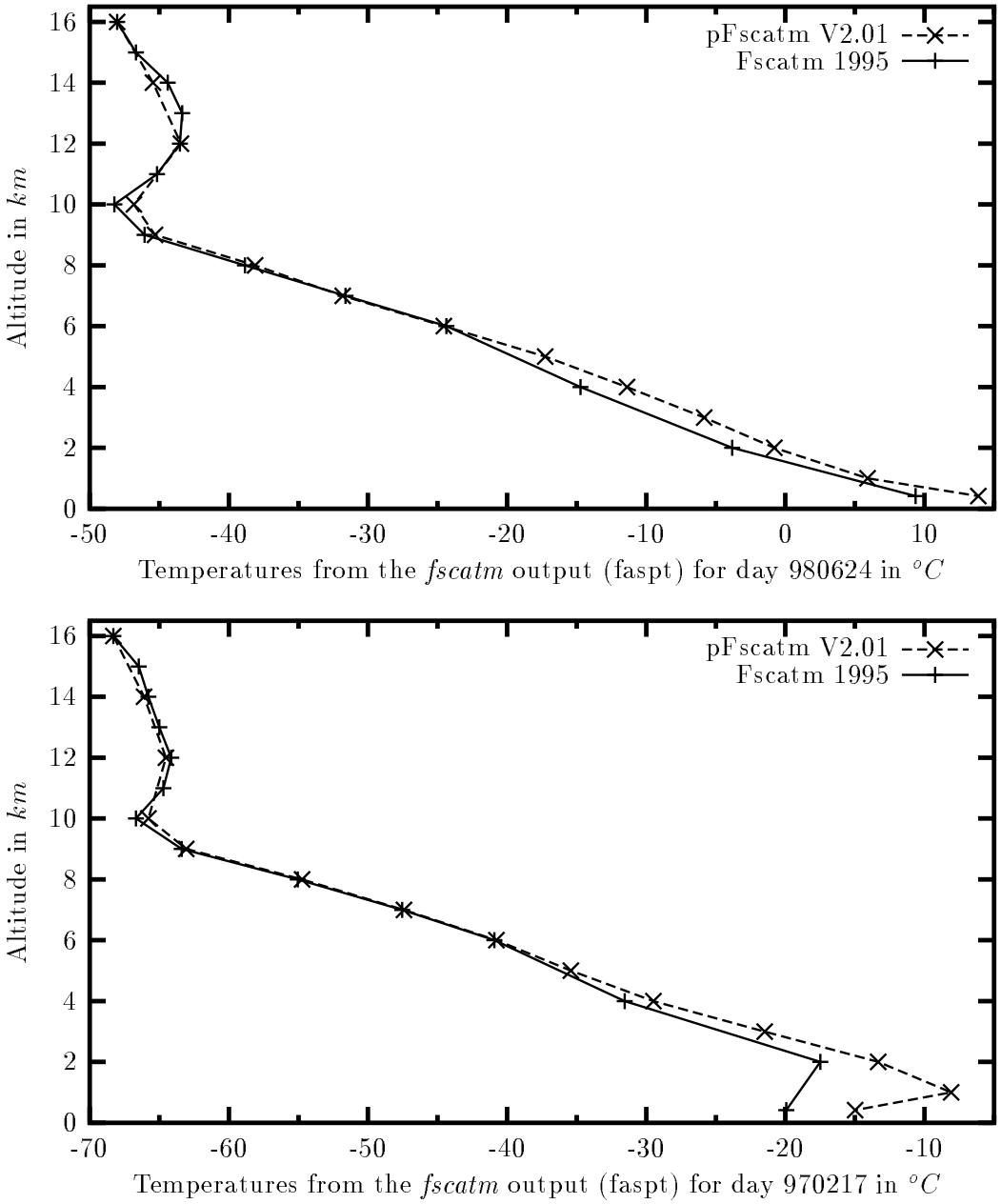

Fig. 9: These plots compare the output of SFIT-FSCATM 1995 and SFIT-FSCATM v2.01 for an identical input temperature profile based on the PTU sonde profiles shown in the previous figure. The upper panel shows the temperature profile for day 980624 (no inversion layer) while the lower panel shows day 970217. SFIT-FSCATM 1995 fails to capture the inversion layer on day 970217 and temperatures from ground to 2 km altitude are about 9 K lower than in the output of SFIT-FSCATM v2.01. Please note that here we used the original *traceinp* layering schemes resulting in 2 km steps near ground for the 1995 version as opposed to table 2, page 12, where we forced the old *traceinp* to use the same layering scheme as the new SFIT–FSCATM V2.0x releases. Note also that the temperatures here are effective temperatures representing the air mass weighted mean temperature for individual model layers of one or two km thickness.

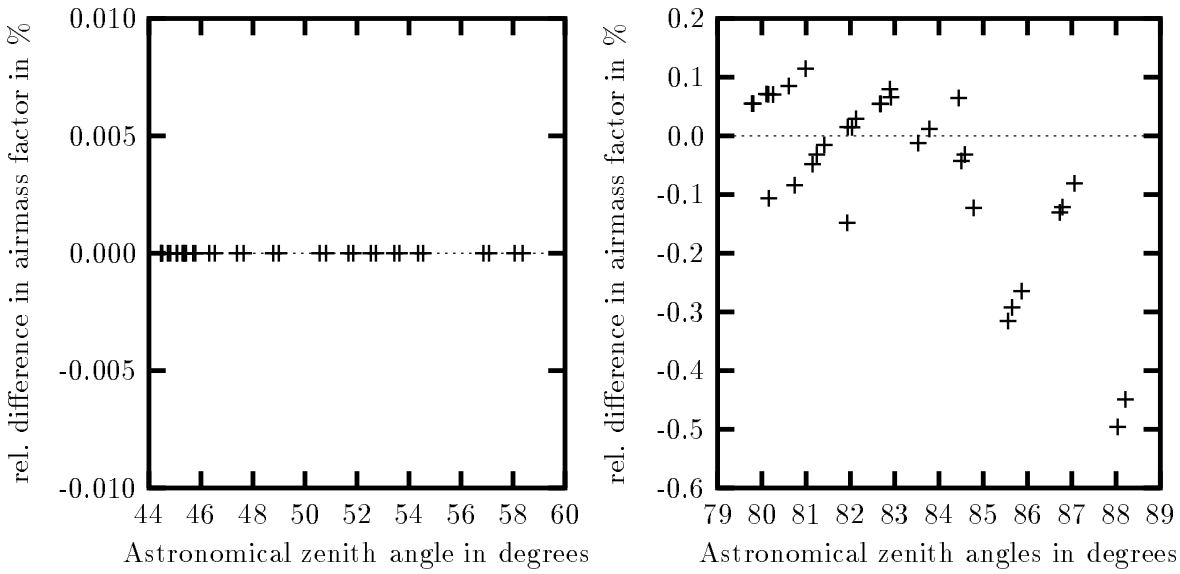

Fig. 10: This plot checks for differences in the total air mass factors between the two versions of SFIT–FSCATM. The left panel indicates that there are no differences for any of the 34 spectra recorded on day 980624. On day 970217 (right panel) small differences in the air mass factors are observed.

D_i scattered around D with a standard deviation of Sd, then the t–test is

$$t = D \cdot \frac{\sqrt{N}}{Sd}. \quad \text{with} \quad D = \frac{1}{N} \sum_{i=1}^{N} D_i \tag{4}$$

The differences 'D' are significant if the result of the t-test is larger than 1.95. Whenever the t–test indicated a significant difference in the total columns retrieved, this is marked with a diamond shaped symbol in Figures 11 and 12.

The results for the individual microwindows and the daily means are tabulated in Appendix A.2 of this document. The effects on the residuals are also listed. The initial choice of VMR a-priori profiles was the 'Reftoon' set (Appendix A.3) which had been corrected for subsidence based on potantial vorticity analysis data from the ECMWF. Once this choice was made, the VMR profiles could only be scaled as a unit for each molecule, because SFIT 1.09 does not allow for profile retrieval. It is shown in the next section that VMR profile retrieval with more advanced algorithms such as SFIT2 are also affected by the changes in SFIT–FSCATM.

On day 980624 with its fairly smooth temperature profile the effects of the changes in SFIT–FSCATM on the TCAs retrieved with SFIT 1.09e are typically small, though significant for CH_3D, CH_4, CHF_2Cl, CO_2, H_2O, HDO, NO_2, and O_3. However, except for water, the total columns change by less than 0.7 % for any species. Compared to other uncertainties in the retrieval of TCAs which add to typically several percent, a re-processing of spectra analysed with SFIT–FSCATM 1995 does not appear necessary nor rewarding in relation to the expected small reduction in uncertainties. However, one should keep in mind that a few temperature sensitive absorption lines (Table 6) can be identified that exceed 1 % change in TCAs.

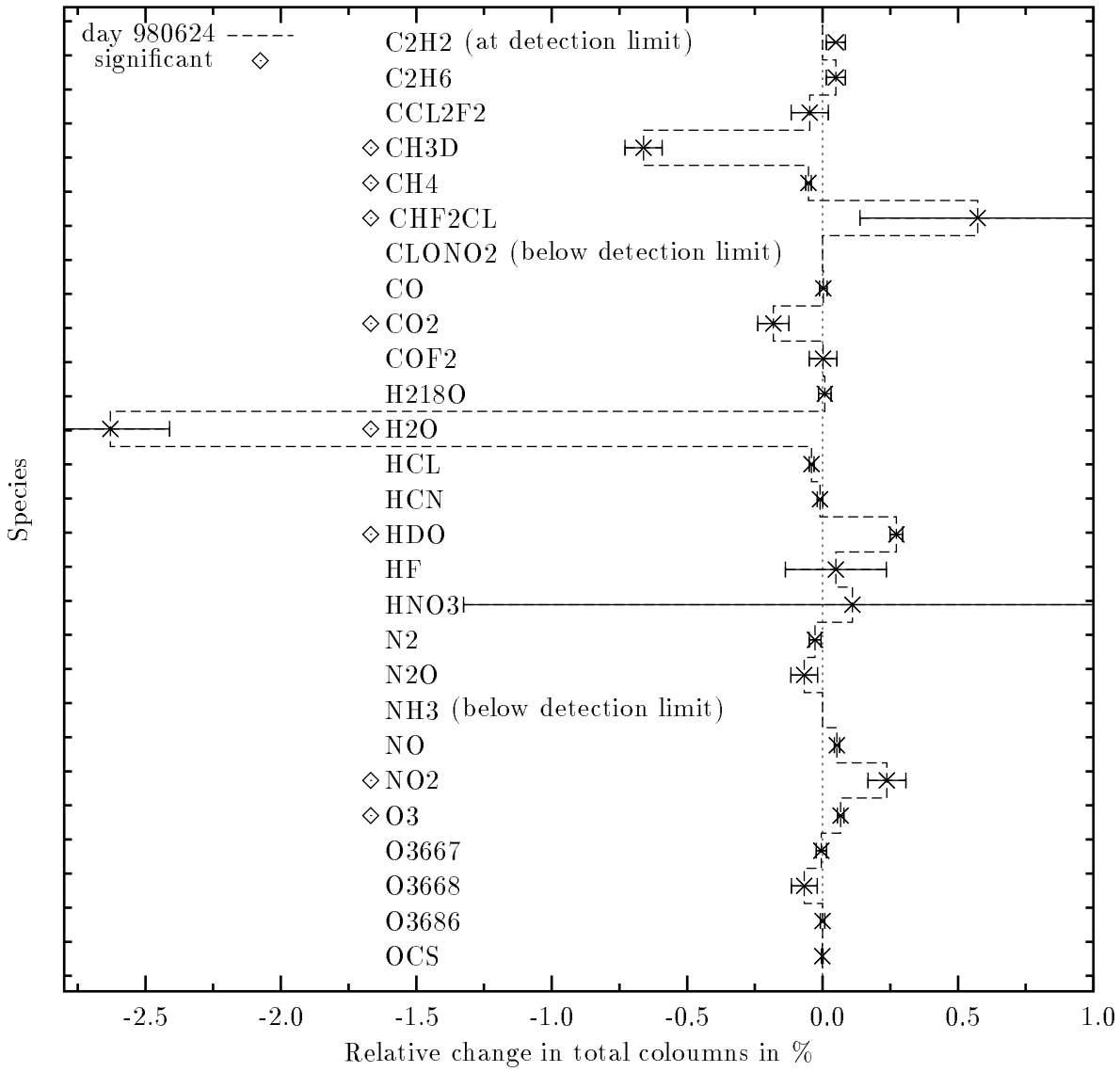

Fig. 11: This figure illustrates the effects of the changes in SFIT–FSCATM on the total columns retrieved with SFIT 1.09e. The changes in the TCAs are shown using SFIT-FSCATM v2.01 as compared to the older SFIT-FSCATM 1995 version. The spectra analysed were recorded at Kiruna on the 24 June, 1998. The temperature profile reported from a local PTU sonde indicates a typical arctic summer day with no inversion layer (compare Fig. 9). The t-test indicates that only few gases show a significant difference (indicated by diamonds).

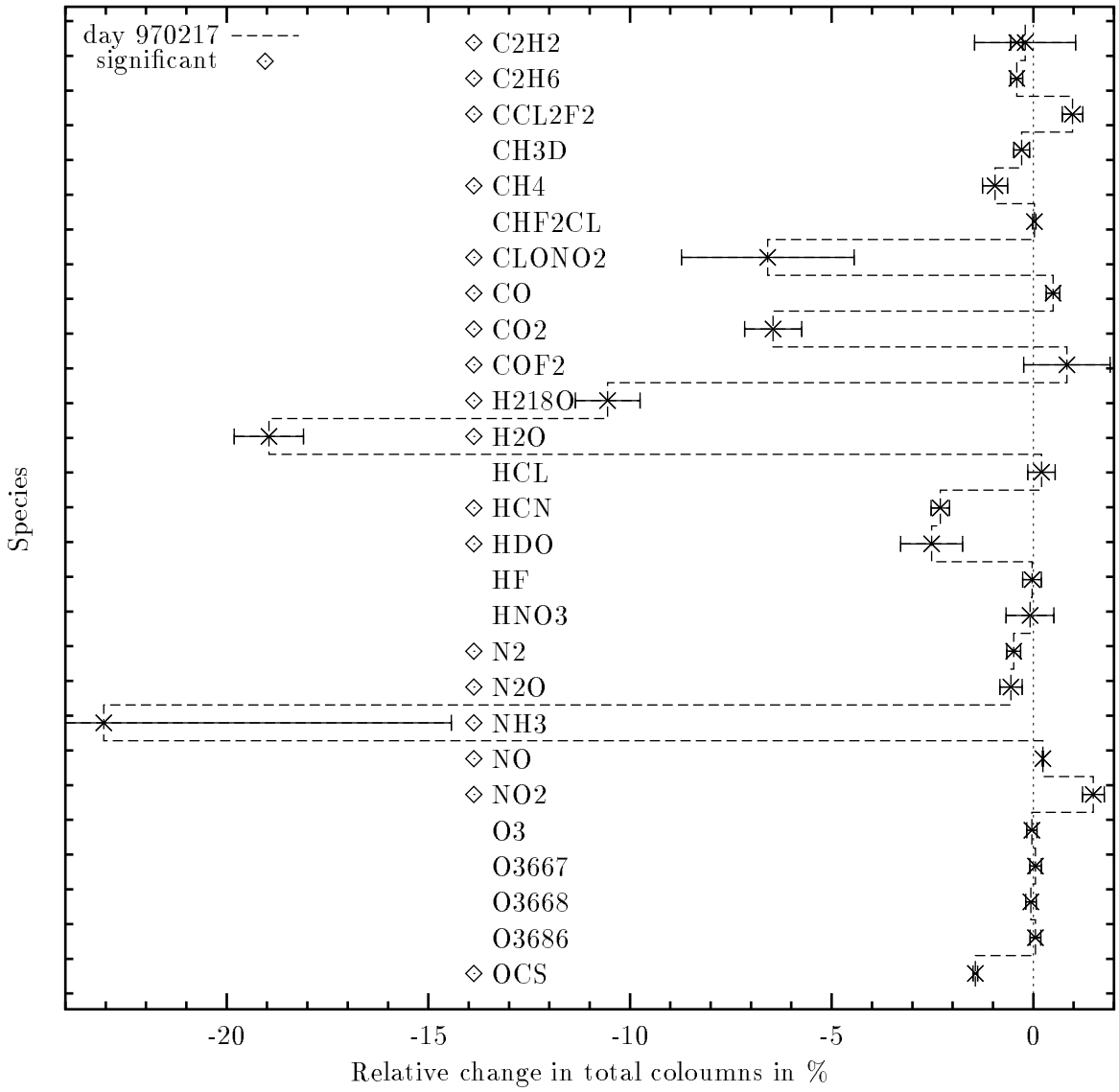

Fig. 12: This figure illustrates the effects of the changes in SFIT–FSCATM on the total columns retrieved with SFIT 1.09e. The changes in the TCAs are shown using SFIT-FSCATM v2.01 as compared to the older SFIT–FSCATM 1995 version. The spectra analysed were recorded at Kiruna on the 17 Feb, 1997. The temperature profile reported from a local PTU sonde indicates a strong inversion layer (compare Fig. 9). As can be expected, the effects on the total columns are much stronger if an inversion layer is present (compare previous figure. Note the different x-scale.). The t-test confirms that the differences are significant in numerous species.

Table 6a: This table lists the differences in the TCAs retrieved with SFIT 1.09 using SFIT-FSCATM v2.01 relative to using SFIT with SFIT-FSCATM 1995 (column "Diff TCA" as defined in equation (3), page 18). The table is ordered by increasing lower state energy E" of the featured line (2nd column) for reasons obvious from Figure 14. The 1-σ uncertainties are calculated under the assumption of Gaussian error distribution and are given in the same units as "Diff TCA". The results of the t–test are listed in column 8. Values exceeding 1.95 indicate that the differences in TCAs are significant. "ChngInSd" is the change in the average stddev; e.g. if the fits obtained with SFIT and SFIT-FSCATM 1995 had an average rms of 0.234 % becoming 0.200 % with SFIT-FSCATM v2.01, we list the difference of -0.034 in the column "ChngInSd". Thus, a negative sign indicates a reduction in the residuals when using the new SFIT–FSCATM version. 'N' is the number of absorption lines analysed times the number of spectra in which they occur.

			Day **980624** (no inversion)					Day **970217** (inversion)				
Species	E" $[cm^{-1}]$	line position	N	Chng in Sd	Diff TCA [%]	abs 1-σ Sd	t-test >1.95 signif	N	Chng in Sd	Diff TCA [%]	abs 1-σ Sd	t-test >1.95 signif
HCl	0	2904.11	8	.000	+0.000	0.000	0.00	12	-.001	+0.330	0.010	39.40
CH_4	10	2819.83	4	-.174	+0.643	0.024	33.90	8	-.069	+0.626	0.457	2.43
CH_4	10	2856.96	4	.000	+0.000	0.000	0.00	8	-.046	+1.575	0.263	26.64
HCl	21	2925.90	16	.001	-0.049	0.014	0.68	24	.015	+0.136	0.560	0.16
O_3	21	3045.30	8	-.000	+0.253	0.009	21.48	12	-.000	-0.041	0.007	0.79
CO	23	2158.30	8	.000	+0.000	0.000	0.00	8	-.077	+3.442	0.054	616.85
CO	23	4274.74	4	.000	+0.000	0.000	0.00	8	.015	-1.701	0.181	45.21
OCS	27	2057.60	8	.000	+0.000	0.000	0.00	8	-.009	-1.382	0.064	84.94
O_3	30	3040.11	16	-.001	+0.247	0.010	24.25	28	.002	-0.021	0.019	0.12
CH_4	31	2651.03	4	.000	+0.000	0.000	0.00	8	.002	-0.135	0.143	0.36
$ClNO_3$	37	780.22	10		at the detection limit			8	-.089	-6.586	2.140	57.32
N_2O	38	2806.32	4	-.000	-0.066	0.001	8.40	8	-.011	-0.425	0.101	5.04
HF	41	4038.96	8	.003	+0.049	0.186	0.04	8	-.001	-0.032	0.232	0.01
$^{667}O_3$	45	1043.42	10	-.000	-0.009	0.027	0.01	8	-.010	+0.052	0.169	0.04
N_2O	46	1159.83	10	-.002	-0.010	0.009	0.04	8	-.018	+0.323	0.416	0.71
HNO_3	47	872.93	10	-.000	+0.271	0.035	6.65	8	.003	+0.006	0.017	0.01
OCS	49	2055.87	8	.000	-0.002	0.004	0.00	8	-.004	-1.756	0.048	183.19
O_3	51	2775.82	4	-.000	+0.266	0.006	24.67	8	-.006	+0.088	0.039	0.56
NO_2	55	2914.65	8	-.000	+0.238	0.070	2.27	12	-.004	+1.489	0.272	28.23
$^{668}O_3$	57	1090.36	10	.003	-0.342	0.100	3.70	8	-.050	+0.147	0.193	0.32
CH_4	63	4285.16	4	.000	+0.008	0.015	0.01	8	.013	-0.449	0.044	12.85
CH_4	63	2835.68	4	.000	-0.024	0.015	0.08	8	-.014	-0.454	0.109	5.37
COF_2	71	1951.95	4	-.000	+0.000	0.000	0.00	4	-.001	+1.065	0.045	49.91
NO	80	1900.08	4	.001	+0.053	0.010	0.59	4	.004	+0.238	0.014	7.89
CO	81	4285.01	4	.000	+0.034	0.024	0.09	8	.013	-0.618	0.330	3.28
NH_3	86	967.35	10		at the detection limit			8	-.032	-23.050	8.617	174.41
C_2H_6	88	2986.71	8	.000	-0.163	0.023	3.29	12	-.004	-0.362	0.206	2.20
CO_2	100	2626.63	4	.001	+0.065	0.011	0.78	8	-.002	-0.358	0.055	6.56
COF_2	104	1233.94	19	.000	-0.021	0.066	0.03	16	.008	-0.223	0.819	0.24
CH_4	105	2657.71	4	.007	+0.856	0.054	27.08	8	-.034	-0.172	0.098	0.86
CH_4	105	2976.45	8	-.023	+0.104	0.016	1.96	12	.036	-0.071	0.031	0.57
HCN	106	3287.25	4	-.000	-0.006	0.007	0.01	4	-.028	-4.434	0.266	147.65
$^{667}O_3$	113	1044.24	20	.000	+0.000	0.000	0.00	16	-.003	+0.056	0.119	0.11
C_2H_6	121	2976.79	8	-.023	+0.339	0.046	7.07	12	.036	-0.478	0.063	12.46
N_2	143	2403.57	4	-.000	+0.000	0.000	0.00	0		"blacked out" at SZA>80^o		
N_2O	150	1231.36	8	.000	+0.036	0.009	0.43	8	-.005	+0.099	0.529	0.05
HNO_3	151	867.64	10	-.000	+0.211	0.033	4.27	8	-.001	-0.024	0.026	0.06
CCl_2F_2	154	923.13	10	-.053	-0.483	0.090	8.20	8	-.063	+0.914	0.078	30.38
CHF_2Cl	169	829.05	10	-.002	+0.572	0.434	2.39	8	.010	+0.025	0.043	0.04
COF_2	172	1230.94	16	.000	+0.041	0.044	0.16	16	-.001	+1.504	1.496	6.05
$^{686}O_3$	172	993.79	10	.000	+0.003	0.005	0.00	8	.000	-0.037	0.050	0.08
$H_2{}^{18}O$	173	3205.42	8	-.048	+1.754	0.024	360.24	12	-.008	+1.271	0.265	21.10
CCl_2F_2	178	1161.04	20	-.001	+0.173	0.042	3.21	15	-.012	+1.019	0.358	11.23
N_2	179	2411.13	4	.000	-0.047	0.030	0.15	3	.003	-0.427	0.053	5.90
CO	202	2057.86	8	.000	-0.006	0.016	0.01	8	-.009	-2.551	0.082	223.49
N_2O	212	2157.69	8	.000	+0.000	0.000	0.00	8	-.077	-1.526	0.050	133.07
$^{686}O_3$	215	990.80	10	.000	+0.002	0.005	0.00	8	-.004	+0.095	0.074	0.34
HDO	217	2660.51	4	-.083	+1.267	0.067	47.94	8	-.047	+1.032	0.530	5.68
N_2	219	2418.65	8	-.000	-0.045	0.027	0.21	6	-.003	-0.509	0.237	2.68
CH_4	220	2742.75	4	.000	+0.000	0.000	0.00	8	.019	+0.733	0.284	5.36
CH_4	220	2903.88	16	.000	+0.000	0.000	0.00	24	-.007	-0.217	0.206	1.12
$^{686}O_3$	220	988.39	10	.000	+0.003	0.005	0.01	8	-.009	+0.222	0.160	0.87
HDO	222	2657.33	4	.007	+1.361	0.029	127.04	8	-.034	+1.038	0.508	6.00
$^{686}O_3$	222	989.12	20	.000	+0.000	0.002	0.00	16	.004	-0.016	0.084	0.01
$H_2{}^{17}O$	224	3249.93	4	.000	+0.000	0.000	0.00	4	-.069	-2.094	0.790	11.10
$^{668}O_3$	230	1043.44	10	-.000	-0.001	0.003	0.00	8	-.010	-0.229	0.161	0.92
N_2O	231	2481.56	8	.001	-0.094	0.008	3.22	12	-.047	-0.358	0.252	1.77
$^{686}O_3$	257	986.30	10	.000	+0.004	0.006	0.01	8	.005	-0.084	0.034	0.58

			Day **980624** (no inversion)					Day **970217** (inversion)				
Species	E" $[cm^{-1}]$	line position	N	Chng in Sd	Diff TCA [%]	abs 1-σ Sd	t-test >1.95 signif	N	Chng in Sd	Diff TCA [%]	abs 1-σ Sd	t-test >1.95 signif
CO_2	258	2481.81	8	.001	-0.276	0.017	12.91	12	-.047	-0.236	0.271	0.71
$^{686}O_3$	264	984.98	10	.000	+0.005	0.006	0.02	8	.005	+0.173	0.076	1.11
HDO	265	1324.81	10	-.064	-0.819	0.027	79.47	8	-.044	-1.377	0.996	5.38
$^{668}O_3$	266	1044.21	20	.000	-0.003	0.005	0.01	16	-.003	-0.094	0.081	0.44
C_2H_2	282	766.73	10		at the detection limit			8	-.036	-0.203	1.252	0.09
OCS	285	2045.58	8	-.000	-0.001	0.004	0.00	8	-.006	-0.884	0.065	33.82
O_3	289	1161.29	10	.000	+0.258	0.012	18.17	8	-.008	-0.039	0.048	0.09
HCN	310	3268.22	4	-.000	-0.012	0.014	0.02	4	-.007	+0.014	0.224	0.00
HCl	313	2775.76	4	-.000	-0.040	0.000	9.27	8	-.006	+0.239	0.025	6.36
CO_2	317	3204.76	8	-.048	+2.262	0.160	90.68	12	-.008	-0.684	0.022	73.36
HNO_3	317	1325.32	20	-.027	-0.619	2.507	0.68	16	-.019	-0.961	1.037	3.56
N_2O	317	1146.12	10	-.001	-0.176	0.012	8.08	8	-.010	-0.842	0.082	24.51
CH_3D	328	1204.33	10	.000	-0.661	0.068	20.12	8	.016	-0.290	0.198	1.20
$^{668}O_3$	328	1002.61	20	.000	-0.001	0.005	0.00	16	.011	-0.054	0.065	0.18
N_2O	340	1193.16	10	.000	+0.000	0.000	0.00	8	-.033	-0.740	0.128	12.06
$^{686}O_3$	351	980.60	10	.000	+0.002	0.005	0.00	8	.003	+0.022	0.043	0.03
O_3	358	781.18	10	.000	+0.229	0.010	16.07	8	-.135	+0.603	0.337	3.06
O_3	372	1146.47	20	-.001	+0.213	0.013	15.12	16	-.006	+0.039	0.028	0.23
$^{686}O_3$	375	979.48	20	.000	+0.002	0.005	0.00	16	-.013	-0.011	0.340	0.00
O_3	377	782.77	10	-.010	+0.297	0.050	5.54	8	-.027	+0.638	0.400	2.88
O_3	396	780.36	10	.000	+0.136	0.015	3.92	8	-.089	-1.189	0.633	6.32
$^{686}O_3$	421	977.92	10	.000	-0.003	0.005	0.01	8	-.003	-0.003	0.099	0.00
$H_2{}^{17}O$	446	3268.06	–	–	–	–	–	4	-.000	-13.978	1.426	274.08
$^{686}O_3$	447	976.78	10	.000	-0.004	0.005	0.01	8	-.000	-0.072	0.044	0.33
O_3	455	787.46	10	.000	+0.003	0.006	0.01	8	-.014	-0.200	0.070	1.63
O_3	478	1044.18	20	.000	-0.000	0.003	0.00	16	-.003	-0.025	0.039	0.06
$^{686}O_3$	495	975.29	10	.000	-0.029	0.025	0.11	8	.001	+0.212	0.192	0.66
CH_4	575	1234.23	10	.000	-0.003	0.009	0.00	8	.016	-1.577	0.135	51.93
N_2O	621	1202.02	20	.001	-0.069	0.121	0.18	16	-.004	-2.079	0.217	79.62
HDO	709	1206.02	10	.000	-0.003	0.009	0.00	8	-.063	-5.754	1.128	83.00
HDO	116	2855.87	4	.000	+0.000	0.000	0.00	8	-.046	-0.563	0.333	2.69
H_2O	782	2819.45	4	-.174	-0.357	0.081	3.16	8	-.069	-6.733	0.424	302.47
HDO	873	1193.51	10	.000	+0.000	0.000	0.00	8	-.033	-8.473	1.165	174.25
CO	887	2055.40	8	.000	+0.006	0.018	0.01	8	-.003	-2.442	0.068	246.30
O_3	945	1002.71	20	.000	+0.000	0.000	0.00	16	.011	-0.185	0.151	0.90
O_3	948	993.71	10	.000	+0.000	0.000	0.00	8	.000	-0.055	0.027	0.31
O_3	1022	990.61	10	.000	+0.000	0.000	0.00	8	-.004	-0.149	0.070	0.89
O_3	1062	989.22	20	.000	+0.000	0.000	0.00	16	.004	-0.181	0.098	1.34
$H_2{}^{18}O$	1075	787.70	10	.000	-0.012	0.016	0.03	8	-.014	-10.977	0.874	389.94
O_3	1092	986.25	10	.000	+0.000	0.000	0.00	8	.005	-0.112	0.041	0.87
CH_4	1096	1202.42	10	.000	-0.297	0.014	19.89	8	-.013	-4.354	0.513	104.59
O_3	1097	1043.40	10	-.000	+0.000	0.000	0.00	8	-.010	+0.143	0.244	0.24
O_3	1102	984.68	10	.000	+0.000	0.000	0.00	8	.005	-0.266	0.130	1.54
O_3	1190	980.40	10	.000	+0.001	0.004	0.00	8	.003	-0.209	0.084	1.47
$H_2{}^{18}O$	1204	3268.04	4	-.000	-0.011	0.013	0.02	4	-.007	-1.117	0.702	3.56
CH_4	1252	1204.04	10	.000	-0.050	0.012	0.67	8	.016	-5.240	0.547	142.01
O_3	1263	988.41	10	.000	+0.000	0.000	0.00	8	-.009	-0.314	0.129	2.17
$H_2{}^{18}O$	1280	1205.08	10	.000	+0.025	0.033	0.06	8	-.063	-13.026	0.879	545.88
CO_2	1346	2419.55	4	.000	-0.417	0.008	41.43	3	-.004	-5.652	0.165	334.57
CO_2	1367	780.50	10	-.001	-0.377	0.007	62.15	8	-.142	-6.408	0.987	117.68
CO_2	1416	967.71	10	-.030	-0.333	0.009	36.89	8	-.032	-7.382	0.861	178.92
CO_2	1431	952.88	10	.000	+0.000	0.000	0.00	8	-.055	-7.479	0.905	174.80
O_3	1448	977.86	10	.000	+0.000	0.000	0.00	8	-.003	-0.167	0.028	2.79
H_2O	1477	2904.43	8	.000	+0.000	0.000	0.00	12	.008	-14.772	0.416	1818.1
O_3	1484	975.17	10	.000	+0.005	0.007	0.01	8	.001	-0.389	0.089	4.77
O_3	1491	979.45	10	.000	+0.000	0.000	0.00	8	-.001	-0.161	0.032	2.27
O_3	1495	976.51	10	.000	+0.003	0.005	0.00	8	-.000	-0.172	0.040	2.09
H_2O	1631	4039.22	8	-.019	-5.043	0.320	224.94	8	-.017	-18.288	0.668	1415.3
CO_2	1662	979.71	10	.000	+0.000	0.000	0.00	8	-.025	-9.054	1.091	212.54
H_2O	1691	922.15	10	-.053	-4.757	0.062	1145.7	8	-.063	-19.410	1.232	864.60
CO_2	1705	936.81	10	-.003	-0.591	0.017	63.92	8	-.033	-9.721	1.047	255.28
CO_2	1724	766.44	10	-.003	-0.529	0.010	87.31	8	-.036	-9.693	1.268	209.51
H_2O	1813	1091.20	10	.003	-6.385	0.515	250.24	8	-.050	-20.730	1.358	895.15
H_2O	1963	953.37	10	.000	-0.003	0.010	0.00	8	-.055	-22.024	0.970	1414.9
CO_2	2203	829.65	10	-.002	-1.113	0.278	14.09	8	.010	-12.406	0.782	556.72
CO_2	2433	780.97	10	.000	-0.411	0.076	7.00	8	-.135	-6.412	0.469	248.09
H_2O	2952	858.55	10	.000	+0.000	0.000	0.00	8	-.010	-33.553	0.801	3973.3
H_2O	3145	1325.15	10	.011	-7.543	0.068	2662.5	8	.005	-35.370	0.420	8425.6

On day 970217 the observed effects are substantially larger as can be expected from the differences in temperature representation (compare Fig. 9b). Differences in some water lines of up to 35 % or in ammonia of 23 % might be looked upon with concern, but the former is commonly avoided by using alternative lines with smaller temperature sensitivity. Ammonia is a difficult species to analyse, because it is a weak absorption located on the shoulder of a highly temperature sensitive water line. Hence, differences in NH_3 should not be overrated.

The differences are significant in all tropospheric species (except CHF_2Cl). The differences

Table 6b: This table is a continuation of Table 6a for the daily mean values typically representing the mean total columns over several absorption lines with different lower state energies.

	Day 980624 (no inversion)					Day 970217 (inversion)				
Species	N	chng in Sd	Diff TCA [%]	abs 1-σ Sd	t-test >1.95 signif	N	chng in Sd	Diff TCA [%]	abs 1-σ Sd	t-test >1.95 signif
C_2H_6	16	-.011	+0.049	0.035	0.28	24	.016	-0.412	0.149	5.57
CCl_2F_2	20	-.027	-0.047	0.068	0.14	16	-.038	+0.973	0.255	14.65
CH_4	58	-.012	-0.052	0.010	1.96	76	-.010	-0.949	0.312	25.21
CO	32	.000	+0.003	0.014	0.00	40	-.012	+0.490	0.167	9.07
CO_2	56	-.013	-0.181	0.058	4.27	55	-.023	-6.452	0.707	436.46
COF_2	22	.000	+0.002	0.051	0.00	20	.003	+0.832	1.072	2.89
$H_2{}^{18}O$	24	.000	+0.008	0.023	0.01	20	-.032	-10.554	0.802	620.76
H_2O	52	-.023	-2.630	0.219	227.72	52	-.036	-18.955	0.861	3010.4
HCl	20	.000	-0.041	0.009	0.82	32	.004	+0.203	0.341	0.69
HCN	8	-.000	-0.010	0.010	0.02	8	-.017	-2.308	0.228	66.14
HDO	32	-.009	+0.273	0.023	18.08	40	-.045	-2.523	0.767	52.46
HNO_3	30	-.009	+0.110	1.435	0.05	24	-.006	-0.083	0.593	0.06
N_2	12	-.000	-0.028	0.022	0.12	6	-.000	-0.488	0.171	3.42
N_2O	60	-.000	-0.068	0.049	0.72	60	-.020	-0.553	0.275	8.61
OCS	16	.000	-0.001	0.003	0.00	16	-.005	-1.437	0.055	149.63
O_3	210	-.001	+0.067	0.012	5.42	186	-.008	-0.035	0.129	0.13
$^{667}O_3$	20	.000	-0.004	0.019	0.00	16	-.006	+0.054	0.143	0.08
$^{668}O_3$	40	.001	-0.067	0.048	0.60	32	-.013	-0.060	0.130	0.15
$^{686}O_3$	110	.000	+0.000	0.008	0.00	88	-.001	+0.051	0.134	0.18

in most of the gases with a mainly stratospheric distribution like HF, HCl, HNO_3, and O_3 are small and insignificant, which is consistent with our understanding of the problem.

That $ClONO_2$ shows a change of almost 7 % is explained through interference from the temperature sensitive CO_2 line at 780.2 cm^{-1} coinciding with the centre of the $ClONO_2$ band. The analysis used the wide/narrow microwindow approach as described in detail in [23] in which CO_2 is first determined in a broad MW including the much stronger and comparatively temperature insensitive CO_2 line at 780.5 cm^{-1}. The CO_2 retrieval is dominated by that stronger line and the weaker, temperature sensitive line interfering with $ClONO_2$ is scaled to the TCA mostly representing the strong CO_2 line. With CO_2 determined, a narrower interval is chosen for the final retrieval of $ClONO_2$, where SFIT is left with no other choice but to compensate the remaining residuals in the $ClONO_2$ band by changing the amount of $ClONO_2$. This is the best approach for retrieving $ClONO_2$ if the temperature profile is accurate, but all advantages are lost, if the temperature profile used is inadequate, because temperature errors will be translated into sytematic errors in the $ClONO_2$ total columns retrieved. This is also true if the user provides an inadequate temperature profile to the new SFIT–FSCATM v2.02 program. Unfortunately, alternative absorption features of $ClONO_2$ have other disadvantages and are of little help to improve the situation.

The temperature sensitivity of a transition depends on its lower state energy E'' and the partition function of the corresponding molecules [24].

Consequently we plotted the differences in derived TCAs as a function of the lower state energy E'' of the featured absorption line as shown in Figure 13 for day 970217. We also expected the differences in TCAs to depend on the distribution over altitude of the molecule studied, because the largest temperature errors are located near ground. Molecules in the stratosphere are

subject to identical atmospheric conditions with either version of SFIT–FSCATM, but molecules in the troposphere, in particular in the lower troposphere, experience substantially different temperatures. Thus we grouped the transition lines according to the corresponding molecule's vertical distribution, more precisely to the fraction of molecules located below 4 km altitude, where most of the temperature differences are manifested.

This results in 4 distinctive groups as indicated in Figure 13. All tropospheric species, but not the stratospheric species, show a clear correlation with the lower state energy. It is also noted that in the given case the older version of SFIT–FSCATM typically leads to an overestimation

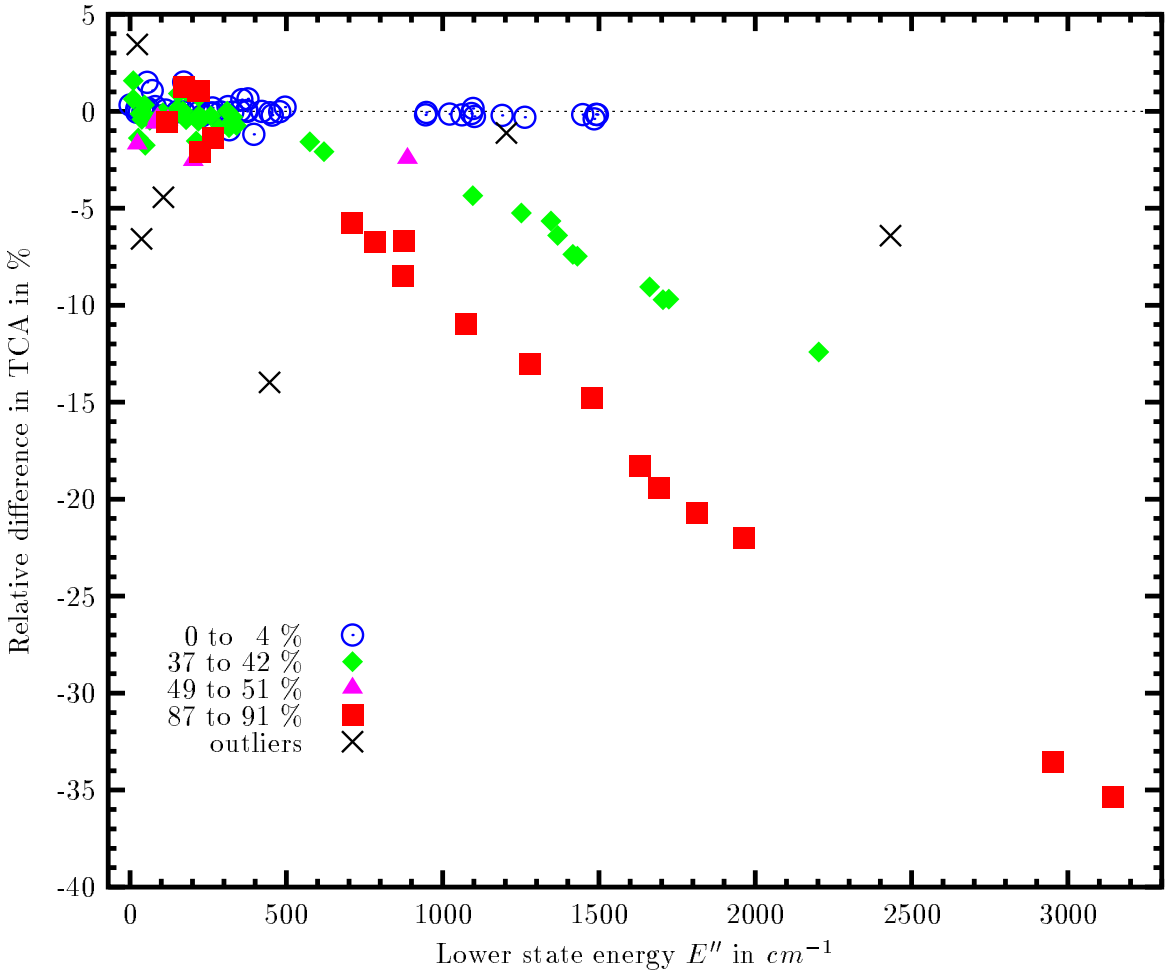

Fig. 13: This plot shows the differences in derived total column amounts ({TCA[FSCATM1995] - TCA[FSCATM V2.01]}/TCA[FSCATM1995]) as a function of the lower state energy of the featured absorption line for day 970217. The absorption lines are grouped according to what fraction of the corresponding molecules are located below 4 km altitude, because that is where most of the differences in temperature are located. **Circles** represent absorption lines from trace gases with less than 3.7 % of their molecules located below 4 km altitude ($ClONO_2$, HF, NO, COF_2, NO_2, HNO_3, HCl, O_3), **Diamonds**, 37 to 41 % (N_2, CO_2, CCl_2F_2, HCN, CH_4, CH_3D, CHF_2Cl, N_2O, OCS), **Triangles** 49 to 51 % (CO and C_2H_6), and **Boxes** more than 87 % (water vapour and its isotopomers). Stratospheric species do not show any significant differences. A few outliers (Crosses) are encountered as discussed in the text.

in retrieved TCAs. At the wrongly modeled lower ambient temperature, more molecules have to be assumed in the calculation to cause the same absorption as at the correct higher temperature. It is expected that the sign of this systematic bias in retrieved total columns depends on whether the ignored temperatures are higher (as in our test case) or lower than a smooth profile through the temperatures at the even values of the altitude.

Besides the $ClONO_2$ lines already discussed, 5 more 'outliers' are identified in Figure 14 (crosses): The most positive value on the ordinate corresponds to the saturated CO line at ν=2158.30 cm^{-1}. The data set discussed included only one saturated absorption line, namely the CO line at ν=2158.30 cm^{-1}. The anticipated differences in a saturated line in terms of line depth and shape as caused by the differences in the model atmosphere's temperature profile are masked and partly disappear in the least squares fitting perfomred due to the saturated nature of this line. Thus it is not surprising that the resulting bias in the TCAs retrieved from this line are different from the results from unsaturated lines.

Other outliers are HCN at ν=3287.25 cm^{-1} (E'' 106 cm^{-1}, 4.4 %), CO_2 at ν=780.97 cm^{-1} (2433 cm^{-1}; 6.4 %), and a pair of interfering heavy water lines at ν= 3268.04 cm^{-1} ($H_2{}^{18}O$ at [E'' 1204 cm^{-1}; 1.1 %] and $H_2{}^{17}O$ at [E'' 446 cm^{-1}; 14.0 %]). The HCN line at ν=3287.25 cm^{-1} causes only a weak absorption with a depth of about 2% located half way down the shoulder of a saturated water line and we ascribe the stronger bias in HCN to this interference. Ammonia falls into the same category (Table 6a), but NH_3 is not included in Figure 13 due to its large error bar.

The $H_2{}^{18}O$ line at ν=3268 cm^{-1} (E"=1204 cm^{-1}) is subject to strong interference from a $H_2{}^{17}O$ line of two third its own strength with a much lower E" of 445.79 cm^{-1}, which in turn shows a stronger effect in TCA changes than expected, suggesting that the interference causes changes in TCAs in such a way that their sum is consistent with the sum of the lower state energies of both water lines involved. The mean over both lines weighted by their individual line strengths yields an effective line of E''= 876.4 cm^{-1} and a TCA change of 6.675 %, which is perfectly in line with all other results for water vapour.

The last outlier is a CO_2 feature at ν=780.97 cm^{-1} (symbol at 2432 cm^{-1}; -6.4 %). It consists of 2 lines of the R-branch of CO_2 with E'' values of 2497 and 2368 cm^{-1}. Why this microwindow behaves different from all the others is not clear. A careful check of the analysis procedure did not reveal any processing errors. All that can be noted is that it is a fairly shallow absorption and that the line shape differs noticeably between the two model atmospheres.

Figure 14 shows a subset of the data from Figure 13 excluding all stratospheric species and the outliers discussed above. The relative differences in the TCAs have been divided by the fraction of molecules located below 4 km altitude to reduce the number of variables further. Based on the linear correlations seen in each group of molecules (Figure 13) and on the differences in the assumed temperature profiles (Figure 9), the simplification made here assumes that all differences observed in the derived TCAs are due to differences in the model atmosphere below 4 km altitude and that these errors scale linearly with the fraction of molecules located in the affected altitude range. In this reduced data set absorption lines with a lower state energy E'' of less than 300 cm^{-1} scatter around zero, while the remaining ones show a clear linear correlation with the error introduced into the TCAs. The latter increases by 1.66 % per 100 cm^{-1} above 300 cm^{-1} in the transition's lower state energy E'' for a molecule entirely contained in the lower troposphere.

By weighting the temperature differences below 4 km altitude by the pressure of each model layer, an effective temperature error of about 8 Kelvin is obtained (Figure 9b, page 19). If a linear response to small temperature errors is assumed, then (from the 1.66 % error in TCA per 100 cm^{-1} in E'') a systematic error in the retrieved TCAs of 0.2 % per Kelvin and per every 100 cm^{-1} above 300 cm^{-1} in E'' is determined. To illustrate this in an example: Assume a

temperature error of 2 K in the altitude range where the majority of an absorbing species is located. If the absorption line studied possesses a lower state energy of 500 cm^{-1}, the total column is subject to a systematic error of 0.8 %, but if it is at 3000 cm^{-1}, then the resulting error increases to 10.8 %. Thus, absorption lines with small lower state energies should be used wherever possible.

It should be noted that although the new version of SFIT–FSCATM is much of an improvement, the model atmosphere can only be as good as the input profiles provided to it. It can be expected that errors in the user provided temperature profile are likely to result in very similar errors as compared to the results of case study 2. Although the biases in the TCAs will scale with the magnitude of any temperature errors, the dependance on the lower state energy should remain basically the same as shown in Figure 14.

In this exercise the solar FTIR spectra were analysed with SFIT 1.09e, which allows only scaling of given *a priori* VMR profiles. The effects on VMR profile retrievals are studied in section 5.3.

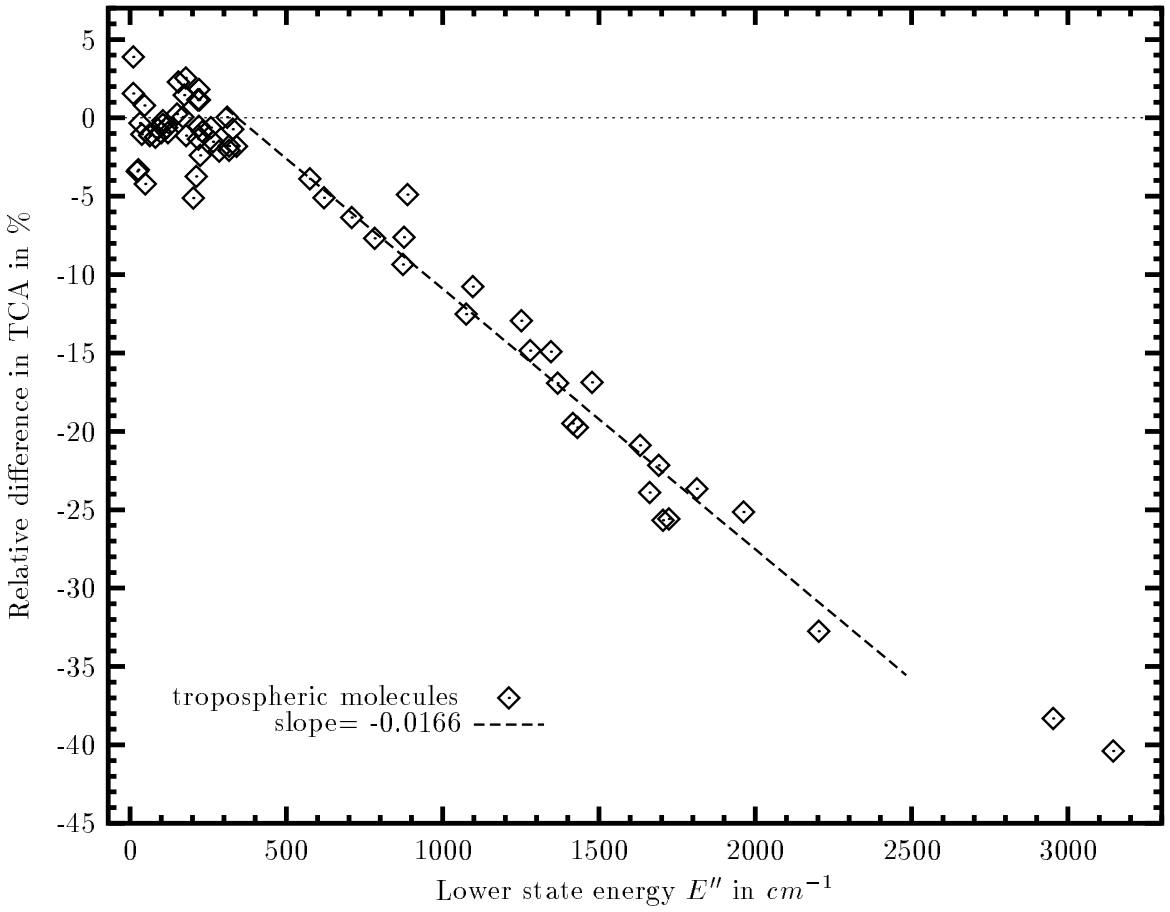

Fig. 14: This plot shows a subset of the data from the previous Figure excluding all stratospheric species and the outliers discussed in the text. To reduce the number of variables further, the relative differences in the TCAs have been divided by the fraction of molecules found below 4 km altitude. The error in the retrieved TCAs increases linearly with the lower state energy of the transition used.

Taking into account the availability of suitable absorption lines with small lower state energies for ground–based observation sites, a re-analysis might be considered only for water vapour, NH_3, CO_2, HCN, and C_2H_2. On observation days with a strong inversion layer or sites at very low altitudes may consider to extend this list to CH_4, $ClONO_2$, CO, and CCl_2F_2. We shall close the discussion of our findings by stressing that it is common practise to select lines with the lowest possible lower state energy and that many of the transitions with high temperature sensitivity were included in this study for demonstrational purposes only. However, in some trace gases the availability of transitions with a low E'' **and** acceptably little interference from other molecules is limited and our results may be used to assign realistic error bars.

5.3 Part 3: Effects on VMR profiles retrieved with SFIT2

This third and last part of the case studies employs the latest version of FSCATM and the VMR profile retrieval code SFIT2 Version 3.74 [7, 8, 9, 10]. It also employs more recent spectroscopic data, namely the year 2000 edition of HITRAN including the 2001 updates for CH_4, C_2H_2, and water vapour [25] (the water vapour data is based on [26]) and the pseudo-linelists [19] as described in the previous sections, but with updated pseudo-lines for $ClONO_2$, which are based on [27]. We used solar spectra from the Wollongong site, located 30 m above sea level on the Australian Pacific coast (34.46°S, 150.88°E). The very low elevation allows to study differences at all altitudes. Water vapour abundances are very high, resulting in omnipresent interferences from highly pressure-broadened water vapour lines. In the previous section it was shown that water vapour is the molecule most sensitive to temperature errors, thus putting our software changes to a stringent test.

49 solar spectra, split evenly over 7 optical filter regions, were recorded with a Bomem model DA-008 FTIR spectrometer with a spectral resolution of 0.004 cm^{-1} on the 9$^{\text{th}}$ Oct, 1999. Details of the instrument, the site, and standard analysis procedures have been described previously [28, 29]. The preparation of the 29-layers model atmosphere with FSCATM has been described in section 5.1 and the temperature profile from the local PTU sonde is shown in Figure 7, page 16. The tropopause is located at 16km altitude. The a-priori VMR profiles used are based on [30] (compare Appendix A.3), but are seasonally adjusted for the local monthly mean tropopause altitude and with HCl, HF, O3, CH4, NO, NO2, and CH4 spline fitted into the HALOE climatology [31] for the apropriate latitude, ClONO2 is replaced with ATMOS observations taken at 33°S [32] (seasonally adjusted), and finally the tropospheric part of the water vapour profile was calculated from the relative humidity data of the PTU sonde.

The four sets of FSCATM output data, i.e. 41/59/S, 41/209/S, 205/209/S, and 205/209/E (see section 5.1), were used one at a time with SFIT 2 resulting in 4 corresponding sets of retrieved total columns and VMR profiles as summarised in Table 7. The selection of suitable absorption features was guided by selecting transitions with small temperature sensitivity and minimum interference, but in some cases the available choices are limited. At any rate we included at least one water vapour retrieval in each optical filter to get a grip on the frequent interferences from water. Unfortunately, many of the traditionally used water lines are saturating at Wollongong and one has to compromise for weaker lines that are often significantly more temperature sensitive (Table 7). Unlike SFIT 1 that we used in the previous section, SFIT2 allows the simultaneous fitting in multiple microwindows. Thus, wherever possible, several lines with different line depth and similar lower state energy were combined in a multi-bandpass fit. This results in a more stable retrieval and typically in a better avaraging kernel; i.e. the sensitivity to VMR profile information is improved and often extended over a larger altitude range. All retrievals assumed an uncertainty of the *a-priori* VMRs of 0.2 at all altitudes and a signal–to–noise ratio consistent with the total standard deviation of the best achieveable fits. In

order to compare the results from a profile retrieval with the tradiational scaling of an assumed a-priori VMR profile, we typically ran SFIT2 twice on each (multi-)bandpass fit: Once in 'SFIT-1' mode allowing only scaling, and a second time allowing for VMR profile retrieval.

The agreement for retrieved TCAs between using FSCATM V2.02 and V2.03 products is excellent (41/209/S versus 41/59/S). Differences are smaller than 0.1%, except for $ClONO_2$ and NO which are both near the detection limit and some of the water vapour lines in case simple scaling and not profile retrievals are employed. This means that the latest improvements made to FSCATM have a very minor effect on the TCAs retrieved and that the results from the previous section 5.2 continue to be fully valid. However, if more accurate temperature data is provided on the input side of FSCATM (205/209/S, 205/209/E)), then the atmosphere provided to SFIT2 is a more accurate image of the true atmosphere. Consequently, small differences are seen in the TCAs retrieved, but there are no principally new findings as compared to section 5.2.

Table 7: *This table lists the relative changes in the retrieved total column amounts using different versions of FSCATM and the profile retrieval program SFIT2. We destinguish 4 model combinations as specified by the number of boundary layers used with each step of FSCATM: the number of input layers (41 or 205), the number of internal layers (59 or 209, corresponding to FSCATM versions 2.02 and 2.03, respectively) and the choice of output layers ('S' Standard non-equidistant 29 layers output and 'E' using Equidistant 1.5km steps throughout the lower atmosphere). The second column 'RM' lists the retrieval method with 'P' indicating profile retrieval and 'S' scaling of a fixed a-priori VMR profile. 'N×M' is the number of spectra times the number of microwindows fitted simultaneously. E'' is the lower state energy of the transition; an asterisk indicates a crude estimate over many transitions in case of unresolved bands. 'SD' is the 1-sigma standard deviation of the mean TCA obtained using the 41/59/S combination and is essentially the same for all model combinations tested here.*

Mole-cule	R M	line position $[cm^{-1}]$	E'' $[cm^{-1}]$	N × M	Model layers: input/internal/output TCA $[cm^{-2}]$ 41/59/S	SD [%]	Difference to 41/59/S [%] 41/209/S	205/209/S	205/209/E
H_2O	S	1959.632	446.5	5×1	6.983E+22	1.50	-0.249	0.008	-0.284
H_2O	P			5×1	7.031E+22	1.22	0.034	-0.206	-0.127
H_2O	S	825.163	586.5	7×2	6.650E+22	2.88	0.127	0.036	0.196
H_2O	P	841.903	552.9	7×2	6.536E+22	1.77	0.019	-0.419	-0.394
H_2O	S	2819.449	782.4	7×1	7.658E+22	7.66	0.172	-0.727	-0.569
H_2O	P			7×1	7.341E+22	6.96	0.017	0.841	-1.252
H_2O	S	3147.925	1475.0	13×2	6.836E+22	2.75	-0.055	-1.088	1.268
H_2O	P	3189.877	1059.6	13×2	6.793E+22	1.68	0.029	-1.077	-1.137
H_2O	S	2144.809	1742.3	14×1	6.419E+22	2.95	0.657	-0.168	0.012
H_2O	P			14×1	6.443E+22	2.91	0.091	1.653	1.093
HDO	S	4130.320	15.5	7×2	6.002E+22	0.57	-1.989	0.617	2.838
HDO	P	4144.494	46.2	7×2	5.855E+22	0.36	-0.063	0.372	-0.019
HDO	S	2612.539	490.4	14×1	6.483E+22	1.16	-0.031	-0.114	0.038
HDO	P			14×1	6.473E+22	0.67	0.033	-0.217	-0.189
HDO	S	1193.513	872.8	7×2	6.400E+22	2.10	0.836	-0.284	1.659
HDO	P	1206.028	709.2	7×2	6.282E+22	0.76	0.019	-0.686	-0.677

Mole-cule	R M	line position $[cm^{-1}]$	E'' $[cm^{-1}]$	N × M	Model layers: input/internal/output TCA $[cm^{-2}]$ 41/59/S	SD [%]	Difference to 41/59/S [%] 41/209/S	205/209/S	205/209/E
CO	P	2057.858 2069.656 2158.300	202.1 102.9 23.0	14×3	2.630E+18	1.35	0.008	0.092	0.052
CO	P	4274.741 4285.009	23.1 80.7	7×2	2.249E+18	0.43	-0.059	0.142	2.114
N_2O	P	1161.479 1163.132 1183.515	30.2 17.6 128.2	7×3	6.333E+18	0.34	0.001	-0.021	-0.023
N_2O	S	2442.277	231.2	7×3	6.270E+18	0.65	-0.042	0.142	0.176
N_2O	P	2447.514 2481.558	128.2 231.2	7×3	6.259E+18	0.41	0.004	0.020	0.047
N_2O	S	2455.244 2465.331	30.2 5.0	14×4	6.321E+18	0.47	-0.053	0.058	0.098
N_2O	P	2471.915 2480.766	55.3 212.0	14×4	6.335E+18	0.32	0.004	-0.033	0.002
N_2O	P	2481.558 2492.385	231.2 588.8	14×2	6.258E+18	0.24	0.005	0.039	0.046
N_2O [A)]	P	2146.516 2153.719	469.9 294.0	14×2	6.672E+18	0.45	-0.036	0.059	0.083
N_2	S	2403.565	143.2	6×3	1.716E+25	0.25	-0.041	0.133	0.153
N_2	P	2411.127	179.0	6×3	1.688E+25	0.23	0.003	0.022	-0.094
N_2 [B)]	P	2418.652	218.8	6×3	1.721E+25	0.24	0.002	0.024	0.062
N_2 [C)]	P			6×3	1.720E+25	0.24	0.003	0.020	0.069
CO_2	P	2492.694	48.6	7×2	7.708E+21	0.16	0.016	-0.184	-0.292
CO_2	S	927.008	1966.2	7×3	7.567E+21	0.77	0.014	-0.055	-0.008
CO_2	P	932.960 936.804	1800.1 1704.9	7×3	7.681E+21	0.75	-0.027	0.402	0.427
CH_4	S	2819.833	10.5	7×1	3.412E+19	5.43	-0.034	0.043	-0.314
CH_4	P			7×1	3.446E+19	2.17	-0.009	-0.504	-0.470
CH_4	P	2651.033 2835.676 2903.876	31.4 62.9 219.9	7×3	3.513E+19	0.32	-0.021	-0.070	-0.184
CH_4	P	4126.656 4265.172 4277.811 4296.150	104.7 157.1 293.2 31.4	7×4	3.426E+19	0.78	-0.028	0.092	-0.140
OCS	P	2045.579 2055.861	285.1 48.7	14×2	9.882E+15	0.59	-0.012	-0.267	0.152
CCl_2F_2	S	1161.043	450*)	7×1	1.107E+16	1.74	-0.031	-0.105	-0.099
CHF_2Cl	P	829.055	169*)	7×1	3.152E+15	2.24	0.037	-0.044	2.774
HCN	P	3268.223	310.3	6×3	5.008E+15	0.38	0.074	0.021	3.068
HCN	P	3287.248 3299.527	106.4 29.6	6×3	5.233E+15	0.34	0.061	0.180	3.814

[A)] Heavy isotopomer expected to give higher TCAs. [B)] As previous N_2 retrieval, but allowing for off-diagonal elements in the k-matrix (FWHM 4km). [C)] as previous run, but assuming an effective apodisation of 85%.

Mole-cule	R M	line position $[cm^{-1}]$	E'' $[cm^{-1}]$	N × M	Model layers: input/internal/output TCA $[cm^{-2}]$ 41/59/S	SD [%]	Difference to 41/59/S [%] 41/209/S	205/209/S	205/209/E
O_3	P	1146.471 1163.422	372.4 253.9	7×2	8.384E+18	0.47	0.031	0.100	0.137
O_3	S	1161.289	289.0	7×1	8.353E+18	1.74	0.018	0.069	0.100
HCl	S	2727.780 2775.761	583.0 312.7	7×3	3.863E+15	0.35	0.073	-0.019	0.159
HCl	P	2925.897	20.9	7×3	3.863E+15	0.35	0.073	-0.019	0.159
HCl	S	2925.897	20.9	7×1	3.786E+15	0.35	0.059	-0.080	0.251
HCl	P			7×1	3.786E+15	0.35	0.059	-0.080	0.251
HNO_3	S	867.232 868.104 868.524 868.970 869.415 872.937	158.6 138.5 130.3 120.1 110.3 46.0	7×9	1.168E+16	0.80	0.005	-0.231	-0.384
HNO_3	P	873.367 873.800 874.232	40.7 35.1 29.9	7×9	1.219E+16	0.80	0.090	-0.314	-0.219
NO_2	P	2914.652	54.6	14×1	3.672E+15	1.13	0.109	-0.163	0.649
HF	S	4038.964	41.1	6×1	1.142E+15	0.62	0.082	-0.038	-0.289
HF	P	4038.964	41.1	6×1	1.130E+15	0.63	0.089	-0.149	-0.478
HF	P	4038.964 4109.936	41.1 246.4	6×2	1.137E+15	0.58	0.087	0.015	-0.211
$ClONO_2$	P	780.220	37*)	7×1	8.524E+14	4.7E)	0.793	-3.163	-1.749
NO	S	1900.082 1903.134	80.3 105.4	3×2	4.616E+15	4.22	-0.424	0.007	-0.014
NO	P	1900.082	80.3	3×1	2.971E+15	1.68	0.166	-0.121	-0.029

E) $ClONO_2$ is near the detection limit.

The agreement between 205/209/S and 205/209/E is very high for in particular scaling, which is consistent with the idea that both sets are based on identical FSCATM input data and differ only in the boundary layer altitude scheme used within SFIT2.

Generally, profile retrievals give smaller residuals and reduce the 1-sigma variation of retrieved TCAs between subsequent spectra (column 'SD' in Table 7). However, the VMR profile retrieval performed poor on water vapour. The retrieved VMR profiles oscillated unrealistically strong yet failed to reproduce the observed line-shape. This behaviour is known and is being addressed[7]. The underlying problem is that SFIT2 assumes a Voigt line-shape for all molecules, which is inadequate for water vapour

The other major finding in employing VMR profile retrievals is that SFIT2 is very susceptible to changes of the stepsize in the 29–layer model atmosphere. Figure 15 illustrates the most extreme examples, comparing retrieved avarage VMR profiles using either the standard altitude scheme (205/209/S, 1km steps below 10km and 2km steps up to 32km, then 3 and 5 km steps above) or the 'quasi-equidistant' scheme (205/209/E, 1.5km steps

[7]Talks on this issue were given by C. Camy-Peyret and by R. Sussmann at the NDSC IRWG Meeting in Bordeaux in Sep 2001.

from 1 to 31km, then 4 and 5km steps above). The larger steps in the lower troposphere cannot represent the strong gradient in water vapour very well and the 205/209/E run for water vapour performs poorer than the 205/209/S run (Table 7) while for most other species the equidistant grid choice is superior.

In the examples of HCN, CO, and OCS (Figure 15 a-c) a sharp step change is seen in the VMR profile between 10 and 12km when using the standard altitude scheme. (A pronounced maximum in the biomass burning tracers HCN and CO in the upper free troposphere is expected – see [29].) The tropopause is known to be at 16km and cannot explain large gradients near 11km altitude. These steps do not show up with the quasi-equidistant grid. thus, they must be considered undesired artefacts of the SFIT2 retrieval method. Both altitude schemes change stepsize again between 30 and 35km and in both cases unexpected oscillations are seen at this altitude in the retrieved profiles of HCl (Figure 15d) underlining that stepsize changes are undesireable at any altitude where

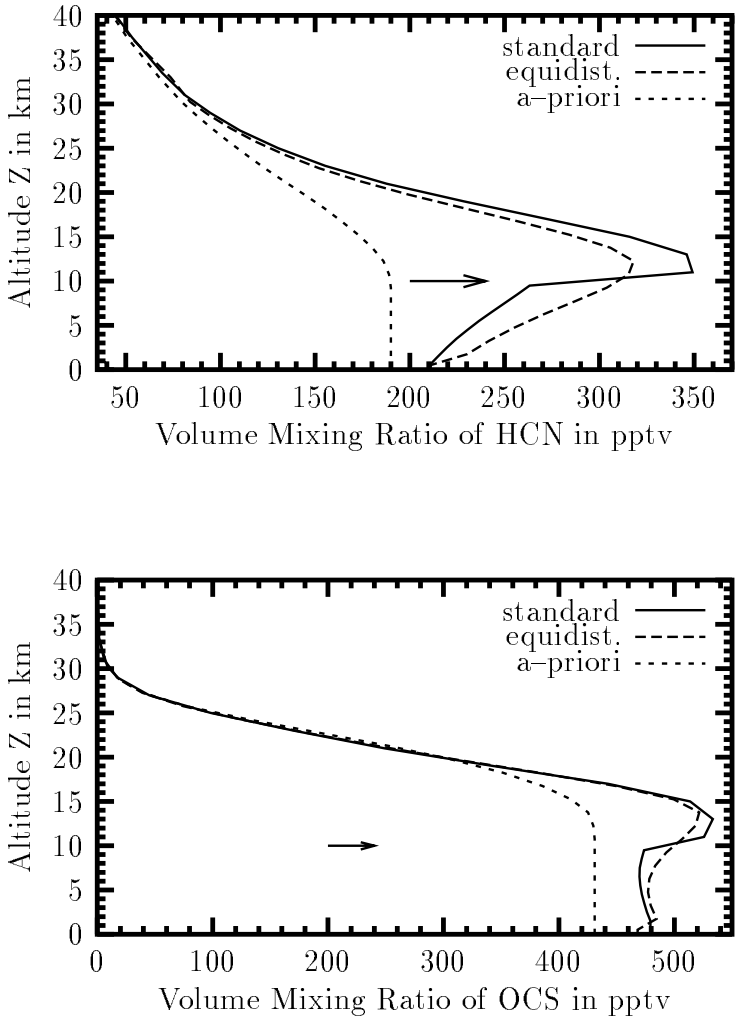

Fig. 15 a and **b:** *Retrieved VMR profiles of HCN (top) and OCS (bottom). The arrow indicates the altitude at which the stepsize is doubled in the standard altitude grid, leading to undesired oscillations.*

there is significant contribution to the TCA and that the problem is not limited to the vicinity of the tropopause as often claimed.

Cases where there are large differences in the retrieved VMR profile shapes between the 205/209/S and the 205/209/E run result also in large differences in terms of TCAs (compare Table 7). However, in most cases the agreement between using profiling and scaling in terms of TCAs is typically good. Due to an accidental scripting error, the scaling runs for HCl were performed with the retrieved HCl profiles from the corresponding profile retrieval run rather than with the a–priori profiles as we did for all other runs. It is comforting to find though, that in the HCl case running SFIT2 in scaling mode comes up with exactly the same results as in the profile retrieval case.

In the case of nitrogen, the correct answer for the TCAs is known. Assuming a constant VMR of 78.1%, a TCA of $1.674e25 cm^{-2}$ is expected. The TCA retrieval employing scaling only returns a TCA that is 2.5% too high (Table 7). Allowing free profile retrieval

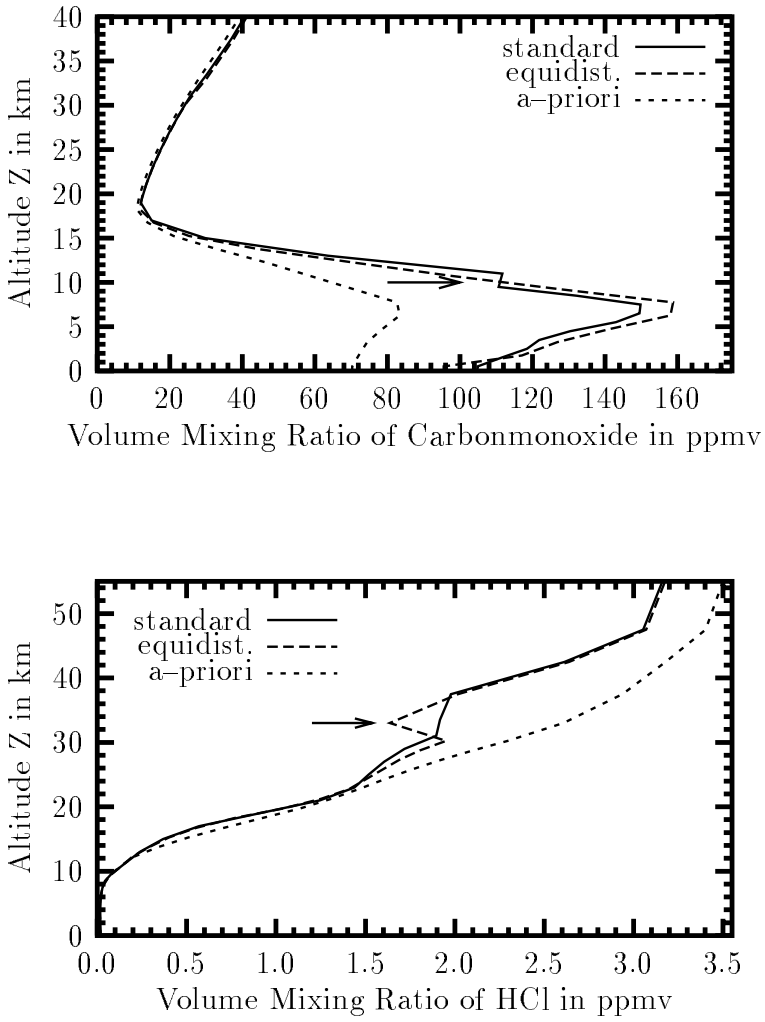

Fig. 15 c and **d:** *Retrieved VMR profiles of CO (top) and HCl (bottom). The arrow indicates the altitude at which the stepsize is doubled in the standard (top) and in both the altitude grids (bottom), leading to undesired oscillations.*

results in slightly better residuals (9% improvement) and it can be concluded that the area of the absorption lines are therefore slightly better matched. The retrieved TCA is only 0.8% higher than the expected value and hence better than the result from scaling. Unfortunately, the retrieved VMR profile shows some (modest) variation with altitude which may indicate an imperfect instrumental line shape. The oscillation-happiness of SFIT2 can be dampened by allowing for off-diagonal elements in the k-matrix at the cost of vertical resolving power - this forces an almost constant VMR profile again and TCAs go up again ('B)'). However, allowing for an effective apodisation of 85% to account for reasonable imperfections in the instrumental line shape has no significant effect on the retrieved TCAs ('C)').

This excursion was taken to demonstrate the importance that some of the improvements made to FSCATM have in practice for the FTIR community. The user has to be able to override the default output altitude scheme for running SFIT2. It may also be a good idea if SFIT2 could be improved to support a user-defined number of model layers to avoid stepsize changes while mainting a small enough stepsize to adequately represent strong gradients in molecules such as water vapour. It is further noted that the differences between all new FSCATM versions 2.01 to 2.03 lead to differences in the retrieved TCAs that are typically much smaller than other uncertainties in the analysis, such as spectroscopic line parameters and the choice of altitude grid, retrieval parameters and retrieval software.

6 Conclusions

The limited vertical resolution in the troposphere implemented in the 1995 version of SFIT–FSCATM can result in misrepresentations in pressure, temperature and air mass. The changes made to SFIT–FSCATM substantially improve the representation of the tropospheric part of the model atmosphere, which is particularly significant if inversion layers are encountered. The differences between the current version 2.03 (Oct 2001) and versions before 1999 are small if the temperature and VMR profiles provided are fairly smooth. High altitude sites are generally less affected than low altitude observation sites. Only in the case of strong inversion layers might a re-analysis of old data be reasonable, but this can be safely restricted to temperature sensitive lines in a few tropospheric species.

Consistent with the conclusion that temperature errors are the main cause of problems with using the previous SFIT–FSCATM version is the fact that differences in the TCAs retrieved show a clear correlation with the lower state energies of the corresponding absorption lines. A systematic error in the retrieved TCAs of about 0.2 % per Kelvin in temperature misrepresentation per every 100 cm^{-1} above 300 cm^{-1} in the lower state energy can be estimated for a molecule entirely contained in the altitude range where the temperature error occurs.

The importance of interference has also been demonstrated. An example of high practical relevance is $ClONO_2$, where the most prominent absorption feature suffers from interference from an underlying, temperature sensitive CO_2 line, resulting in an error in the retrieved TCAs of $ClONO_2$ of 7 % in spite of the entirely stratospheric distribution of $ClONO_2$.

The update was also used to improve the consistency of the boundary layer schemes, the quality of the first guess for the atmospheric bending and the number of NDSC sites supported in the SFIT specific implementation. The greatly improved flexibility of the code that now allows the support of user-specified boundary layers in both input and output files allows a more accurate representation of the true atmosphere in particular if PTU sondes or other high resolution data are available. It was also shown that the choice of output layers is very important when VMR profile retrievals are performed.

In addition, the number of molecules has been expanded to include replacement–CFCs, which are expected to reach detection limits in the near future. The corresponding default VMRs have been updated according to recent measurements.

Acknowledgements – Research at the University of Denver was supported in part by NSF and in part by NASA. Acknowledgment is made to the National Center for Atmospheric Research, which is supported by the National Science Foundation, for computer time used in this research. We wish to thank the Australian Research Council and the New Zealand Foundation for Research, Science, and Technology for funding; the Upper Atmosphere Research Program for funding NASA Langley; our colleagues at the Swedish Institute of Space Physics and their collaboration partners for their support in recording the solar spectra, the Atmospheric Watch Section of the Australian Bureau of Meteorology and the Swedish Space Corporation at Esrange for use of their PTU sonde data, and all our colleagues from the infrared working group of the NDSC for their encouraging support.

Appendix A.1: List of observation sites supported

Sites inherently supported by the *traceinp.exe* program from the SFIT–FSCATM v2.02 release for SFIT are listed in Table A1.1. 16 new sites have been added since the SFIT–FSCATM 1995 release distributed with SFIT 1.09e. The altitude of the South Pole site has been corrected from 2800 to 2850 m and Mauna Loa from 3459 to 3398 m in version 2.02. Moreover, a number of minor corrections have been applied to observation latitudes, longitudes, elevations, and earth radii. The formerly used equatorial and polar earth radii were 6378.69 and 6356.91 km, respectively. The new numbers are 6378.140 km (equatorial) and 6356.755 km (polar) [33] resulting in differences of 0.02 % or less.

Table A1.1: List of pre-calculated observation sites in *traceinp* (revis. level 1.14, Oct 2001), most of which have NDSC status. The sites are ordered by latitude rather than by the tag number under which they are known to the software. Latitudes are treated as positive for north latitude and negative for south latitude.

tag-No	Site	Latitude	Longitude	Altitude [m]
7	Eureka, Canada	80.05 °N	86.42 °W	610
8	Ny-Ålesund, Spitsbergen	78.92 °N	11.94 °E	20
15	Kiruna, Sweden	67.84 °N	20.41 °E	419
19	Poker Flat RR, Alaska	65.119°N	147.433°W	505
13	Harestua, Norway	60.217°N	10.753°E	596
12	Bremen, Germany	53.107°N	8.854°E	27
18	NPL Teddington, UK	51.424°N	0.343°W	30
25	Zugspitze, German Alps	47.422°N	10.987°E	2964
2	Jungfraujoch, Swiss Alps	46.549°N	7.986°E	3580
16	Moshiri, Japan	44.367°N	142.267°E	280
20	Rikubetsu, Japan	43.457°N	143.766°E	370
17	Mt Bancroft, California	37.584°N	118.235°W	3801
6	Denver, Colorado	36.673°N	104.963°W	1643
11	Billings, Oklahoma	36.605°N	97.485°W	317
23	Tsukuba, Japan	36.048°N	140.116°E	31
21	Table Mountain, California	34.382°N	117.677°W	2258
14	JPL Pasadena, California	34.200°N	118.172°W	350
4	Kitt Peak, Arizona	31.90 °N	111.60 °W	2090
22	Teneriffe, Canarian Islands	28.294°N	16.490°W	2367
1	Mauna Loa, Hawaii	19.539°N	155.578°W	3398
24	Wollongong, Australia	34.45 °S	150.88 °E	30
3	Lauder, New Zealand	45.045°S	169.684°E	370
10	Arrival Heights, Antarctica	77.83 °S	166.67 °E	200
5	South Pole, Antarctica	89.83 °S		2850
9	User specified at run time	any	any	0 - 4000

Appendix A.2: Tables of results from case study 2

The results from all retrieval calculations for the spectra of 24 June 1998 and 17 February 1997 are presented in tables A.2.1 and A.2.2, respectively. These tables list the effects of the changes in SFIT–FSCATM onto the retrieval parameters of SFIT 1.09e for individual absorption features and for the mean values for each atmospheric constituent.

The differences between the TCAs retrieved with SFIT using the new SFIT–FSCATM version relative to using the *sfit–fscatm 1995* version have also been calculated and are listed in Table 6 in section 5.2 (page 23). The results presented in Table 6 are based on the individual results listed here in Tables A.2.1 and A.2.2. Please note that the subsidence applied to the a priori VMR profiles on day 970217 was determined with *optivmr* from the SFIT-Tools [15] as described in detail in [34] using the model atmosphere of SFIT-FSCATM 1995. This may explain why the residuals of the retrievals are sometimes better with the old SFIT-FSCATM 1995 model atmosphere. (On day 980624 no subsidence correction was applied to the VMR profiles.)

Table A.2.1: This table lists the total column amounts (TCAs) retrieved with SFIT 1.09 using either SFIT-FSCATM v2.01 or SFIT-FSCATM 1995 for the observation day **980624** from case study 2. The lower state energy E" of the featured line is listed in the second column after the name of the molecule. The "mean flag" defines which microwindows contribute to the daily mean and in which way. Values ≥ 1 mean that this absorption line contributes to the daily mean values, with '1' indicating an independent absorption (normal case) and a '2' that a pair of 2 microwindows featuring the same absorption line form together the equivalent of one independent microwindow A zero indicates that we do not trust the TCAs obtained and they are not contributing to the 'mean' value of the given species. Reasons for this are distrust in the HITRAN spectroscopic data or interference. "Line position" identifies the main absorption feature in terms of wavenumbers. "N" is the number of microwindows times the number of independent spectra analysed. "Aver. rms" is the average value of the total standard deviation (rms) for a single fit as achieved with SFIT. "AoRMS" is the Absorption depth over rms ratio for the featured line and serves as its weight in the calculation of the mean TCA. The latter are given in $molec/cm^{-2}$ for zenith geometry along with their 1-σ standard deviation. Gaussian error distribution is assumed in this calculation; i.e. σ improves with $\sqrt{N}$.

		mean		SFIT 1.09e using FSCATM 1995				SFIT 1.09e using FSCATM v2.01			
Species	E"	flag/ line		aver. rms	aver. AoRMS	TCA	Sd of TCA	aver. rms	aver. AoRMS	TCA	Sd of TCA
	$[cm^{-1}]$	position	N	[%]	[1]	$[cm^{-2}]$	[%]	[%]	[1]	$[cm^{-2}]$	[%]
CH_4	105	0 2657.71	4	0.218	57.07	3.7770E+19	0.821	0.225	59.06	3.8022E+19	0.867
CH_4	105	0 2976.45	8	0.270	128.37	3.5061E+19	0.440	0.247	140.43	3.5095E+19	0.435
CH_4	63	0 4285.16	4	0.222	92.21	3.4057E+19	0.155	0.222	92.20	3.4060E+19	0.159
CH_4	1096	1 1202.42	10	0.158	233.60	3.5030E+19	0.234	0.158	233.29	3.4926E+19	0.233
CH_4	1252	1 1204.04	10	0.134	165.31	3.5484E+19	0.156	0.134	164.24	3.5466E+19	0.156
CH_4	575	1 1234.23	10	0.152	80.77	3.4447E+19	1.002	0.152	80.77	3.4446E+19	1.002
CH_4	31	1 2651.03	4	0.135	127.46	3.4697E+19	0.241	0.134	127.92	3.4697E+19	0.241
CH_4	220	1 2742.75	4	0.238	349.85	3.4984E+19	0.119	0.238	351.51	3.4984E+19	0.119
CH_4	10	1 2819.83	4	0.565	82.08	3.4204E+19	0.115	0.391	120.34	3.4424E+19	0.108
CH_4	63	1 2835.68	4	0.083	210.17	3.5252E+19	0.328	0.084	208.04	3.5243E+19	0.326
CH_4	10	1 2856.96	4	0.182	464.15	3.5112E+19	0.069	0.182	463.13	3.5112E+19	0.069
CH_4	220	2 2903.88	16	0.218	199.96	3.3950E+19	0.160	0.218	201.38	3.3951E+19	0.160
CH_4		mean	58	0.190	195.37	3.4887E+19	0.161	0.178	197.89	3.4861E+19	0.161
C_2H_2	282	1 766.73	10		at the detection limit				at the detection limit		
C_2H_2	214	0 3250.67	4		below detection limit				below detection limit		
C_2H_6	121	1 2976.79	8	0.270	20.80	2.0023E+16	0.580	0.247	24.39	2.0084E+16	0.575
C_2H_6	88	1 2986.71	8	0.234	28.37	1.9937E+16	0.515	0.234	26.84	1.9903E+16	0.514
C_2H_6		mean	16	0.252	24.58	1.9973E+16	0.354	0.241	25.61	1.9990E+16	0.352
CCl_2F_2	154	1 923.13	10	0.304	32.36	1.0084E+16	0.381	0.251	39.84	1.0036E+16	0.369
CCl_2F_2	178	2 1161.04	20	0.292	64.19	1.0045E+16	0.197	0.292	64.35	1.0062E+16	0.195
CCl_2F_2		mean	20	0.298	48.27	1.0058E+16	0.225	0.272	52.10	1.0052E+16	0.220
CHF_2Cl	169	1 829.05	10	0.327	5.93	2.5330E+15	2.514	0.325	5.88	2.5481E+15	2.558

Species	E" [cm^{-1}]	mean flag/ line position	N	SFIT 1.09e using FSCATM 1995 aver. rms [%]	aver. AoRMS [1]	TCA [cm^{-2}]	Sd of TCA [%]	SFIT 1.09e using FSCATM v2.01 aver. rms [%]	aver. AoRMS [1]	TCA [cm^{-2}]	Sd of TCA [%]
CH_3D	328	1 1204.33	10	0.134	8.16	3.8849E+19	2.976	0.134	8.15	3.8607E+19	2.998
$ClNO_3$	37	1 780.22	10	at the detection limit				at the detection limit			
CO	887	1 2055.40	8	0.283	219.87	1.9797E+18	0.304	0.283	222.17	1.9798E+18	0.301
CO	202	1 2057.86	8	0.207	54.67	2.1812E+18	0.226	0.207	56.52	2.1810E+18	0.223
CO	23	1 2158.30	8	0.212	472.92	1.9540E+18	0.174	0.212	472.91	1.9540E+18	0.174
CO	23	1 4274.74	4	0.182	52.60	2.1294E+18	0.528	0.182	52.60	2.1294E+18	0.528
CO	81	1 4285.01	4	0.222	54.97	2.1112E+18	1.056	0.222	55.71	2.1115E+18	1.043
CO		mean	32	0.226	200.31	1.9877E+18	0.147	0.226	201.44	1.9882E+18	0.146
CO_2	1724	0 766.44	10	0.382	204.71	7.2900E+21	0.222	0.379	206.08	7.2514E+21	0.221
CO_2	1367	0 780.50	10	0.333	155.22	7.1946E+21	0.369	0.332	155.30	7.1676E+21	0.369
CO_2	2497	0 780.97	10	0.327	11.54	7.2883E+21	0.891	0.327	11.72	7.2576E+21	0.907
CO_2	2203	0 829.65	10	0.327	10.18	8.9863E+21	1.087	0.325	10.31	8.8850E+21	1.032
CO_2	258	0 2481.81	8	0.138	25.36	8.4180E+21	0.889	0.139	27.58	8.4012E+21	0.890
CO_2	1705	1 936.81	10	0.185	259.86	7.3681E+21	0.176	0.181	264.13	7.3245E+21	0.177
CO_2	1431	1 952.88	10	0.218	289.21	7.3757E+21	0.176	0.218	296.74	7.3756E+21	0.176
CO_2	1416	1 967.71	10	0.252	248.58	7.4733E+21	0.268	0.223	282.29	7.4475E+21	0.268
CO_2	1662	1 979.71	10	0.236	226.85	7.4665E+21	0.149	0.236	237.48	7.4664E+21	0.149
CO_2	1346	1 2419.55	4	0.152	72.12	7.5337E+21	0.211	0.152	79.39	7.5022E+21	0.214
CO_2	100	1 2626.63	4	0.138	76.56	7.7841E+21	0.872	0.138	75.97	7.7889E+21	0.869
CO_2	317	1 3204.76	8	0.331	25.45	7.3974E+21	0.396	0.284	32.52	7.5681E+21	0.420
CO_2		mean	56	0.227	197.20	7.4304E+21	0.092	0.215	208.71	7.4183E+21	0.095
COF_2	172	2 1230.94	16	0.144	1.23	3.6249E+14	6.486	0.144	1.28	3.6336E+14	6.482
COF_2	104	2 1233.94	19	0.146	1.71	3.8392E+14	5.365	0.146	1.65	3.8225E+14	5.366
COF_2	71	1 1951.95	4	0.102	3.62	4.0978E+14	4.425	0.102	3.62	4.0988E+14	4.423
COF_2		mean	22	0.137	1.89	3.8793E+14	4.575	0.137	1.88	3.8738E+14	4.576
$H_2{}^{17}O$	224	0 3249.93	4	0.380	14.46	5.9578E+22	5.268	0.380	14.18	5.9570E+22	5.269
$H_2{}^{18}O$	173	0 3205.42	8	0.331	135.38	4.0123E+22	3.237	0.284	167.90	4.1002E+22	3.244
$H_2{}^{18}O$	1075	1 787.70	10	0.302	25.08	2.8245E+22	3.096	0.302	25.07	2.8240E+22	3.092
$H_2{}^{18}O$	1280	1 1205.08	10	0.274	52.46	3.4129E+22	3.284	0.274	52.41	3.4140E+22	3.293
$H_2{}^{18}O$	1204	1 3268.04	4	0.094	48.13	4.4976E+22	5.703	0.094	49.40	4.4987E+22	5.702
$H_2{}^{18}O$		mean	24	0.256	40.33	3.4761E+22	1.808	0.256	40.52	3.4823E+22	1.806
H_2O	3145	0 1325.15	10	0.637	43.69	3.5235E+22	3.469	0.647	42.06	3.2574E+22	3.458
H_2O	1631	0 4039.22	8	0.329	303.54	3.6539E+22	0.872	0.310	322.54	3.4712E+22	0.820
H_2O	2952	1 858.55	10	0.326	211.21	3.7972E+22	3.417	0.326	211.02	3.7960E+22	3.417
H_2O	1691	1 922.15	10	0.304	321.44	3.4373E+22	2.935	0.251	394.46	3.2810E+22	2.941
H_2O	1963	1 953.37	10	0.218	344.19	3.5940E+22	3.103	0.218	344.74	3.5940E+22	3.105
H_2O	1813	1 1091.20	10	0.250	401.48	3.5275E+22	2.947	0.253	397.76	3.3090E+22	3.079
H_2O	782	1 2819.45	4	0.565	132.70	3.5743E+22	1.363	0.391	190.58	3.5617E+22	1.410
H_2O	1477	1 2904.43	8	0.277	290.77	3.6190E+22	3.253	0.277	290.78	3.6190E+22	3.253
H_2O		mean	52	0.297	300.77	3.5752E+22	1.157	0.274	318.62	3.4788E+22	1.177
HCl	313	1 2775.76	4	0.102	148.70	4.9675E+15	0.590	0.102	148.83	4.9655E+15	0.590
HCl	0	1 2904.11	8	0.130	36.65	5.0338E+15	0.620	0.130	37.96	5.0340E+15	0.621
HCl	21	2 2925.90	16	0.124	173.70	5.0796E+15	0.228	0.125	174.25	5.0769E+15	0.228
HCl		mean	20	0.122	113.88	5.0444E+15	0.270	0.122	114.65	5.0423E+15	0.270
HCN	310	1 3268.22	4	0.094	12.82	6.7170E+15	4.300	0.094	14.36	6.7181E+15	4.294
HCN	106	1 3287.25	4	0.168	10.38	7.8891E+15	0.924	0.168	13.89	7.8911E+15	0.922
HCN		mean	8	0.131	11.60	7.2416E+15	1.714	0.131	14.12	7.2949E+15	1.699
HDO	265	0 1324.81	10	0.788	117.96	3.2582E+22	3.019	0.724	128.00	3.2298E+22	3.019
HDO	873	1 1193.51	10	0.185	390.73	2.9495E+22	3.293	0.185	390.60	2.9494E+22	3.293
HDO	709	1 1206.02	10	0.274	288.45	3.0670E+22	3.277	0.274	288.20	3.0670E+22	3.275
HDO	222	1 2657.33	4	0.218	285.25	2.6580E+22	1.252	0.225	284.77	2.6871E+22	1.296
HDO	217	1 2660.51	4	0.350	184.96	2.6476E+22	1.314	0.266	240.61	2.6793E+22	1.348
HDO	116	1 2855.87	4	0.182	108.27	2.4890E+22	1.614	0.182	111.36	2.4885E+22	1.615
HDO		mean	32	0.237	284.55	2.9038E+22	1.373	0.228	291.72	2.9039E+22	1.374
HF	41	1 4038.96	8	0.211	121.10	1.4364E+15	0.211	0.214	122.79	1.4371E+15	0.241
HNO_3	151	1 867.64	10	0.278	11.19	1.3135E+16	1.118	0.278	11.39	1.3163E+16	1.126
HNO_3	47	1 872.93	10	0.257	12.50	1.1878E+16	0.960	0.256	12.78	1.1908E+16	0.960
HNO_3	317	2 1325.32	20	0.712	4.31	1.4403E+16	1.811	0.686	4.57	1.4331E+16	1.359
HNO_3		mean	30	0.416	9.33	1.2769E+16	1.038	0.407	9.58	1.2791E+16	0.828
N_2	143	1 2403.57	4	0.158	111.58	1.6599E+25	0.166	0.157	111.14	1.6599E+25	0.166
N_2	179	1 2411.13	4	0.127	66.25	1.6794E+25	0.429	0.127	68.18	1.6786E+25	0.433
N_2	219	2 2418.65	8	0.149	107.21	1.7012E+25	0.631	0.149	107.46	1.7007E+25	0.637
N_2		mean	12	0.144	95.01	1.6800E+25	0.308	0.144	95.60	1.6797E+25	0.311
N_2O	212	0 2157.69	8	0.212	133.76	5.7521E+18	0.052	0.212	136.70	5.7521E+18	0.052
N_2O	317	1 1146.12	10	0.225	144.49	5.9652E+18	0.066	0.224	144.86	5.9548E+18	0.068
N_2O	46	1 1159.83	10	0.295	153.34	5.8447E+18	0.152	0.293	154.16	5.8441E+18	0.150
N_2O	340	1 1193.16	10	0.185	149.95	5.9316E+18	0.191	0.185	149.31	5.9316E+18	0.191
N_2O	621	2 1202.02	20	0.139	68.75	6.0644E+18	0.301	0.140	68.42	6.0602E+18	0.313
N_2O	150	1 1231.36	8	0.145	35.98	5.7110E+18	2.336	0.145	35.97	5.7130E+18	2.337
N_2O	231	1 2481.56	8	0.138	298.86	6.0691E+18	0.094	0.139	296.77	6.0633E+18	0.096
N_2O	38	1 2806.32	4	0.105	93.31	6.0597E+18	1.006	0.104	93.94	6.0552E+18	1.006
N_2O		mean	60	0.185	136.96	5.9705E+18	0.271	0.185	136.75	5.9661E+18	0.272
NH_3	86	1 967.35	10	at the detection limit				at the detection limit			
NO	80	1 1900.08	4	0.487	15.59	5.2310E+15	0.839	0.488	15.02	5.2336E+15	0.840
NO_2	55	1 2914.65	8	0.107	9.41	4.0627E+15	2.513	0.107	9.68	4.0740E+15	2.499
OCS	27	0 2057.60	8	0.207	70.32	9.8517E+15	0.312	0.207	71.42	9.8522E+15	0.312
OCS	285	1 2045.58	8	0.273	26.48	9.9973E+15	0.243	0.273	28.97	9.9968E+15	0.244
OCS	49	1 2055.87	8	0.306	58.31	9.9336E+15	0.159	0.306	58.32	9.9334E+15	0.159
OCS		mean	16	0.290	42.40	9.9535E+15	0.133	0.290	43.64	9.9545E+15	0.133
O_3	396	0 780.36	10	0.349	69.79	8.1376E+18	0.578	0.349	70.06	8.1488E+18	0.578
O_3	358	1 781.18	10	0.327	81.98	8.2746E+18	0.794	0.327	82.50	8.2940E+18	0.794
O_3	377	1 782.77	10	0.463	58.36	8.0233E+18	0.723	0.452	60.26	8.0474E+18	0.721
O_3	455	1 787.46	10	0.302	64.68	8.2399E+18	0.784	0.302	64.89	8.2399E+18	0.786
O_3	1484	1 975.17	10	0.144	38.75	8.0085E+18	0.532	0.144	39.02	8.0085E+18	0.533
O_3	1495	1 976.51	10	0.149	30.82	8.0685E+18	0.934	0.149	30.95	8.0679E+18	0.933
O_3	1448	1 977.86	10	0.167	34.15	8.1619E+18	0.674	0.167	34.53	8.1623E+18	0.674
O_3	1491	1 979.45	10	0.156	23.74	8.3793E+18	1.092	0.156	24.35	8.3756E+18	1.092
O_3	1190	1 980.40	10	0.206	121.50	8.3549E+18	0.652	0.206	121.50	8.3551E+18	0.651
O_3	1102	1 984.68	10	0.235	170.80	8.3445E+18	0.686	0.235	170.79	8.3445E+18	0.686

Species	E"	mean flag/ line		SFIT 1.09e using FSCATM 1995				SFIT 1.09e using FSCATM v2.01			
				aver.	aver.		Sd of	aver.	aver.		Sd of
				rms	AoRMS	TCA	TCA	rms	AoRMS	TCA	TCA
	$[cm^{-1}]$	position	N	[%]	[1]	$[cm^{-2}]$	[%]	[%]	[1]	$[cm^{-2}]$	[%]
O_3	1092	1 986.25	10	0.194	190.59	8.2189E+18	0.764	0.194	190.60	8.2189E+18	0.764
O_3	1263	1 988.41	10	0.225	53.72	8.2992E+18	0.618	0.225	53.72	8.2992E+18	0.618
O_3	1062	2 989.22	20	0.400	153.39	8.2117E+18	0.718	0.400	153.39	8.2117E+18	0.718
O_3	1022	1 990.61	10	0.281	181.84	8.2788E+18	0.597	0.281	181.84	8.2788E+18	0.597
O_3	948	1 993.71	10	0.314	196.23	8.2718E+18	0.520	0.314	196.23	8.2718E+18	0.520
O_3	945	2 1002.71	20	0.376	143.84	8.3234E+18	0.347	0.376	146.23	8.3228E+18	0.347
O_3	1097	1 1043.40	10	0.354	59.26	8.2944E+18	0.785	0.354	59.27	8.2944E+18	0.785
O_3	478	2 1044.18	20	0.386	65.72	8.2531E+18	0.521	0.386	65.72	8.2531E+18	0.521
O_3	372	2 1146.47	20	0.212	138.81	8.2085E+18	0.421	0.210	141.18	8.2259E+18	0.423
O_3	289	1 1161.29	10	0.290	98.03	8.1731E+18	0.572	0.291	98.71	8.1945E+18	0.570
O_3	51	1 2775.82	4	0.102	58.57	8.0194E+18	0.668	0.102	60.62	8.0416E+18	0.668
O_3	30	2 3040.11	16	0.167	133.71	7.8471E+18	0.354	0.166	134.77	7.8669E+18	0.354
O_3	21	1 3045.30	8	0.105	75.54	7.8882E+18	0.582	0.105	75.04	7.9080E+18	0.583
O_3		mean	210	0.259	99.86	8.2177E+18	0.137	0.258	100.37	8.2228E+18	0.137
$^{667}O_3$	45	1 1043.43	10	0.354	290.44	1.1782E+19	1.941	0.354	290.52	1.1781E+19	1.943
$^{667}O_3$	113	2 1044.24	20	0.386	273.24	1.0632E+19	1.499	0.386	273.24	1.0632E+19	1.499
$^{667}O_3$		mean	20	0.370	281.84	1.1225E+19	1.380	0.370	281.88	1.1224E+19	1.380
$^{668}O_3$	328	2 1002.61	20	0.376	22.02	9.7752E+18	0.831	0.376	23.42	9.7830E+18	0.832
$^{668}O_3$	230	1 1043.44	10	0.354	20.06	9.1542E+18	0.540	0.354	20.06	9.1541E+18	0.539
$^{668}O_3$	266	2 1044.21	20	0.386	15.07	9.1935E+18	0.860	0.386	16.18	9.2043E+18	0.866
$^{668}O_3$	57	1 1090.36	10	0.250	13.76	1.0339E+19	0.710	0.253	13.54	1.0310E+19	0.744
$^{668}O_3$		mean	40	0.341	17.73	9.5853E+18	0.453	0.342	18.30	9.5803E+18	0.458
$^{686}O_3$	495	1 975.29	10	0.144	15.78	9.6325E+18	0.988	0.144	15.24	9.6365E+18	0.978
$^{686}O_3$	447	1 976.78	10	0.149	19.77	9.9247E+18	1.312	0.149	20.64	9.9274E+18	1.312
$^{686}O_3$	421	1 977.92	10	0.167	20.61	9.6638E+18	1.076	0.167	18.32	9.6623E+18	1.076
$^{686}O_3$	375	2 979.48	20	0.196	21.50	9.5246E+18	0.978	0.196	22.61	9.5247E+18	0.978
$^{686}O_3$	351	1 980.60	10	0.206	24.96	9.3785E+18	0.745	0.206	24.42	9.3781E+18	0.744
$^{686}O_3$	264	1 984.98	10	0.235	28.37	9.4082E+18	0.910	0.235	28.37	9.4087E+18	0.910
$^{686}O_3$	257	1 986.30	10	0.194	39.26	9.2575E+18	0.711	0.194	39.26	9.2579E+18	0.710
$^{686}O_3$	220	1 988.39	10	0.225	32.28	9.1000E+18	1.391	0.225	32.28	9.1003E+18	1.391
$^{686}O_3$	222	2 989.12	20	0.400	20.67	9.3045E+18	0.806	0.400	20.68	9.3045E+18	0.806
$^{686}O_3$	215	1 990.80	10	0.281	27.49	9.1058E+18	0.641	0.281	27.49	9.1060E+18	0.641
$^{686}O_3$	172	1 993.79	10	0.314	19.83	9.4060E+18	0.559	0.314	19.83	9.4063E+18	0.560
$^{686}O_3$		mean	110	0.228	24.59	9.3876E+18	0.279	0.228	24.47	9.3875E+18	0.279

Table A.2.2: This table lists the TCAs retrieved with SFIT 1.09 using either SFIT-FSCATM v2.01 or SFIT-FSCATM 1995 for the observation day **970217** from case study 2. The quantities and symbols listed are the same as in Table A.2.1.

Species	E"	mean flag/ line		SFIT 1.09e using FSCATM 1995				SFIT 1.09e using FSCATM v2.01			
				aver.	aver.		Sd of	aver.	aver.		Sd of
				rms	AoRMS	TCA	TCA	rms	AoRMS	TCA	TCA
	$[cm^{-1}]$	position	N	[%]	[1]	$[cm^{-2}]$	[%]	[%]	[1]	$[cm^{-2}]$	[%]
C_2H_2	282	1 766.73	8	0.678	12.75	6.6404E+15	0.623	0.642	13.93	6.6356E+15	0.691
C_2H_2	214	0 3250.67	4	0.502	8.97	5.6675E+15	2.107	0.432	11.20	5.9395E+15	1.895
C_2H_6	121	1 2976.79	12	0.604	50.41	3.4043E+16	0.734	0.640	49.91	3.3903E+16	0.751
C_2H_6	88	1 2986.71	12	0.625	65.15	3.4005E+16	0.483	0.621	66.95	3.3886E+16	0.498
C_2H_6		mean	24	0.614	57.78	3.4022E+16	0.413	0.630	58.43	3.3893E+16	0.424
CH_3D	328	1 1204.33	8	0.254	24.81	4.0453E+19	0.944	0.270	23.30	4.0319E+19	0.971
CH_4	105	0 2657.71	8	0.278	187.93	3.5780E+19	0.533	0.244	206.72	3.5689E+19	0.496
CH_4	105	0 2976.45	12	0.604	150.31	3.5472E+19	0.402	0.640	143.63	3.5457E+19	0.404
CH_4	63	0 4285.16	8	0.645	107.86	3.4145E+19	0.282	0.658	105.88	3.3994E+19	0.269
CH_4	1096	1 1202.42	8	0.370	231.43	3.7395E+19	0.584	0.357	240.95	3.5766E+19	0.737
CH_4	1252	1 1204.04	8	0.254	222.73	3.8284E+19	0.810	0.270	212.44	3.6252E+19	0.994
CH_4	575	1 1234.23	8	0.172	262.77	3.5393E+19	0.463	0.188	242.13	3.4846E+19	0.504
CH_4	31	1 2651.03	8	0.251	234.23	3.4878E+19	0.226	0.253	235.58	3.4832E+19	0.193
CH_4	220	1 2742.75	8	0.666	143.53	3.5599E+19	0.150	0.685	144.69	3.5863E+19	0.249
CH_4	10	1 2819.83	8	0.351	258.12	3.4702E+19	0.634	0.282	336.49	3.4931E+19	0.468
CH_4	63	1 2835.68	8	0.151	410.81	3.5274E+19	0.251	0.136	448.32	3.5121E+19	0.223
CH_4	10	1 2856.96	8	0.357	287.72	3.3904E+19	0.367	0.311	336.61	3.4438E+19	0.265
CH_4	220	2 2903.88	24	0.797	127.46	3.3843E+19	0.377	0.789	131.95	3.3774E+19	0.359
CH_4		mean	76	0.396	236.06	3.5422E+19	0.148	0.386	252.12	3.5041E+19	0.155
CCl_2F_2	154	1 923.13	8	0.548	83.00	9.7100E+15	0.210	0.485	93.39	9.7987E+15	0.185
CCl_2F_2	178	2 1161.04	16	0.622	116.54	9.7766E+15	0.226	0.609	119.03	9.8789E+15	0.151
CCl_2F_2		mean	16	0.585	99.77	9.7489E+15	0.187	0.547	106.21	9.8436E+15	0.136
CHF_2Cl	169	1 829.05	8	0.377	29.66	2.5212E+15	0.351	0.387	29.18	2.5216E+15	0.359
$ClNO_3$	37	1 780.22	8	0.469	10.91	2.6291E+15	4.049	0.380	12.48	2.4445E+15	3.942
CO	887	1 2055.40	8	0.575	109.42	2.6909E+18	0.762	0.573	119.50	2.6266E+18	0.764
CO	202	1 2057.86	8	0.509	41.54	2.5604E+18	0.099	0.500	47.65	2.4949E+18	0.116
CO	23	1 2158.30	8	0.436	230.84	2.3923E+18	0.100	0.359	281.62	2.4746E+18	0.111
CO	23	1 4274.74	8	0.716	67.29	2.3962E+18	0.971	0.731	66.14	2.3556E+18	0.914
CO	81	1 4285.01	8	0.645	78.39	2.3950E+18	0.932	0.658	81.26	2.3798E+18	0.833
CO		mean	40	0.576	105.50	2.4684E+18	0.269	0.564	119.23	2.4806E+18	0.249

Species	E" [cm^{-1}]	mean flag/ line position	N	SFIT 1.09e using FSCATM 1995 aver. rms [%]	aver. AoRMS [1]	TCA [cm^{-2}]	Sd of TCA [%]	SFIT 1.09e using FSCATM v2.01 aver. rms [%]	aver. AoRMS [1]	TCA [cm^{-2}]	Sd of TCA [%]
CO_2	1724	0 766.44	8	0.678	157.51	8.5739E+21	0.542	0.642	169.56	7.7414E+21	0.534
CO_2	1367	0 780.50	8	0.584	158.33	8.0182E+21	0.483	0.443	204.08	7.5019E+21	0.655
CO_2	2497	0 780.97	8	0.604	13.19	7.9845E+21	0.488	0.469	19.77	7.4706E+21	0.602
CO_2	2203	0 829.65	8	0.377	19.94	9.9998E+21	0.837	0.387	18.68	8.7590E+21	0.764
CO_2	258	0 2481.81	12	0.586	27.95	8.2199E+21	0.633	0.539	35.48	8.2026E+21	0.577
CO_2	1705	1 936.81	8	0.295	278.24	8.4803E+21	0.510	0.261	305.71	7.6396E+21	0.799
CO_2	1431	1 952.88	8	0.294	348.66	8.3158E+21	0.478	0.239	433.16	7.6934E+21	0.731
CO_2	1416	1 967.71	8	0.309	335.64	8.3469E+21	0.497	0.277	376.22	7.7305E+21	0.751
CO_2	1662	1 979.71	8	0.447	194.00	8.6086E+21	0.670	0.422	204.10	7.8269E+21	0.979
CO_2	1346	1 2419.55	3	1.778	16.48	8.7156E+21	5.268	1.773	16.15	8.2265E+21	5.358
CO_2	100	1 2626.63	8	0.179	219.77	7.7184E+21	0.111	0.178	221.62	7.6907E+21	0.091
CO_2	317	1 3204.76	12	0.375	85.59	7.5169E+21	0.287	0.367	88.52	7.4645E+21	0.291
CO_2		mean	55	0.400	219.76	8.2374E+21	0.243	0.377	244.31	7.6916E+21	0.290
COF_2	172	2 1230.94	16	0.141	5.36	4.2902E+14	1.690	0.140	5.71	4.3479E+14	1.500
COF_2	104	2 1233.94	16	0.152	5.10	4.5965E+14	2.308	0.160	4.70	4.5716E+14	2.119
COF_2	71	1 1951.95	4	0.100	15.25	3.7596E+14	1.598	0.099	15.52	3.7996E+14	1.584
COF_2		mean	20	0.137	7.24	4.1530E+14	1.732	0.140	7.27	4.1715E+14	1.570
$H_2{}^{17}O$	446	0 3268.06	4	0.183	–	4.8458E+21	5.918	0.295	–	4.1685E+21	6.208
$H_2{}^{17}O$	224	0 3249.93	4	0.502	8.10	8.4834E+21	5.743	0.432	11.12	8.2824E+21	6.182
$H_2{}^{18}O$	173	0 3205.42	12	0.375	94.63	5.2343E+21	2.921	0.367	97.32	5.2965E+21	2.962
$H_2{}^{18}O$	1075	1 787.70	8	0.309	18.70	4.5888E+21	3.393	0.295	19.45	4.0805E+21	3.536
$H_2{}^{18}O$	1280	1 1205.08	8	0.418	18.93	5.5622E+21	2.191	0.355	22.05	4.8276E+21	2.336
$H_2{}^{18}O$	1204	1 3268.04	4	0.183	11.60	6.0229E+21	7.377	0.176	12.55	5.9539E+21	7.639
$H_2{}^{18}O$		mean	20	0.327	17.37	5.2046E+21	1.865	0.295	19.11	4.6714E+21	2.021
H_2O	3145	0 1325.15	8	2.656	6.32	7.4545E+21	1.725	2.661	6.67	4.8191E+21	1.862
H_2O	1631	0 4039.22	8	0.427	217.47	6.3901E+21	2.872	0.410	223.63	5.2013E+21	2.853
H_2O	2952	1 858.55	8	0.304	112.77	8.1636E+21	1.511	0.294	113.88	5.4217E+21	1.476
H_2O	1691	1 922.15	8	0.548	142.59	5.7513E+21	1.664	0.485	159.94	4.6342E+21	1.641
H_2O	1963	1 953.37	8	0.294	160.84	6.5466E+21	1.611	0.239	200.76	5.1006E+21	1.643
H_2O	1813	1 1091.20	8	0.517	175.08	5.9326E+21	1.838	0.467	197.53	4.7043E+21	2.105
H_2O	782	1 2819.45	8	0.351	171.80	5.6031E+21	3.343	0.282	212.14	5.2242E+21	3.439
H_2O	1477	1 2904.43	12	1.041	66.27	6.2553E+21	1.993	1.048	65.61	5.3322E+21	2.004
H_2O		mean	52	0.550	132.69	6.2804E+21	0.733	0.514	151.18	5.0321E+21	0.787
HCl	313	1 2775.76	8	0.387	112.53	4.3123E+15	0.306	0.381	114.20	4.3226E+15	0.298
HCl	0	1 2904.11	12	0.333	57.67	4.3888E+15	0.393	0.332	58.80	4.4032E+15	0.395
HCl	21	2 2925.90	24	0.404	149.75	4.3103E+15	0.127	0.419	145.48	4.3160E+15	0.178
HCl		mean	32	0.373	105.91	4.3269E+15	0.168	0.377	105.15	4.3361E+15	0.179
HCN	310	1 3268.22	4	0.183	11.91	2.7144E+15	2.267	0.176	12.90	2.7142E+15	2.131
HCN	106	1 3287.25	4	0.276	13.01	3.1085E+15	2.450	0.248	19.41	2.9698E+15	2.308
HCN		mean	8	0.229	12.46	2.9201E+15	1.397	0.212	16.16	2.8678E+15	1.303
HDO	265	0 1324.81	8	2.179	37.91	3.3368E+21	1.674	2.135	38.70	3.2916E+21	1.855
HDO	873	1 1193.51	8	0.441	118.15	3.5391E+21	1.532	0.408	127.28	3.2386E+21	1.779
HDO	709	1 1206.02	8	0.418	148.01	3.5946E+21	1.590	0.355	171.99	3.3836E+21	1.772
HDO	222	1 2657.33	8	0.278	175.83	3.0600E+21	3.385	0.244	191.41	3.0718E+21	3.501
HDO	217	1 2660.51	8	0.381	137.00	3.0523E+21	3.299	0.334	154.25	3.0813E+21	3.423
HDO	116	1 2855.87	8	0.357	34.74	2.7821E+21	3.544	0.311	41.76	2.7709E+21	3.614
HDO		mean	40	0.375	122.75	3.2637E+21	1.015	0.330	137.34	3.1647E+21	1.086
HF	41	1 4038.96	8	0.356	222.06	1.6945E+15	2.452	0.356	222.89	1.6943E+15	2.518
HNO_3	151	1 867.64	8	0.481	44.13	2.0737E+16	1.418	0.480	44.96	2.0729E+16	1.425
HNO_3	47	1 872.93	8	0.450	52.02	2.0342E+16	1.234	0.453	52.20	2.0343E+16	1.234
HNO_3	317	2 1325.32	16	2.417	8.23	2.4446E+16	1.488	2.398	8.35	2.4223E+16	1.425
HNO_3		mean	24	1.116	34.79	2.0833E+16	0.968	1.110	35.17	2.0815E+16	0.936
N_2	143	1 2403.57	0		"blacked out", SZA>80^o				"black out" at SZA>80^o		
N_2	179	1 2411.13	3	3.337	9.71	1.8462E+25	9.920	3.340	9.83	1.8406E+25	9.864
N_2	219	2 2418.65	6	1.735	29.15	1.6951E+25	2.119	1.732	28.91	1.6864E+25	2.100
N_2		mean	6	2.536	19.43	1.7329E+25	4.388	2.536	19.37	1.7255E+25	4.366
N_2O	212	0 2157.69	8	0.436	143.69	5.9140E+18	0.404	0.359	174.63	5.8234E+18	0.418
N_2O	317	1 1146.12	8	0.473	176.58	5.9505E+18	0.586	0.463	180.88	5.9008E+18	0.560
N_2O	46	1 1159.83	8	0.639	146.54	5.7494E+18	0.574	0.622	150.83	5.7673E+18	0.421
N_2O	340	1 1193.16	8	0.441	173.90	5.9460E+18	0.812	0.408	192.49	5.9026E+18	0.767
N_2O	621	2 1202.02	16	0.268	146.03	6.1916E+18	0.451	0.265	144.71	6.0612E+18	0.491
N_2O	150	1 1231.36	8	0.160	146.20	5.6064E+18	0.861	0.155	151.37	5.6123E+18	0.696
N_2O	231	1 2481.56	12	0.586	193.64	6.0218E+18	0.372	0.539	226.48	6.0004E+18	0.306
N_2O	38	1 2806.32	8	0.187	205.32	6.0983E+18	0.369	0.175	217.19	6.0723E+18	0.344
N_2O		mean	60	0.406	171.34	5.9549E+18	0.197	0.386	183.63	5.9232E+18	0.179
NH_3	86	1 967.35	8	0.309	3.48	6.2291E+13	11.594	0.277	4.76	4.8400E+13	14.376
NO	80	1 1900.08	4	0.307	61.02	2.7512E+15	3.330	0.311	60.24	2.7574E+15	3.332
NO_2	55	1 2914.65	12	0.224	6.63	1.1239E+15	4.205	0.221	7.87	1.1433E+15	4.142
OCS	27	0 2057.60	8	0.509	74.58	1.0303E+16	0.552	0.500	80.17	1.0163E+16	0.548
OCS	285	1 2045.58	8	0.474	38.58	1.0118E+16	0.520	0.468	43.47	1.0027E+16	0.501
OCS	49	1 2055.87	8	0.765	66.91	1.0455E+16	0.512	0.761	67.31	1.0272E+16	0.516
OCS		mean	16	0.620	52.74	1.0332E+16	0.332	0.615	55.39	1.0176E+16	0.328
O_3	396	0 780.36	8	0.469	135.81	9.5311E+18	1.152	0.380	166.79	9.4180E+18	0.897
O_3	358	1 781.18	8	0.604	129.23	9.2743E+18	0.527	0.469	167.34	9.3364E+18	0.633
O_3	377	1 782.77	8	0.440	182.74	9.3178E+18	0.654	0.413	197.34	9.3774E+18	0.801
O_3	455	1 787.46	8	0.309	205.09	9.4552E+18	0.850	0.295	212.77	9.4388E+18	0.821
O_3	1484	1 975.17	8	0.202	53.29	9.3746E+18	1.916	0.202	53.23	9.3343E+18	1.891
O_3	1495	1 976.51	8	0.208	40.88	9.2326E+18	1.804	0.208	42.18	9.2214E+18	1.800
O_3	1448	1 977.86	8	0.248	45.70	9.5608E+18	1.848	0.244	47.44	9.5474E+18	1.851
O_3	1491	1 979.45	8	0.248	26.98	9.4218E+18	1.874	0.247	27.75	9.3958E+18	1.866
O_3	1190	1 980.40	8	0.354	151.01	9.6482E+18	1.460	0.357	149.99	9.6264E+18	1.427
O_3	1102	1 984.68	8	0.372	213.13	9.6426E+18	1.450	0.377	210.47	9.6159E+18	1.398
O_3	1092	1 986.25	8	0.356	218.09	9.4982E+18	1.372	0.361	215.20	9.4871E+18	1.356
O_3	1263	1 988.41	8	0.388	70.42	9.7664E+18	1.868	0.379	71.75	9.7373E+18	1.816
O_3	1062	2 989.22	16	0.549	154.72	9.5143E+18	0.860	0.553	153.89	9.4959E+18	0.836
O_3	1022	1 990.61	8	0.562	158.83	9.5008E+18	1.422	0.558	160.27	9.4856E+18	1.394
O_3	948	1 993.71	8	0.593	168.17	9.5250E+18	1.257	0.593	168.11	9.5201E+18	1.265
O_3	945	2 1002.71	16	0.626	124.70	9.4022E+18	0.843	0.637	123.38	9.3863E+18	0.822
O_3	1097	1 1043.40	8	0.864	55.80	9.3917E+18	1.241	0.854	56.54	9.4029E+18	1.173

Species	E" [cm^{-1}]	mean flag/ line position	N	SFIT 1.09e using FSCATM 1995 aver. rms [%]	aver. AoRMS [1]	TCA [cm^{-2}]	Sd of TCA [%]	SFIT 1.09e using FSCATM v2.01 aver. rms [%]	aver. AoRMS [1]	TCA [cm^{-2}]	Sd of TCA [%]
O_3	478	2 1044.18	16	0.803	79.65	9.5150E+18	0.868	0.800	79.97	9.5124E+18	0.866
O_3	372	2 1146.47	16	0.477	171.16	9.1597E+18	0.459	0.471	173.29	9.1627E+18	0.462
O_3	289	1 1161.29	8	0.605	113.40	9.1947E+18	0.719	0.597	116.10	9.1904E+18	0.737
O_3	51	1 2775.82	8	0.387	81.27	9.0734E+18	0.273	0.381	86.87	9.0811E+18	0.274
O_3	30	2 3040.11	28	0.534	143.06	9.0130E+18	0.197	0.536	142.15	9.0112E+18	0.197
O_3	21	1 3045.30	12	0.311	112.32	9.0970E+18	0.364	0.311	113.06	9.0933E+18	0.365
O_3		mean	186	0.456	123.14	9.3794E+18	0.222	0.447	126.12	9.3746E+18	0.220
$^{667}O_3$	45	1 1043.43	8	0.864	124.23	1.1588E+19	0.621	0.854	125.71	1.1591E+19	0.683
$^{667}O_3$	113	2 1044.24	16	0.803	135.36	1.0720E+19	0.701	0.800	135.78	1.0725E+19	0.722
$^{667}O_3$		mean	16	0.833	129.79	1.1135E+19	0.561	0.827	130.75	1.1142E+19	0.589
$^{668}O_3$	328	2 1002.61	16	0.626	46.70	1.0942E+19	0.765	0.637	45.87	1.0940E+19	0.763
$^{668}O_3$	230	1 1043.44	8	0.864	39.87	1.0900E+19	1.026	0.854	40.30	1.0875E+19	1.052
$^{668}O_3$	266	2 1044.21	16	0.803	27.77	1.0769E+19	0.761	0.800	28.92	1.0763E+19	0.768
$^{668}O_3$	57	1 1090.36	8	0.517	36.12	1.1043E+19	0.918	0.467	40.50	1.1048E+19	0.958
$^{668}O_3$		mean	32	0.702	37.62	1.0923E+19	0.471	0.689	38.90	1.0918E+19	0.478
$^{686}O_3$	495	1 975.29	8	0.202	45.94	1.0734E+19	0.825	0.202	45.87	1.0754E+19	0.812
$^{686}O_3$	447	1 976.78	8	0.208	56.14	1.0669E+19	1.018	0.208	57.23	1.0659E+19	1.031
$^{686}O_3$	421	1 977.92	8	0.248	53.71	1.0583E+19	1.127	0.244	54.29	1.0584E+19	1.152
$^{686}O_3$	375	2 979.48	16	0.347	51.59	1.0296E+19	0.563	0.335	53.97	1.0295E+19	0.618
$^{686}O_3$	351	1 980.60	8	0.354	58.87	1.0500E+19	1.004	0.357	58.09	1.0505E+19	1.018
$^{686}O_3$	264	1 984.98	8	0.372	79.90	1.0541E+19	0.927	0.377	79.06	1.0559E+19	0.951
$^{686}O_3$	257	1 986.30	8	0.356	87.39	1.0367E+19	0.881	0.361	86.24	1.0358E+19	0.876
$^{686}O_3$	220	1 988.39	8	0.388	84.01	1.0214E+19	0.746	0.379	85.90	1.0237E+19	0.793
$^{686}O_3$	222	2 989.12	16	0.549	51.69	1.0405E+19	0.577	0.553	51.42	1.0402E+19	0.591
$^{686}O_3$	215	1 990.80	8	0.562	57.60	1.0138E+19	0.635	0.558	58.15	1.0147E+19	0.649
$^{686}O_3$	172	1 993.79	8	0.593	48.35	1.0363E+19	0.705	0.593	48.31	1.0359E+19	0.709
$^{686}O_3$		mean	88	0.380	61.38	1.0425E+19	0.228	0.379	61.68	1.0429E+19	0.233

Appendix A.3: Reference volume mixing ratio profiles

FSCATM must be provided with a set of a-priori Volume Mixing Ratio (VMR) profiles. The distribution package of SFIT 1.09 provides the 'refmod95' file, which has been a reference for many users or at least served as an example for building their own set specific to a certain observing location. Another common set of VMR profiles, the 'spitprim.set', has been compiled by Geoffrey C. Toon, JPL Pasadena [35], but is often better known as the 'Reftoon' set after interpolation to the 41 standard altitudes of the 'refmod95' file. These profiles are based on MkIV balloon FTIR spectra out of Fort Summer recorded on the 25-Sep-1993 (possibly with supplementary observations from other flights out of Ft. Summer and Palestine, Texas, around this time.), which obtained good quality spectra down to 4 km tangent height. These profiles contain the correct tracer correlations and seem to provide a good a priori guess, especially for the long-lived species. Many of the MkIV VMR profiles used are published in a compendium of UARS Correlative Measurements [30].

We used the opportunity of the FSCATM revision to update the refmod95 file resulting in the refmod99 file. Compared to refmod95 we incorporated the following changes: A number of profiles were scaled with a constant factor to account for long-term trends in their total abundances. Many multiplication factors were estimated from [36] and are documented in the file itself. Some profiles including CH4, N2O, and CO2 showed some unlikely 'kinks' in refmod95 and we decided to replace them with profiles from the 'Reftoon' set. We also replaced some profiles for which better information has become available since the creation of the refmod95 file. The following list summarises the changes. The last 6 molecules had not been included in previous refmod files:

CO2	Profile from G.C. Toon, (Balloon-FTIR data, 1993) *1.022
N2O	Profile from G.C. Toon, (Balloon-FTIR data, 1993) *1.0129
CH4	Profile from G.C. Toon, (Balloon-FTIR data, 1993) *1.0465
NH3	Profile from G.C. Toon, (Balloon-FTIR data, 1993) *0.1
CCL3F	Profile from G.C. Toon, (Balloon-FTIR data, 1993) *0.8434
CH3CCL3	Profile from G.C. Toon, (Balloon-FTIR data, 1993) *0.7273
CCL4	Profile from G.C. Toon, (Balloon-FTIR data, 1993) *0.7923
CHF2CL	Profile from G.C. Toon, (Balloon-FTIR data, 1993) *1.51
COCL2	GC Toon et al, GRL, p.2835-2838, 2001; [37]
CH3BR	Reftoon (NH: 9 to 11 pptv, SH: 7.8 to 8.8 pptv, IGAC Jan 2000)
CH3I	Profile from G.C. Toon, (Balloon-FTIR data, 1993)
HCOOH	Profile from G.C. Toon, (Balloon-FTIR data, 1993)
CHCL2F	Profile from G.C. Toon, (Balloon-FTIR data, 1993)
SF6	Profile from G.C. Toon, (Balloon-FTIR data, 1993) *2.600
CH3D	Profile from G.C. Toon, (Balloon-FTIR data, 1993) *1.0465
HCN	Profile from G.C. Toon, *0.76 (Mahieu, JAC, 299-310, 1995); [38]
HBR	I.G. Nolt et al, GRL 24, 281-284, 1997 (assumed constant); [39]
COCLF	ATMOS standard VMR *2 (J.Kaye et al, JGR, 12865-12881, 1991); [40]
H2S	T.W. Andreae et al, JGR 96, 18753–18760, 1991 (assumed const); [41]
OCLO	assumed constant
F134A	shape as CH2FCF3, scaled to CMDL Rep 24, 1998; [36]
C3H8	M. Kanakidou et al., JGR 96, 15395-15413, 1991 (c2h6 *0.3); [42]
F142B	shape as C2H3F2CL, scaled to CMDL Rep 24, 1998; [36]
CFC113	shape as C2F3CL3, ground concentr.: WMO Report 44, 1999, Table 1-2
F141B	shape as C2H3FCl2, scaled to CMDL Rep 24, 1998; [36]

Comments:

CH3Br , IGAC Newsletter No.19, Jan 2000, http://web.mit.edu/igac/www/. Profile of CH3Br from Reftoon – scaled to a concentration of 9pptv in the lower troposphere (compromise between 9 - 11 and 7.8 - 8.8 pptv for the northern and southern hemisphere, respectively). Stratosphere estimated from [43] and splined into the aforementioned profile.

CH3I, Vertical distribution as CH3Br, but scaled to 3 ppt in the troposphere as suggested by *Cox* et al. [44].

Appendix A.4: The SFIT–FSCATM distribution package

There is a choice between different sets of binaries to run on a PC that were created using different compilers.

- Microsoft powerstation FORTRAN (Win-NT 4.0x; rinsland@larc.nasa.gov))
- GNU open source f2c/gcc, (multi-platform OS/2, DOS, Win32; arndt@uow.edu.au).
- DEC/Compaq Visual FORTRAN 5.0d (Win-NT 4.04, n.jones@niwa.cri.nz)

In case of platform specific questions in running these programs, please contact the person listed with the version you are using. For a Unix or Linux version please contact Aaron Goldman, (email goldman@acd.ucar.edu). All binaries were created from an identical source code (including the Unix version not included in the PC distribution for SFIT 1.09).

The executables differ in the way extended memory and DPMI are handled and you may find that either of them runs more stably on your system. However, the output created shows no differences between the alternatives. More details are given in the readme files on the diskette.

For further questions on FSCATM, SFIT, or the case studies & *traceinp*, please contact Aaron Goldman, Curtis Rinsland or Arndt Meier, respectively.

References

[1] Gallery WO, Kneizys FX, Clough SA. Air Mass Computer Program for Atmospheric Transmittance/Radiance Calculation: FSCATM. Envir Res Paper ERP-828/AFGL-TR-83-0065, Air Force Geophysical Laboratory, Hanscom AFB, MA 01731, 1983.

[2] Kneizys FX, Shettle EP, Abreu LW, Chetwynd JH, Anderson GP, Gallery WO, Selby JEA, Clough SA. Users guide to LOWTRAN7. AFGL-TR-88-0177, Air Force Geophysical Laboratory AFGL(OPI), Hanscom AFB, MA 01731, 1988.

[3] Clough SA, Iacono MJ. Line-by-Line Calculations of Atmospheric Fluxes and Cooling Rates 2: Application to Carbon Dioxide, Ozone,Methane, Nitrous Oxide, and the Halocarbons. J Geophys Res, 1995;100:16519–16535.

[4] Edwards DP. GENLN2 A General Line–by–line Atmospheric Transmittance and Radiance Model. NCAR Technical Note, NCAR/TN-367+STR, Boulder, CO 80307, 1992.

[5] Rinsland CP, Levine JS, Zander R, Goldman A, Sze ND, Ko MKW, Johnson DW. Infrared measurements of HF and HCl total column abundances above Kitt Peak, 1977–1990: Seasonal cycles, long-term increases, and comparisons with model calculations. *J Geophys Res (D: Atmosph)*, 1991;96:15523–15540.

[6] Rinsland CP, Smith MAH, Rinsland PL, Goldman A, Brault JW, Stokes GM. Ground-based Infrared Spectroscopic Measurements of Atmospheric Hydrogen Cyanide. *J Geophys Res (D: Atmosph)*, 1982;87:11119–11125.

[7] Rinsland CP, Goldman A, Connor BJ, Stephen TM, Jones NB, Wood SW, Murcray FJ, David SJ, Blatherwick RD, Zander R, Mahieu E, Demoulin P. Correlation relationships of stratospheric molecular constituents from high spectral resolution, ground-based infrared solar absorption spectra. *J Geophys Res (D: Atmosph)*, 2000;105:14637–14652.

[8] Rinsland CP, Jones NB, Connor BJ, Logan JA, Pougatchev NS, Goldman A, Murcray FJ, Stephen TM, Pine AS, Zander R, Mahieu E, Demoulin P. Northern and southern hemisphere ground-based infrared spectroscopic measurements of tropospheric carbon monoxide and ethane. *J Geophys Res (D: Atmosph)*, 1998;103:28197–28217.

[9] Connor BJ, Jones NB, Wood SW, Keys JG, Rinsland CP, Murcray FJ. Retrieval of HCl and HNO3 profiles from ground-based FTIR data using SFIT2. In RD Bojkov and G Visconti, editors, *Proc XVIII Quadr Ozone Symp*, pages 485–488, L'Aquila, Italy, 1998. Parco Scientifico e Technologico d'Abruzzio.

[10] Pougatchev NS, Connor BJ, Rinsland CP. Infrared measurements of the ozone vertical distribution above Kitt Peak. *J Geophys Res (D: Atmosph)*, 1995;100:16689–16697.

[11] Kurylo MJ. Network for the Detection of Stratospheric Change. *Proc Soc Photo Opt Instrum Eng*, 1991;1491:169–174. See also http://www.ndsc.ws/.

[12] Kurylo MJ, Zander R. The NDSC – its status after 10 years of operation. In *Proc. XIX Quad. Ozone Symp.*, Sapporo, Japan: Hokkaido Univ, 2000. p. 167–168.

[13] Meier A, Goldman A, Manning PS, Stephen TM, Rinsland CP, Jones NB, Wood SW. Improvements to Air Mass Calculations for Ground-Based Infrared Measurements. *J Quant Spectrosc Radiat Transfer*, this issue, 2002.

[14] Mohr PJ, Taylor BN. CODATA recommended values of the fundamental physical constants: 1998. *Rev Mod Phys*, 2000;72:351–495. Also available online from NIST: http://physics.nist.gov/cuu/Constants/index.html.

[15] Meier A. The SFIT-Tools - a comprehensive set of auxiliary programs for running SFIT 1.09e and SFIT2, 1994–2001. Electronic access: http://www.uow.edu.au/~arndt/sftools.htm.

[16] Goldman A. Report of the FTIR retrieval intercomparison of the NDSC 1996. Annual Meeting of the infrared working group of the NDSC, University of Denver, Denver CO, April 1996.

[17] Meier A, Toon GC, Rinsland CP, Goldman A. Spectroscopic Atlas of Atmospheric Microwindows in the Middle Infra–Red. Technical Report IRF report No 123, Swedish Institute of Space Physics, Kiruna, 1997.

[18] Rothman LS, et al. The HITRAN Molecular Spectroscopic Database and HAWKS (HITRAN Atmospheric Workstation) 1996 edition. *J Quant Spectrosc Radiat Transfer, special issue 'HITRAN'*, Nov 1998;60(5):665–710.

[19] Toon GC. Pseudo-linelists, line parameters fitted to laboratory cross-section measurements. private comm., 2001. Linelists and descriptions are available electronically from ftp://mark4sun.jpl.nasa.gov/pub/pseudolines.

[20] Varanasi P. Absorption spectra of HCFC–22 around 829 cm^{-1} at atmospheric conditions. *J Quant Spectrosc Radiat Transfer*, 1992;47(4):251–255.

[21] Varanasi P, Li Z, Nemtchinov V, Cherukuri A. Spectral absorption coefficient data on HCFC–22 and SF_6 for remote-sensing applications. *J Quant Spectrosc Radiat Transfer*, 1994;52(3/4):323–332.

[22] Varanasi P, Nemtchinov V. Thermal infrared absorption coefficients of CFC–12 at atmospheric conditions. *J Quant Spectrosc Radiat Transfer*, 1994;51(5):679–687.

[23] Reisinger AR, Jones NB, Matthews WA, Rinsland CP. Southern hemisphere midlatitude ground–based measurements of $ClONO_2$: Method of analysis, seasonal cycle, and long–term trend. *J Geophys Res (D: Atmosph)*, 1995;100:23183–23193.

[24] Penner SS. *Quantitative Molecular Spectroscopy and Gas Emissivities.* Addison-Wesley, Reading MA, 1959. LCCC 59–7546.

[25] Rothman LS, et al. Current updates to the HITRAN molecular spectroscopic database, 2001. Electronic access at: http://www.hitran.com.

[26] Toth RA. Air- and N_2-broadening parameters of water vapor: 604 to 2271 cm^{-1}. *J Molec Spectrosc*, 2000;201:218–243.

[27] Birk M. Cross-sections of ClONO2 under a variety of atmospheric conditions. DLR Deutsche Forschungs- and Versuchsanstalt für Luft- und Raumfahrttechnik, Oberpfaffenhofen, Germany, private comm., 2001. Linelists and descriptions are available electronically from ftp.dfd.dlr.de/pub/spectroscopic_database/ClONO2/ (cross-sections) and ftp.dfd.dlr.de/pub/spectroscopic_database/ofp_report_german/ (data description).

[28] Griffith DWT, Jones NB, Matthews WA. Interhemispheric ratio and annual cycle of carbonyl sulfide (OCS) total columns from ground–based FTIR spectra. *J Geophys Res (D: Atmosph)*, 1998;103:8447–8454.

[29] Rinsland CP, Meier A, Griffith DWT, Chiou LS. Ground-based measurements of tropospheric CO, C2H6, and HCN from australia at 34°S during 1997-1998. *J Geophys Res (D: Atmosph)*, 2001;106:20913–20924.

[30] Peterson DB, Margitan JM, editors. *Upper atmospheric research satellite correlative measurements program (UARS–CMP) balloon data atlas.* NASA, Washington DC, 1995.

[31] Randel WJ, Wu F, Russell III JM, Zawodny JM, Nash J. *Interannual changes in stratospheric constituents and global circulation derived from satellite data.* AGU Monograph 123. American Geophysical Union, 2000. Electronic access to HALOE observations and numerous references are available at http://haloedata.larc.nasa.gov/.

[32] Brown TL, Gunson MR, Chang AY. ATMOS Level 2 Version 2 Description. Technical Report TLB-95-01, NASA, May 1995. Further information is available online at http://isis.dlr.de/ftp/atmos/atmos/version2/.

[33] Zombeck MV. *Handbook of Astronomy and Astrophysics.* Cambridge University Press UK, Cambridge, 2nd edition, 1990.

[34] Meier A. *Determination of atmospheric trace gas amounts and corresponding natural isotopic ratios by means of ground-based FTIR spectroscopy in the high arctic*, volume 236 of *Reports on Polar Research.* Alfred–Wegener–Institute, Bremerhaven, 1997. ISSN 0176-5027.

[35] Toon GC. JPL Pasadena, private communication, Aug 2001. see also http://mark4sun.jpl.nasa.gov/m4-balloon.html.

[36] Climate Monitoring and Diagnostics Laboratory Summary Report No 24 1996-1997. CMDL Report 24, US Dept of Commerce, NOAA, and Env Res Lab, Boulder CO, Dec 1998.

[37] Toon GC, Blavier J-F, Sen B, Drouin BJ. Atmospheric $COCl_2$ measured by solar occultation spectrometry. *Geophys Res Let*, 2001;28:2835–2838.

[38] Mahieu E, Demoulin P, Delbouille L, Roland G, Rinsland CP, Zander R. Vertical column abundances of HCN deduced from ground-based infrared solar spectra: Long-term trend and variability. *J Atmosph Chem*, 1995:20:299–310.

[39] Nolt IG, et al. Stratospheric HBr concentration profile obtained from far-infrared emission spectroscopy. *Geophys Res Let*, 1997;24:281–284.

[40] Kaye J, Douglas AR, Jackman CH, Stolarski RS, Zander R, Roland G. Two-Dimensional Model Calculation of Fluorine–Containing Reservoir Species in the Stratosphere. *J Geophys Res (D: Atmosph)*, 1991;96:12865–12881.

[41] Andreae TW, Cutter GA, Hussain N, Radford-Knoery J, Andrae MO. Hydrogen Sulfide and Radon in and over the Western North Atlantic. *J Geophys Res (D: Atmosph)*, 1991;96:18753–18760.

[42] Kanakidou M, Singh HB, Valentin KM, Crutzen PJ. A Two-Dimensional Study of Ethane and Propane Oxidation in the Troposphere. *J Geophys Res (D: Atmosph)*, 1991;96:15395–15413.

[43] Kourtidis K, Borchers R, Fabian P. Distribution of Methyl Bromide in the Stratosphere. *Geophys Res Let*, 1998;25:505–508.

[44] Cox RA, Bloss WJ, Jones RL, Rowley DM. OIO and the Atmospheric Cycle of Iodine. *Geophys Res Let*, 1999;26:1857–1860.

[45] Rinsland CP, Boughner RE, Larsen JC, Stokes GM, Brault JW. Diurnal Variations of Atmospheric Nitric Oxide: Ground-based Infrared Spectroscopic Measurements and their Interpreation with Time-dependent Photochemical Model Calculations. *J Geophys Res (D: Atmosph)*, 1984;89:9613–9622.

Glossary

ECMWF European Center for Medium Range Weather Forecast

NDSC Network for the Detection of Stratospheric Change, http://www.ndsc.ncep.noaa.gov/

SFIT 1.xx Nonlinear least squares fitting program for ground-based solar FTIR spectra, by C.P. Rinsland, LARC. (Allows scaling of a given set of a-priori VMR profiles, but not profile retrieval.)

SFIT 2 is being jointly developped by the SFIT 1 creators and NIWA Lauder. The concept goes much further though, as it is primarily a profile retrieval program. However, the model atmosphere used in the SFIT2 retrieval is provided through SFIT–FSCATM in the same way as for SFIT 1.

SZA Solar Zenith Angle, typically given in degrees.

TCA Total Column Amount (in $molec/cm^{-2}$)

VMR Volume Mixing Ratio